Block Copolymer Ion Gels for CO_2 Separations

A DISSERTATION
SUBMITTED TO THE FACULTY OF THE GRADUATE SCHOOL
OF THE UNIVERSITY OF MINNESOTA
BY

Yuanyan Gu

IN PARTIAL FULFILLMENT OF THE REQUIREMENTS
FOR THE DEGREE OF
DOCTOR OF PHILOSOPHY

Adviser: Timothy P. Lodge

August 2013

Acknowledgements

The past five years in graduate school has been a challenging as well as rewarding experience for me. The completion of this thesis research is truly a milestone in my life, and it could not be achieved without the support from many people. First and foremost, I would like to thank my advisor, Prof. Tim Lodge, for his invaluable guidance, encouragement and support during my graduate career. Tim has been an outstanding teacher and mentor, from whom I have learned much about how to conduct good research. His enthusiasm, patience and thoroughness toward scientific research will always inspire me in my future career. I thank Prof. Edward Cussler, who provided very generous help and insightful guidance to this thesis project. Especially in the starting stage, the interaction with Prof. Cussler always stimulated my scientific interest toward research and generated great ideas.

I must also thank many past and present Lodge group and Polymer group members for their help and support. I thank Dr. Zhifeng Bai, Dr. Brad Jones, Dr. Hau-Nan Lee and Dr. Chun Liu for getting me started on my research in Lodge lab; Dr. Sipei Zhang, Dr Keun Hyung Lee, Lucas McIntosh, and Dr. Jae-Hong Choi for collaboration on multiple projects. I benefited a lot from the discussion with Dr. Shingo Kobayashi, Dr. Yuewen Xu, Dawen Niu and Dr. Jihua Zhang on polymer synthesis; and Can Zhou, Aaron Hedegaard, Yuqiang Qian, Luca Martinetti, Dr. David Giles, Dr. Milana Trifkovic, Dr. Ligeng Yin and Dr. Megan Hoarfrost on polymer characterization and application. Many other people have also helped me through instrument training, providing chemicals and helpful discussions: Dr. Sara Arvidson, Dr. Soo-Hyung Choi, Tim Gillard, Dr. Ashish

Gaikwad, Dr. Mingjing Ha, Prof. Marc Hillmyer, Matt Irwin, Dr. Yu Lei, Dr. Ken-Hsuan Liao, Dr. Joe Lott, Jie Lu, Prof. Chris Macosko, Dr. Ameara Mansour, John McAllister, Dr. Luciana Meli, Dr. Michelle Mok, Dr. Adam Moughton, Zhen Ren, Dr. Jie Song, Dr. Myungeun Seo, Dr. Peter Simone, Dr. Joshua Speros, Soonyong So, Dr. Rajiv Tarabagil, Chris Thurber and Yanfei Wu.

Last but not least, I owe my deepest gratitude to my parents and my fiancée, Lingjun, for their endless love, care, encouragement and support. Without them I would have never achieved this far in my journey of life. They are the reason why I am here today.

To Dad, Mom and Lingjun

Abstract

Block copolymer ion gel is composed of a polymer network formed by self-assembly of triblock copolymers, and an ionic liquid which can selectively dissolve the polymer mid-block. In this thesis project, the target is to study the gas separation performance of ion gels for CO_2 separation, and seek ways to optimize their properties in terms of the gas separation performance and mechanical strength. Ionic liquids have shown great promise as novel CO_2-separation media, largely due to their highly selective gas solubility and non-volatility. It is discovered that the polymer networks not only provides the mechanical support to the ionic liquid, but help improve the gas separation performance as well.

To study the CO_2 separation performance of block copolymer ion gels, model ion gel systems that comprise 1-ethyl-3-methylimidazolium bis(trifluoromethylsulfonyl)amide ([EMI][TFSA]), a low viscosity ionic liquid, and a triblock copolymer with a polymerized ionic liquid mid-block was prepared. The synthesis of the triblock copolymer was successfully achieved through a sequential controlled polymerization and post-polymerization reactions. The gas separation performance was measured on a supported ion gel membrane, which is prepared by filling a porous PVDF support with ion gels. It was discovered that the polymerized ionic liquid gels exhibit high gas permeability due to the high liquid fraction. Moreover, the permeation selectivity is significantly increased from that of the neat ionic liquid. Comparisons with Robeson plots also indicate very promising separation performance for ion gels. Two other ion gels formed by self-assembly of poly(styrene-*b*-ethylene oxide-*b*-styrene) (SOS) and

poly(styrene-*b*-methyl methacrylate-*b*-styrene) (SMS) in [EMI][TFSA] were also examined for the CO_2 separation application. The separation performance of ion gels was found to be strongly dependent on the polymer mid-block. This effect is further confirmed by gas solubility test, as PEO can increase the solubility ratio for both CO_2/N_2 and CO_2/CH_4 gas pairs.

To achieve applications in industrial processes, it is highly desirable to enhance the mechanical properties of ion gels. A novel ion gel based on poly[(styrene-r-vinylbenzyl azide)-*b*-ethylene oxide-*b*-(styrene-r-vinylbenzylazide)] (SOS-N_3) was synthesized. Such a triblock copolymer ion gel can be chemically cross-linked by high temperature annealing and UV-irradiation. After cross-linking, the mechanical strength of the gel showed significant improvement, with 400% increase in the tensile strength and almost one order of magnitude increase in toughness. The mechanical stability of the supported ion gel membranes was also enhanced. More importantly, the mass transport properties are retained after the cross-linking. Because the cross-linking reaction is restricted to the styrene domains, it does not affect the mass transport path. This study demonstrates a promising approach to improve the mechanical properties of a dilute gel without interfering with the gas separation performances.

Overall, block copolymer ion gels represent a promising class of materials for CO_2 separation applications. Through rational choice of ionic liquid and block copolymers, the properties of ion gels can be further optimized for gas separation applications.

Table of Contents

List of Tables

List of Figures

List of Schemes

Chapter 1

Background

This chapter provides an overview of previously published work that motivates the research described in this thesis. In Section 1.1, basic concepts and recent progress in membrane technologies for gas separation are reviewed, with an emphasis on the recent developments of novel materials for CO_2-related separation membranes. Section 1.2 introduces the background of ionic liquids and their potential applications in CO_2 separation and absorption. The chemical design, physical chemical properties and other applications of ionic liquids are also briefly discussed in this section. As a way to achieve the materials application of ionic liquids, combining ionic liquids with polymer systems have attracted significant research attention. Section 1.3 reviews the recent developments in this area, with detailed discussion on polymer solubilization in ionic liquids, block copolymers in ionic liquids, ion gels and polymerized ionic liquids. Previous studies in the fields of ion gels and polymerized ionic liquids are especially pertinent to this thesis project. Section 1.4 describes the key motivation for this thesis and outlines the following chapters.

1.1 Membrane technology in CO_2 separation

The separation of gas mixtures using polymeric membranes has been commercially utilized since the late 1970s.[1,2] Although the possibility of using membranes in gas separation was recognized much earlier, the commercialization of gas separation

membranes generated a significant amount of interest from both academia and industry.[3,4] In 1979, Monsanto introduced the PRISM membrane system for hydrogen separation, which was the first gas separation membrane introduced in an industrial process.[5] This polysulfone hollow-fiber membrane was a big success and widely used for hydrogen recovery from the purge gas streams of ammonia plants.[6] Since then, the rate of growth of this technology has been phenomenal. Progress was made possible by the development of new membrane materials, new processing techniques and new operational procedures. So far, membrane-based gas separation has grown into a 200 million dollar/year industry, which is still under rapid development.[7,8] Compared to the more established gas separation technologies (e.g., chemical and physical absorption, pressure swing adsorption and cryogenic distillation), membrane separation has the advantages of lower energy cost, better safety, and less maintenance requirement. As the cost of energy increases, membrane separation becomes a more economically favorable choice due to the simple separation process and operation.

A gas separation membrane works by allowing a certain type of gas to pass through the membrane while blocking others. Therefore, the key parameters for the performance of a gas separation membrane are the permeability (P) of a specific component, which usually is the "fast gas", and the selectivity (α), which describes the separation efficiency. In dense membranes, gas permeation follows the well-known "dissolution-diffusion" mechanism, which means that gas molecules first dissolve into the membrane material and then diffuse through it.[9] Based on this mechanism, the permeability of a certain gas is determined by the product of gas solubility (S) and diffusivity (D), while

the selectivity (also referred to as permselectivity) is determined by the permeability ratio of two different gases on the same type of membranes, as shown in Equation 1.1. Hence, the selectivity of a membrane is also determined by the diffusivity ratio and the solubility ratio, as shown in Equation 1.2.

$$P = D \times S \tag{1.1}$$

$$\alpha_{i/j} = \frac{P_i}{P_j} = \frac{D_i}{D_j} \times \frac{S_i}{S_j} \tag{1.2}$$

Here, it is important to point out that there are two different types of selectivity: ideal and real selectivity. Ideal selectivity is calculated from the permeability ratio of two different pure gases in a given membrane, while the real selectivity is the permeability ratio of these two gases in a gas mixture and across the same membrane. Typically, the real selectivity can be considerably lower than the ideal selectivity for some polymeric gas separation membranes, which is attributed to either membrane plasticization or the competitive absorption of different components in gas mixtures.[10,11] When discussing the performance of a gas separation membrane, it is also necessary to distinguish between permeability and permeance. The former is a material property which is independent of the membrane structure and design, while the latter is a membrane property which equals the permeability divided by the membrane thickness.

A high-performance gas separation membrane requires both high selectivity and high permeability, which, however, is hard to achieve at the same time. A Robeson plot is a widely applied metric to compare the gas separation performances of polymer membranes, as shown in Figure 1.1.[2,3] On this plot, the selectivity of a gas pair is plotted against the permeability of the more permeable gas on a log-log scale. The empirical

"upper bound" on this plot, which shows the well-known flux/selectivity tradeoff of membrane separation, represents the best permeability/selectivity combination of the existing membranes.[12] Hence, one of the main targets in this research field is to obtain polymer membranes with performance exceeding the upper bound. Usually, commercial membranes exhibit performances that lie somewhat below the upper bound, reflecting the fact that many factors including cost, operational condition, membrane stability may affect the choice of materials for commercial membranes.[1,8]

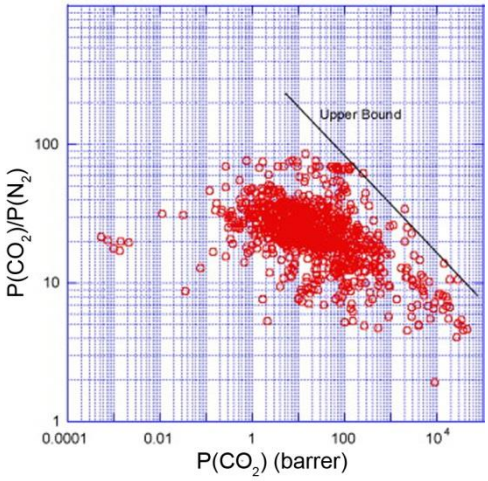

Figure 1.1 Robeson Plot for CO_2/N_2 separation[2]

Among various gas separation targets, CO_2 separation from mixed gas streams is becoming an increasingly important area, largely due to the growing demand to limit greenhouse gas emission. Carbon capture and sequestration from point sources such as coal-fire power plants requires separating CO_2 from flue gases (CO_2/N_2 separation).[13–16] Also, CO_2 removal from raw wellhead gas is essential to the production of home-use natural gas qualified for pipeline transportation (CO_2/CH_4 separation). Traditional amine-

absorption has proved to be an efficient technology for CO_2 separation in industrial processes, where amine-based solvents (e.g. monoethanolamine) are used to capture CO_2 through simple acid-base reactions.[17,18] However, the major disadvantage of amine-absorption is the high energy cost during desorption, where the CO_2-rich amine solution is heated up to 120-140 ℃ to release CO_2 and regenerate the solvent.[19] Due to the highly-corrosive nature of the degraded amine sorbents, this technology also requires constant maintenance, which limits applications in remote areas.[17]

Membrane separation currently occupies a small, yet growing, sector in CO_2 separation. The advantages of smaller unit size, simpler operation and better safety makes it particularly attractive in small- and medium-scale applications where continuous monitoring is impractical. In the early 1980s, the anisotropic cellulose acetate membrane was first introduced into natural gas processing for CO_2 removal by Grace Membrane Systems.[20] Currently, cellulose acetate is still widely used in most CO_2 membrane separation units, but polyimide membranes and perfluoropolymer membranes have started to challenge its market position.[8,21–25] Recent developments in this area have also been highlighted by several breakthroughs in the application of novel membrane materials. A group of polymers known as “polymers of intrinsic microporosity” (PIM) have been recently synthesized by Budd and coworkers.[26,27] By incorporating various spiro-centers which force the polymer chains to form a loosely packed morphology, these ladder-type polymers have structural characteristics similar to molecular sieves. The significantly increased free volume allows facile gas permeation through the membrane, and some of the PIMs have exceeded the Robeson upper bound.[28,29] Other materials such

as metal organic frameworks, polymer-zeolite composite membranes, inorganic silica membranes and ionic liquids have also shown great promise in gas separation performance.[30–34] Introducing these emerging technologies into membrane separation offers great potential for improving gas separation performance.

1.2 Ionic liquids

Ionic liquids have become a research focus as new solvents and materials in the past two decades. Their history, however, can be traced back to the early 20th century. The first ionic liquid, ethyl ammonium nitrate ($[EtNH_3][NO_3]$, m.p. 12 °C), was reported by Walden in 1914,[35] but it was not until the discoveries of binary ionic liquids based on mixtures of trihalogenoaluminates and 1,3-dialkylimidazolium or *N*-alkylpyridinium that the modern age of ionic liquids truly began.[36,37] The binary ionic liquids were initially investigated as solvents in solution electrochemistry and liquid electrolytes in batteries. But these ionic liquids, especially the halogenoaluminate anions, are very sensitive to moisture and air, which limits their further applications beyond the laboratory. In the early 1990s, studies was directed to search for air- and moisture-stable anions as an alternative.[38,39] In particular, ionic liquids based on tetrafluoroborate ($[BF_4]$) and bis(trifluoromethylsulfonyl)amide ([TFSA]) anions have exhibited remarkable stability to air and water, which increase their potential for various kinds of applications.[40–42] Since then, the scientific community has shown a continuously increasing interest in this area of research.

Ionic liquids are defined as a class of salts with melting points below 100 °C. In fact, most of the ionic liquids reported in the literature are salts with melting points lower than room temperature, which are also termed "room temperature ionic liquids" (RTILs). Generally, ionic liquids are composed of organic cations and either organic or inorganic anions. These ions usually have asymmetric and bulky structures, which can significantly reduce the inter-ionic interactions and disrupt crystal formation, thus leading to the low melting points.[43] Among all the ionic components used in ionic liquids, the most commonly used cations include 1,3-dialkylimidazolium, *N*-alkylpyridinium, *N*,*N*-dialkylpyrollidinium, tetraalkylphosphonium and tetra-alkylammonium, while [BF_4], [TFSA], hexafluorophosphate ([PF_6]) and triflate [TfO] are the most prevalent anions.[38,44] More importantly, the physicochemical properties of ionic liquids can be tuned through different combination of anions and cations, which provides great design flexibility for applications.[45] The chemical structures of these common ions are shown in Figure 1.2.

Ionic liquids have received a great deal of attention in engineering applications because of their unique combination of properties. Most ionic liquids have negligible vapor pressures (10^{-11}~10^{-10} mbar) and are usually non-flammable. It is also recognized that ionic liquids have high chemical and thermal stability as well as wide liquid ranges due to their high decomposition temperatures (above 300 °C for some ionic liquids). Thus, ionic liquids are widely studied as novel "green solvents" to replace conventional organic solvents in chemical synthesis and catalysis. Additionally, the chemical structure of both the cations and the anions can be tailored to make various kinds of organic or inorganic molecules, polar or non-polar, soluble in ionic liquids. One specific example is

the discovery of ionic liquids as solvents in cellulose processing, which has attracted considerable research interest from both academia and industry.[46] As molten salts at room temperature, ionic liquids also exhibit high ionic conductivities and high capacitance values that are comparable to aqueous electrolytes, yet they have wider electrochemical windows (spanning up to 6 V in some cases), meaning that they can be stable at higher oxidation or reduction potentials.[47] Because of their exceptional electrical properties and high stability, ionic liquids have also been widely studied as functional materials for various electrochemical devices such as lithium-ion batteries, transistors, solar cells and supercapacitors.[48,49] Ionic liquids also show other special properties such as selective gas solubility (which will be discussed later in this section) and the capability to absorb microwaves.[50,51]

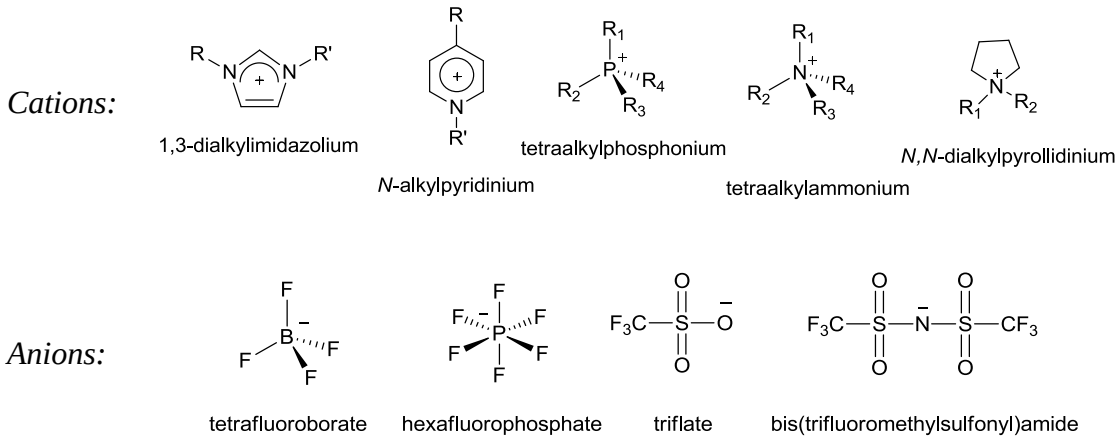

Figure 1.2 Chemical structures of common cations and anions in ionic liquids

Because the availability of numerous cations and anions provides virtually unlimited combinations, ionic liquids have been termed “designer solvents”: by changing the chemical structure of component ions, the physicochemical properties of ionic liquids can

be tailored to meet specific application requirements.[45] This provides an almost infinite platform for chemistry researchers to synthesize, understand and explore the application of this novel class of materials. Watanabe and coworkers have conducted a systematic study into the physicochemical properties of ionic liquids by changing the alkyl chain length in 1-alkyl-3-methylimidazolium cations.[52–54] Their research indicates that the temperature dependence of the ionic conductivity, viscosity and self-diffusion coefficient follows the Vogel-Fulcher-Tamman equation, while density shows a linear dependence. By increasing the alkyl chain length on the cation, the ionic association of the ionic liquids decreases dramatically.[55] Additionally, certain functional groups can be chemically incorporated introduced into ionic liquids to impart specific properties. These ionic liquids are thereby named "task-specific ionic liquids". Recent developments have shown great promise to facilitate cellulose processing, gas absorption and separation, chemical synthesis and catalysis, as well as drug delivery. One recent advance in this area is task-specific ionic liquids for heavy metal ion extraction from aqueous systems, pioneered by Visser and Rogers.[56] In such ionic liquids, functionalized imidazolium cations with thioether, urea, or thiourea derivatized side chains act as metal ligating moieties, whereas the perfluorinated anions provide the desired water immiscibility for liquid-liquid extraction.

Despite their wealth of useful properties and potential applications, ionic liquids naturally possess several shortcomings. First, although the number of commercially available ionic liquids is increasing, they are still relatively expensive compared to conventional solvents, which limit their application in large-scale industrial processes.

Second, the physical and chemical properties of ionic liquids are very sensitivity to halide impurities or residual water: for instance, the viscosity of [BMI][PF_6] can be increased by 48% with only 2.5 wt% of LiBr impurities.[57] In ionic liquid-based electrochemical devices such as transistors or solar cells, device performances can also be significantly affected by moisture. Third, the toxicity and biodegradability for most ionic liquids have not been systematically studied.[58] Although their low vapor pressure may reduce air pollution compared to conventional organic solvents, ionic liquids can still cause severe water pollution if they are released to aquatic environments.[59] Because of their high stability, ionic liquids may even become very persistent pollutants. These environmental risks have also stimulated debate about the "green" nature of ionic liquids. A number of practical issues need to be solved to enable the large-scale applications of ionic liquids.

1.2.1 Ionic liquids in CO_2 separation

As mentioned earlier, CO_2 separation and absorption has become an increasingly important area due to the significant need to reduce green-house gas emission. Most of the research focuses on developing new polymeric materials to enhance separation performance.[1,5,20,60] Liquid-facilitated transport has been proposed as an alternative route to achieve efficient gas separation in the early 1970s.[61] The high gas permeability comes from the low viscosity of liquids, while the high selectivity comes from the selective gas solubility of the liquids. However, there have been very few practical applications of liquid membranes due to the low membrane stability. The major cause of this low stability is the loss of liquid phase from the membrane support by evaporation.[62] Ionic liquids can effectively avoid this problem due to their non-volatility and high thermal

stability. Moreover, ionic liquids generally show selective solubility of CO_2 over other gases such as N_2 and CH_4, which makes them promising CO_2-selective separation media.

Brennecke and coworkers first reported the solubility of CO_2 and several other gases in ionic liquids.[63] When they studied the application of supercritical CO_2 to extract solutes from ionic liquid solutions, they discovered that CO_2 is actually quite soluble in several pyridinium- and imidazolium-based ionic liquids. For instance, at a pressure of 50 bar, the CO_2 solubility in [BMI][PF_6] is as high as 50 mol%.[64] Further experimental studies have also confirmed this phenomenon at both higher and lower pressures.[65–67] Naturally, it is desirable to understand the underlying mechanism of this interesting phase behavior. Gas solubility in ionic liquids is a thermodynamic process governed by the interaction between ionic liquids and gas molecules. Recently, Anthony et al. systematically studied the solubilization of several different gases in imidazolium-based ionic liquids.[64,68] Their results suggest that the high solubility of CO_2 can be attributed to the interaction between the quadrupole moment of the CO_2 molecule and the electrical charge of the ionic liquid.[69] This specific interaction enhances the solubilization of CO_2 in ionic liquids over other gases such as N_2 and CH_4, which have significantly smaller or zero quadrupole moments. Other interactions, such as weak Lewis acid-base interactions and hydrogen-bonding, could also have some influence on CO_2 solubility in certain ionic liquids.[65]

Additionally, the tunable structure of ionic liquids provides unique flexibility in tailoring gas separation performance. Over the past several years, a group of ionic liquids with the general formula [RMI][TFSA], 1-*R*-3-methylimidazolium bis(trifluoromethyl-

sulfonyl)amide (*R* represents a certain functional group), presents a versatile platform for comparative studies of gas solubility in ionic liquids.[70] In order to improve the solubility and selectivity of CO_2, a series of functional groups including alkyl, ether, fluoroalkyl, hydroxyl and nitrile have been incorporated into imidazolium cations.[45,71–75] Results show that polar groups such as nitriles, hydroxyl, and oligo(ethylene glycol) are more effective than the non-polar alkyl chains. However, it is necessary to point out that the physical solubility of CO_2 in imidazolium-based ionic liquids is still relatively low compared to the chemical absorption of traditional amine-based solvents such as monoethanolamine and diethanolamine.[70] Therefore, research efforts have been made to incorporate specific functional groups into ionic liquids to exceed the limit of physical absorption. For instance, Bates et al. reported the synthesis of an amine-functionalized ionic liquid which can capture CO_2 through chemical complexation.[76] This type of "task-specific ionic liquid" can absorb 50 mol% of CO_2 even at a low pressure. More recently, equimolar CO_2 absorption has been achieved in a special class of anion-functionalized ionic liquid, where the amino acid anions can achieve a 1:1 complexation with CO_2.[77] The chemical absorption agent can also be doped into the ionic liquids to enhance CO_2 uptake. Camper et al. reported that amine ionic liquid solutions (molar ratio 1:1) can be an efficient CO_2 separation medium.[73] Unsurprisingly, the CO_2 capture efficiency of amine-IL solution is similar to that of the traditional amine-based solvent, but the use of ionic liquids significantly reduced amine degradation and evaporation, which improves the energy efficiency of separation.

Supported ionic liquid membranes (SILMs), prepared by impregnating a porous support with ionic liquid, provide a good method to assess the viability of using ionic liquids in membrane separation.[78] Previous studies have shown promising results for separation of CO_2/N_2 and CO_2/CH_4 gas pairs. For instance, Scovazzo et al. studied the effects of moisture, temperature, mixed gas operation, and operational time on separation performances of these SILMs, and demonstrated long-term stability in low pressure operations.[79] A critical analysis of ionic liquid membranes relative to the Robeson upper bound was also provided as a guide for relevant research.[80] The effects of water on ionic liquid gas separation performances have also been investigated.[81] However, as the ionic liquid is retained in the porous support merely by capillary forces, these membranes are not stable for high pressure applications such as CO_2/CH_4. Therefore, it is desirable to develop solid-state materials which can maintain the separation properties of ionic liquids. Bara et al. prepared a membrane using a cross-linked difunctional ionic liquid with higher stability.[82] The ability to tune the separation performances was also demonstrated by incorporating various functional groups. In 2011, Jansen et al. also developed ionic liquid gel membranes using poly(vinylidene fluoride-*co*-hexafluoropropylene) and [EMI][TFSA] for CO_2 gas separations.[83] The mechanical properties and gas separation performances have been examined for a wide range of polymer weight fractions from 20 to 80 wt%. The membrane with the highest ionic liquid content exhibits a CO_2 permeability of *ca*. 500 barrers, which is close to pure ionic liquids.

1.3Polymers in ionic liquids

As discussed in the previous section, ionic liquids have been recognized as a new class of solvent or liquid electrolyte for various applications. Since the development of ionic liquids with high air- and moisture-stability, incorporating ionic liquids into various polymer systems has become a fast-growing area.[48,84,85] Initial research interest in this field was to use ionic liquids as alternative solvents in polymerization reactions and polymer processing.[38] Later, ionic liquid-based functional materials via combinations of polymers and ionic liquids have attracted great attention. In this field, block copolymers have received special interest because of their interesting self-assembly phase behavior and flexibility in material design.[86] Another area of interest is to incorporate ionic liquid into polymer systems through covalent bonding. Polymerized ionic liquids, prepared by polymerization of ionic liquid monomers, have shown promising gas separation performance as well as interesting ion conducting properties. Here, a brief description of current research in this field is provided, with specific focus on polymer solubilization in ionic liquids, block copolymer self-assembly, ion gels and polymerized ionic liquids.

1.3.1 Ionic liquids as solvents in polymer systems

The most straightforward method to obtain a polymer-ionic liquid composite is through simple dissolution of polymer in an ionic liquid. However, there have been relatively few studies investigating polymer solubility in ionic liquids. In general, the solubility of a chemical compound in a solvent is determined by thermodynamics, but the kinetic factors may also play an important role in this regard. Dissolution of a polymer in a solvent requires diffusion of the solvent into the polymer first, leading to swelling or plasticization that precedes the formation of a homogeneous solution.[87] Due to the high

viscosity of ionic liquids (usually 20-1000 times higher than conventional molecular solvents), the time scale to reach solubility equilibrium can be significantly longer. In a study reported by Snedden et al., the solubility of 17 different homopolymers and copolymers in three different ionic liquids were systematically studied in dilute solutions.[88,89] The results on solubility trends are fairly empirical. Moreover, the authors reported the observation of phase separation between polymer and ionic liquid over periods of days or weeks in many initially homogeneous systems. This phenomenon is believed to be caused by the slow kinetics in reaching solubility equilibrium because of the higher visocosity or potential degradation in ionic liquids. Another interesting result from Watanabe et al. shows that polymers which can form strong hydrogen bonds, such as poly(acrylic acid), poly(methacrylic acid) and poly(vinyl alcohol), are insoluble in a common ionic liquid 1-ethyl-3-methylimidazolium bis(trifluoromethylsulfonyl)amide ([EMI][TFSA]). In contrast, polymethacrylates and polyacrylates such as poly(methyl methacrylate) and poly(2-ethylhexyl acrylate) are soluble in [EMI][TFSA].[90,91]

In the study of polymer solubility in ionic liquids, the temperature dependence is of particular interest. Both upper critical solution temperature (UCST, the critical temperature above which a mixture is miscible in all proportions) and lower critical solution temperature (LCST, the critical temperature below which a mixture is miscible in all proportions) phase behavior have been found in ionic liquids. For instance, Ueki and Watanabe first reported the UCST behavior of poly(N-isopropylacrylamide) (PNIPAm) in [EMI][TFSA], which is so far the only reported UCST system.[91] This is quite interesting because PNIPAm is also well-known for its LCST behavior in aqueous

solutions. In polymer/ionic liquid systems, LCST behavior is more commonly discovered. It has also been reported that both homopolymer poly(benzyl methacrylate) (PBzMA) and random copolymer poly(styrene-*co*-methyl methacrylate) (PS-*co*-PMMA) exhibit LCST behavior in [EMI][TFSA].[92] In these systems, the LCST can be tuned by changing the ionic liquid or the distribution of solvatophobic (benzyl) and solvatophilic (methacrylate) groups in the polymer chains. More recently, Lee and Lodge discovered the LCST behavior of poly(ethylene oxide) (PEO), a widely used hydrophilic polymer, in the ionic liquids 1-ethyl-3-methylimidazolium tetrafluoroborate ([EMI][BF_4]), 1-butyl-3-methylimidazolium tetrafluoroborate ([BMI][BF_4]) and their blends, where the LCST can be easiliy tuned by changing the composition of the blends.[93] It was also proposed that hydrogen bonds between PEO and ionic liquid provide the driving force for the LCST phase behavior.[94] The fact that poly(ethyl glycidyl ether) (PEGE), a PEO derivative, shows a LCST in the [EMI][TFSA] also supports this hypothesis.[95]

Cellulose processing has become another important area where ionic liquids are used as solvents. While cellulose is known to be insoluble in water and most conventional molecular solvents, it was discovered that imidazolium-based ionic liquids with strong hydrogen bond accepting anions, such as halides, show high solubility for cellulose.[46,96] Rogers and coworkers conducted a series of studies on the dissolution mechanism of cellulose in ionic liquids, where they found that polymer solubilization is through the strong hydrogen bond interaction between the hydroxyl protons of cellulose and the halide anions of the ionic liquids.[46,97–99] It was also suggested that cations with shorter alkyl chain lengths helps improve cellulose solubility. Regeneration of cellulose from

ionic liquid solutions was also investigated. Powders, films, fibers and many other macroscopic morphologies can be obtained via different processing procedures.[100–102] The regenerated cellulose shows minimal changes in molecular weight and other properties. In more recent efforts, application of ionic liquids has been further extended to not only other biopolymers including hemicellulose and lignin, but to the direct extraction of these polymers from biomass as well.[103] The high solubility of cellulose-based materials in ionic liquids provides new opportunities in the processing of these most abundant materials in nature.

1.3.2 Block copolymer self-assembly in ionic liquids

Block copolymers are composed of two or more chemically distinct polymer blocks covalently linked to each other. It is well established that block copolymers can self-assemble into various morphologies either in bulk or in a selective solvent.[86] Using ionic liquids as a solvent for block copolymers has spurred new interest in this area, as the non-volatility and tunable solvation properties allows for new examinations of the phase behavior in block copolymer/solvent mixtures.[104] Moreover, it provides a unique platform for designing novel materials through the combination of the attractive properties from ionic liquids and the well-defined nanostructures from self-assembled block copolymers.

Investigation in this area began with the study of micelle formation in dilute ionic liquid solutions. He and Lodge first reported a comprehensive study on the self-assembly behavior of diblock copolymer poly(butadiene-*b*-ethylene oxide) (PB-PEO) in 1-butyl-3-methylimidazolium hexafluorophosphate ([BMI][PF_6]).[104] In this system, the non-polar PB is insoluble micelle cores, while polar PEO is soluble in ionic liquid and forms the

micelle corona. It was discovered that PB-PEO diblock copolymers exhibit the "universal" block copolymer micelle structures, ranging from spheres to worm-like micelles to vesicles upon decreasing the chain length of the ionic liquid-compatible block. Similar to aqueous systems, block copolymer micelle formation in ionic liquids is not controlled by thermodynamics but kinetics, as evidenced by the polymorphism in these PB-PEO micelles and the dependence of the micelle morphologies on preparation method. The kinetically trapped micelle structure reflects the high amphiphilic nature of PB-PEO and the extremely low compatibility of PB in [BMI][PF_6]. Due to the non-volatile nature and wide liquid range of ionic liquids, the ergodicity of micelle formation can be studied in ionic liquids using different preparation methods and high temperature annealing. Meli et al. studied the relaxation of PB-PEO block copolymer micelles in [EMI][TFSA] and [BMI][TFSA].[105,106] They found that the large aggregates formed through direct dissolution of the polymer in ionic liquids will relax to smaller, monodispersed micelles. In contrast, smaller micelles formed by cosolvent evaporation method cannot be further relaxed through high temperature annealing. Moreover, the relaxation rate increased with increased polymer concentration, indicating that the mechanism for micelle equilibration is mainly through micelle fusion/fission instead of unimer exchange.

The discoveries of thermo-sensitive ionic liquid/polymer systems have led to the development of stimuli-responsive materials that can respond to temperature changes. Ueki et al. reported a successful example where diblock copolymer PBzMA-*b*-PNIPAm displays doubly thermosensitive micellization in [EMI][TFSA].[107] Because the LCST of PBzMA and the UCST of PNIPAm are combined in this system, the block copolymer

can form micelles below the UCST of the PNIPAm block and above the LCST of the PBzMA block. The resulting micelles can therefore undergo a micelle-unimer-inverse micelle morphology change upon temperature increase. The same micelle-unimer-inverse micelle morphology transition is also observed in PEO-PNIPAm diblock copolymers in [EMI][BF_4]/[BMI][BF_4] blends, where both the UCST and LCST can be adjusted by changing the mixing ratio of the two cations.[108]

The thermo-responsive behavior of micelles has also been used to create "micelle shuttles" between ionic liquids and water. Such systems are of particular interest for developing recoverable delivery vehicles in biphasic catalysis. In 2007, He and Lodge reported the first micelle shuttle based on PB-PEO micelles which shows a reversible transfer between water and [BMI][[PF_6].[109] Due to the higher solubility of PEO in water than in [BMI][PF_6], PB-PEO micelles preferentially stay in the aqueous phase at ambient temperature, and will transfer to the ionic liquid phase if the temperature is increased to above 75 ℃. The transfer process is fully thermo-reversible and can be repeated many times. The driving force of the phase transfer is the LCST behavior of the PEO corona in water: as the relative affinity of PEO corona to water and ionic liquid is variable with temperature, the micelles will migrate to the phase that dissolves PEO better. The transfer mechanism, thermodynamics and kinetics were systematically studied using dynamic light scattering and turbidity tests.[110] It was discovered that dissolved solutes in the aqueous phase, such as salt and sugar, can also affect the transfer temperature and rate. Furthermore, the work was extended by replacing PB with a thermosensitive PNIPAm block, which exhibits a UCST in ionic liquid [EMI][TFSA] and an LCST in water.[111] The

PNIPAm-PEO micelles display an interesting micellization-transfer-demicellization phase behavior upon temperature increase, which allows for transportation and delivery of chemicals from water to ionic liquid phase and back. Recently, an exciting discovery in this area is the "vesicle shuttle": by decreasing the volume fraction of ionic liquid-soluble PEO block, PB-PEO block copolymer can be used to prepare vesicles which also show reversible phase transfer between water and ionic liquids.[112,113] An obvious advantage of this system is that the vesicle interiors can transfer larger amounts ionic liquid and chemicals dissolved in ionic liquid to the aqueous phase. Due to the low glass transition temperature of PB (*ca.* 5 ℃), the vesicle bilayers formed by liquid PB block is quite permeable, thereby chemicals outside the vesicle can diffuse through the membrane into the vesicles, and vice versa. Such a system is very promising as nanocarriers and nanoreactors for reactions and catalysis involving ionic liquids.

In medium and high concentrations, ionic liquids are usually incorporated into block copolymer matrices to develop nanostructured materials for electrochemical applications. Generally, ionic liquids preferentially swell one phase to generate an ion conductive path, while the unswollen phase(s) provide mechanical strength. Simone et al. first investigated the lyotropic phase behavior of concentrated block copolymer/ionic liquid solutions based on the system of PB-PEO in two different ionic liquids [EMI][TFSA] and [BMI][PF_6].[114] The lyotropic phase behavior of block copolymers in ionic liquids was found to resemble that of the block copolymers in conventional molecular solvents. In addition to the classical diblock copolymer microstructures including body-centered cubic lattices of spheres, hexagonally packed cylinders and lamellae, coexistence of

lamellae, cylinders and disordered networks were also observed in this system. They also studied the lyotropic phase behavior of PS-PEO in [EMI][TFSA].[115] The ionic conductivity of the block copolymer solutions was found to be dependent on the concentration of ionic liquid as well as the volume fraction of the swollen PEO phase. A handful of other diblock copolymer/ionic liquid systems have been studied for ion and proton conductive materials as well. For instance, Virgili et al. investigated self-assembly behavior and ionic and protic conductivity of poly(styrene-*b*-2-vinylpyridine) in imidazolium bis(trifluoromethylsulfonyl)amide ([Im][TFSA]), a protic ionic liquid.[116] The dependence of the self-assembled morphology on temperature, distribution of ionic liquids in different phases, proton transport mechanism and ionic conductivity were also systematically studied.[117]

1.3.3 Ion gels

The fluid nature of ionic liquids poses potential challenges in practical applications, such as ionic liquid leakage and lack of mechanical strength. To solve this issue while retaining the high ion and mass transport properties from ionic liquids (e.g., ionic conductivity and gas permeability), efforts have made to incorporate a three dimensional network structure into the ionic liquids, which can simultaneously provide mechanical support and mass transport paths.[118–121] Small molecule gelators, macromolecules, colloidal particles and carbon nanotubes have been successfully used to achieve this goal in certain ionic liquids, which results in solid-state materials referred to as ion gels (or ionogels).[122,123] Their superior transport properties as well as tunable mechanical properties have enabled applications in electrochemical devices as well as gas separation

membranes.[124–126] The following discussion will mainly focus on polymeric ion gels, which comprise a few volume percent of polymer network swollen in ionic liquid, as they are directly relevant to this thesis project.

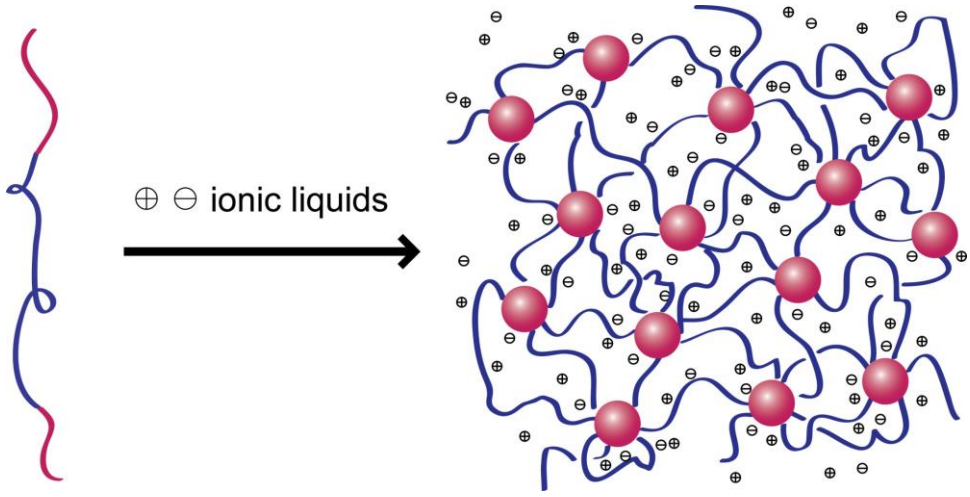

Figure 1.3 Block copolymer ion gels through triblock copolymer self-assembly[132]

Polymeric ion gels can be divided into chemical and physical gels, depending on the nature of cross-linking junctions in the network. Chemical crosslinking can be realized by direct polymerization of vinyl monomers in the ionic liquids in the presence of a crosslinker, or polyaddition reaction of macromers with multifunctional reactive groups.[120] One representative example reported by Watanabe and co-workers involves using *in situ* polymerization of methylmethacylate (MMA) dissolved in [EMI][TFSA] with a small amount of ethylene glycol dimethacrylate as the cross-linker, to prepare transparent, flexible, self-standing ion gels.[118] At the lowest polymer concentration (30 mol% of MMA), the ion gel shows a conductivity of almost 6 mS/cm at room temperature, while the ion gel with the highest polymer concentration (80 mol% MMA)

shows a high modulus on the order of 0.1 GPa. These ion gels have been successfully used in electrochemical devices including actuators and capacitors.[53] Rogers et al. demonstrated that rubbery and transparent ion gels can also be synthesized by crosslinking disuccimidylpropyl poly(ethylene glycol) with four-arm tetraamine PEG crosslinkers in ionic liquids.[120] More recently, epoxy-based and polyurethane-based ion gels have been developed through radical polymerization in ionic liquids.[127,128] These chemical ion gels exhibit enhanced mechanical strength and reasonable ionic conductivities (on the order of 10^{-5} to 10^{-3} mS/cm). However, because the ion gel network is permanently locked by covalent bonds, their structure cannot be tuned once chemical cross-linking reaction is completed.

Physical crosslinking provides an alternative method to achieve gelation in ionic liquids. Weaker interactions such as microphase separation, hydrogen bonding and crystallization are utilized to form network structures of physical ion gels.[83,129–131] Among these methods, block copolymer self-assembly is particularly versatile because the structure and properties of ion gels can be easily tuned through variations of polymer chemical structure, block length and architecture.[132] In 2007, He and Lodge reported the first block copolymer (BCP) ion gel based on an ABA-triblock copolymer with ionic liquid insoluble end-block (A) and soluble mid-block.[133] In the presence of ionic liquids, the insoluble A blocks will self-associate and form crosslinking junctions interconnected by soluble B blocks, as shown in Figure 1.3. For example, through self-assembly of poly(styrene-*b*-ethylene oxide-*b*-styrene) (SOS) in 1-butyl-3-methylimidazolium hexfluorophosphate ([BMI][PF_6]), a physically cross-linked ion gel can be prepared with

addition of as little as 4 wt% polymer, and the ionic conductivity of 5 and 10 wt% gels were only slightly decreased from the neat ionic liquid. The storage modulus (G') for the gels is a few kilopascals. Using these highly conductive ion gels, Lee et al. developed a polymer thin-film transistor with high capacitance and high operational frequency (~1kHz).[126]

Recently, thermoreversible ion gels were further developed by replacing the insoluble PS end-blocks with thermal-sensitive poly(*N*-isopropylacrylamide) (PNIPAm, corresponding triblock denoted as NON) block, which exhibits a UCST phase behavior in the ionic liquid [EMI][TFSA].[119,134] Such ion gels show solid-like behavior at low temperatures and become liquid when the temperature is higher than the gelation temperature (T_{gel}) as the end-block is soluble in ionic liquid. Nevertheless, the 10 wt% NON ion gel is a liquid at ambient temperature because its T_{gel} is only 17 °C, which poses difficulty for potential applications. To increase the T_{gel} above room temperature, insoluble PS blocks were incorporated into the end-blocks to obtain a NSOSN pentablock copolymer.[134] The resulting ion gel shows a sol-gel transition at 48 °C. In another case, SOS ion gels with short PS end-blocks were also found to be thermoreversible due to the low energy barrier for PS chain pullout from the cores.[135] At elevated temperatures, the association strength in the micelle core is weak enough for measurements to access the time scale of reversible chain pullout, thus a liquid-like behavior is observed at high temperatures. In this case, the SOS ion gel essentially forms a viscoelastic solution of congested micelles with PS cores and PEO coronas when the temperature is higher than T_{gel}. The thermoreversibility of ion gel is of particular interest in material processing and

device fabrication as ion gels can be processed in the liquid state and utilized in the solid state. Using these thermoreversible ion gels, transfer printing of patterned ion gel layers using PDMS stamps onto thin-film transistors has been achieved.[136]

1.3.4 Polymerized ionic liquids

Combining polymers and ionic liquids into composite materials has been proved a successful strategy to create various novel functional materials. Interestingly, functionalization of polymers with certain groups of ionic liquids has also been explored as a way of developing a new class of polyelectrolytes named polymerized ionic liquids (PILs).[137] By directly incorporating ionic liquid functionalities into the macromolecular structures, the resulted polymers are expected to possess both the functional properties of ionic liquids and the flexibility and mechanical strength of macromolecules. PILs can be prepared by polymerization of ionic liquid monomers, where a polymerizable group is covalently linked to either the cation or anion moieties of an ionic liquid. A series of PIL systems such as polycation, polyanion, copolymer, polyion complex and poly(zwitterion) have been documented, as shown in Figure 1.4.[138,139] The properties of PILs can be readily tuned by changing the chemical structure of ionic species, introducing flexible monomer, or changing the polymer architecture. [48]

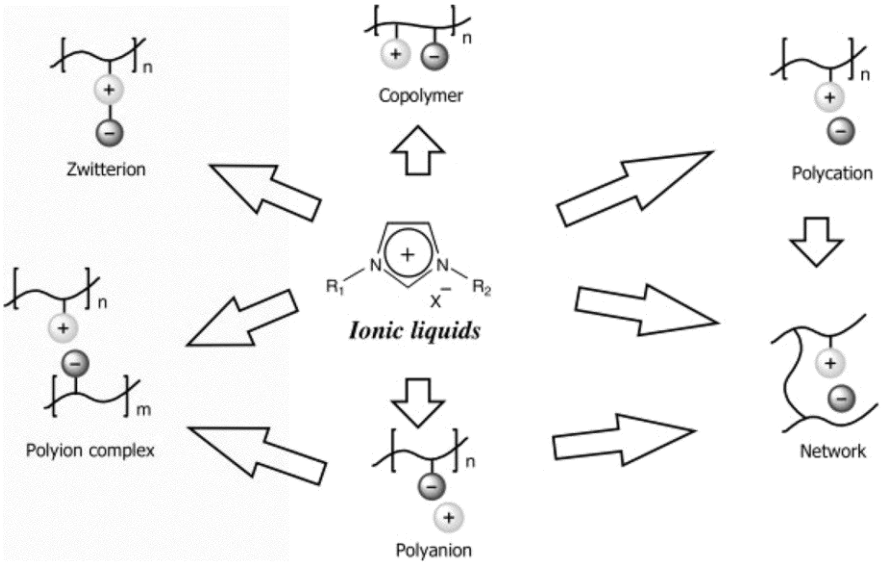

Figure 1.4 Various forms of polymerized ionic liquids

Ohno et al. reported the synthesis of the first polymerized ionic liquid, poly(1-ethyl-3-vinylimidazolium) bis(trifluoromethylsulfonyl)amide, which shows a low T_g of −75.4 °C.[140] Subsequent studies on similar systems have focused on developing PILs as solid state electrolytes that could potentially substitute ionic liquids in electrochemical devices.[141,142] However, due to the elevated glass transition temperature, confined ion mobility and the reduced amount of conductive species after polymerization, the ionic conductivity of a PIL is significantly lower than that of a corresponding neat ionic liquid.[48,143] Apart from electrochemical devices, applications of PILs have also expanded to a variety of areas such as microwave absorption, CO_2 sorption, gas separation, thermoresponsive materials, catalysis and nanoparticle dispersions.[144–147]

Synthetic strategies for PILs can be divided to two categories: (1) direct polymerization of ionic liquid monomers, and (2) chemical modification of existing

polymers to incorporate ionic liquid functionalities.[148] In each strategy, various polymerization techniques have been successfully applied, including radical polymerization, step-growth polymerization and ring opening metathesis polymerization.[149–151] So far, most of the PILs reported are prepared through free radical polymerization of ionic liquid monomers, because of high tolerance of toward impurities, moistures and other active functional groups.[84] In most cases, the ionic liquid monomers for free radical polymerization have a polymerizable unit in the cation: a vinyl, styrenic, acryloyl or methacryloyl functional group.[137] It is also highly desirable to synthesize PILs through controlled polymerization techniques, such as anionic polymerization and controlled radical polymerization, for controlling the PIL molecular weight as well as achieving various polymer architectures. In 2004, Shen et al. first reported polymerization of 2-(1-butylimidazolium)ethylmethacrylate tetrafluoroborate and 1-(4-vinylbenzyl)-3-butyl imidazolium tetrafluoroborate through atom transfer radical polymerization (ATRP).[152,153] Their results revealed that in order to achieve controlled polymerization, reaction conditions such as conversion rate, catalyst/ligand ratio, solvent polarity as well as polymerization temperature should be well adapted to the ionic liquid monomer reactivity. The lowest dispersity values achieved, however, were 1.38 and 1.24 for the above mentioned two monomers, respectively, which are higher than what ATRP can achieve for most common monomers.

The synthesis of block copolymers containing at least one PIL block has attracted considerable attention in the past few years. Almost simultaneously, several groups reported the successful synthesis of PIL block copolymers using different polymerization

techniques. For instance, Texter et al. used ATRP to synthesize a symmetric ABA-triblock copolymer with two PIL endblocks from a difunctional poly(propylene oxide) macroinitiator.[84,154] Elabd and coworkers prepared a diblock copolymer through sequential RAFT polymerization of MMA and a methacryloyl-based ionic liquid monomer.[155,156] Moreover, nitroxide mediated polymerization (NMP) and ring opening metathesis polymerization (ROMP) among several other techniques have been employed to prepare for PIL-containing block copolymer or the precursors for PILs.[150] Waymouth and coworkers made use of NMP to syntheisze a diblock copolymer polystyrene-*b*-poly(4-vinylbenzyl chloride) (PS-PVBC) and the ionic liquid functionalities are introduced as a side group through reaction of 1-methylimidazole with the vinylbenzyl chloride repeating units.[157] Additionally, surface initiated ATRP and NMP have also been used to synthesize PIL from a substrate.[158]

CO_2 separation and absorption using PILs is of particular interest for this thesis project. Pure ionic liquids exhibit several important properties that make them potentially useful in this application, including negligible vapor pressure, high gas uptake and reversible absorption-desorption of CO_2. In 2005, Shen et al. first reported that PILs exhibit even higher CO_2 absorption than the corresponding ionic liquid monomers.[144,159] Since 2006, Gin and Noble et al. have reported extensively on the gas absorption and separation behavior of PIL-based materials.[82,160–163] They discovered that PILs based on tetraalkylammonium cations and [BF_4] anion generally show higher CO_2 absorption than commonly used imidazolium-based PILs with [PF_6] and [TFSA], although the underlying absorption mechanism is still unclear for CO_2. More recently, the gas separation

performance of PIL membranes for gases such as CO_2, N_2, CH_4, H_2, C_3H_6 as well as C_3H_4 are also under investigation.[82] These studies showed promising results for CO_2 related separation because PIL membranes generally have high selectivity for CO_2, which is similar to pure ionic liquids. The introduction of cross-linkable ionic liquid monomers and the development of PIL/ionic liquid composite membranes can significantly improve the permeability due to the higher gas diffusion rate in ionic liquids.[161] Recently, Simons et al. found that PILs with pendant imidazolium cations may effectively resist membrane plasticization due to the reversible swelling of the polymer by CO_2, which is similar to the reversible CO_2 sorption in ionic liquids.[164] Although the research in this area has shown very promising results for using PILs for CO_2 uptake or separation, more fundamental and extensive research is needed for a systematic understanding of the structure-property relationships in PIL for gas permeation and absorption properties.

1.4 Research Motivation and Overview

The motivation for this thesis project was grounded in the previous success of block copolymer ion gels and the need to develop ionic liquid materials for CO_2 separation. As mentioned in Section 1.2.1, membrane separation of CO_2 using ionic liquids has been demonstrated through supported ionic liquid membranes (SILMs). However, the poor stability of SILMs limits their applications beyond the laboratory. The displacement of liquids will happen with sufficient trans-membrane pressure difference. Hence, it is desirable to impart a solid-state structure to the ionic liquids to improve the membrane stability. Block copolymer ion gels present a unique system combining the properties of

ionic liquids and the mechanical strength of macromolecules. More importantly, our previous studies showed that the ionic conductivity of 10 wt% ion gels are very close to the pure ionic liquids, indicating that the self-assembled polymer networks have minimal influences on mass transport. Therefore, this thesis project focuses on the development of block copolymer ion gels as novel CO_2 gas separation media.

The rest of the chapters are organized as follows: Chapter 2 introduces the synthesis and gas separation studies of ABA triblock copolymer ion gels with polymerized ionic liquid (PIL) mid-blocks. Inspired by the enhanced gas separation performance of cross-linked PIL composite membranes, we incorporated an acrylate-based PIL mid-block into the ion gels to improve gas separation efficiency. The synthetic strategy, ion gel membrane preparation and the rheological properties are discussed in detail. The overall results from this project show that ion gel shows a very high gas permeability which is close to the pure ionic liquids. Moreover, the PIL mid-block has improved the selectivity for both CO_2/CH_4 and CO_2/N_2 gas pairs.

The research described in Chapter 3 involves using ion gels with more commonly used polymers as mid-blocks, poly(ethylene oxide) (PEO) and poly(methyl methacrylate) (PMMA). Therefore, the polymers are much easier to synthesize. Due to the high ionic liquid fractions, these ion gels also exhibit rapid gas transport as well as high selectivity. The selectivity is also influenced by the choice of mid-block: PEO-based ion gels shows higher selectivity than PMMA-based ion gels and pure ionic liquids. Gas solubility tests on ionic liquid and polymer solutions indicate that PEO can suppress the solubility of N_2 and CH_4, and thereby enhancing the separation performance.

Chapter 4 describes a novel strategy to enhance the mechanical properties of ion gels without affecting their mass transport properties. In this study, cross-linkable azide functionalities were introduced into the PS end-blocks of a model block copolymer ion gel. The azide groups can be chemically cross-linked by either UV-irradiation or heating. Thus a physical network can first form in the ionic liquid via block copolymer self-assembly, where the micelle cores can be further cross-linked through the reaction of azide groups. This is the first time both chemical cross-linking and physical cross-linking are combined in the same block copolymer ion gel. The mechanical properties, mass transport rates as well as the self-assembled microstructure of ion gels were investigated. It was discovered that the plateau modulus, morphology and gas permeability remain the same, whereas the toughness is increased by over 700%. By marrying the enhanced mechanical strength of a chemical gel with the processability of a physical gel, a novel type of ion gel with high toughness and high mass transport rate is developed.

Chapter 5 provides a summary of the whole project and an outlook on the future work in CO_2 separation using ion gels. Additionally, initial efforts on UV-induced cross-linking of the ion gels and the small angle neutron scattering investigation of homopolymer conformation in ionic liquids were also described in the Appendices.

1.5 References

(1) Baker, R. W.; Lokhandwala, K. *Ind. Eng. Chem. Res.* **2008**, *47*, 2109–2121.

(2) Robeson, L. M. *J. Membr. Sci.* **2008**, *320*, 390–400.

(3) Robeson, L. M. *J. Membr. Sci.* **1991**, *62*, 165–185.

(4) Yampolskii, Y. *Macromolecules* **2012**, *45*, 3298–3311.

(5) Stern, S. A. *J. Membr. Sci.* **1994**, *94*, 1–65.

(6) *Membrane Separations Technology: Principles and Applications*; Noble, R. D.; Stern, S. A., Eds.; 2nd Ed.; Elsevier, 1995; p. 718 pp.

(7) Koros, W. J.; Fleming, G. K. *J. Membr. Sci.* **1993**, *83*, 1–80.

(8) Wind, J. D.; Paul, D. R.; Koros, W. J. *J. Membr. Sci.* **2004**, *228*, 227–236.

(9) Koros, W. J.; Fleming, G. K.; Jordan, S. M.; Kim, T. H.; Hoehn, H. H. *Prog. Polym. Sci.* **1988**, *13*, 339–401.

(10) Wind, J. D.; Staudt-Bickel, C.; Paul, D. R.; Koros, W. J. *Ind. Eng. Chem. Res.* **2002**, *41*, 6139–6148.

(11) Visser, T.; Koops, G. H.; Wessling, M. *J. Membr. Sci.* **2005**, *252*, 265–277.

(12) Freeman, B. D. *Macromolecules* **1999**, *32*, 375–380.

(13) Chu, S. *Science* **2009**, *325*, 1599.

(14) Balat, H.; Oz, C. *Energy Exploration & Exploitation* **2007**, *25*, 357–392.

(15) Luby, P.; Susta, M. R. *Power* **2007**, *151*, 40,42,44–48,50.

(16) Schrag, D. P. *Science* **2007**, *315*, 812–813.

(17) Babcock, R. E.; Spillman, R. W.; Goddin, C. S.; Cooley, T. E. *Energy Progress* **1988**, *8*, 135–142.

(18) Rochelle, G. T. *Science* **2009**, *325*, 1652–1654.

(19) Hammond, G. P.; Akwe, S. S. O. *Int. J. Energ. Res.* **2007**, *31*, 1180–1201.

(20) Freeman, B. D.; Pinnau, I. *ACS Symp. Ser.* **1999**, *733*, 1–27.

(21) Pinnau, I.; Toy, L. G. *J. Membr. Sci.* **1996**, *109*, 125–133.

(22) Belov, N. A.; Zharov, A. A.; Shashkin, A. V; Shaikh, M. Q.; Raetzke, K.; Yampolskii, Y. P. *J. Membr. Sci.* **2011**, *383*, 70–77.

(23) Alentiev, A. Y.; Yampolskii, Y. P.; Shantarovich, V. P.; Nemser, S. M.; Plate, N. A. *J. Membr. Sci.* **1997**, *126*, 123–132.

(24) Costello, L. M.; Koros, W. J. *J. Polym. Sci., Part B: Polym. Phys.* **1995**, *33*, 135–146.

(25) Tanaka, K.; Okano, M.; Toshino, H.; Kita, H.; Okamoto, K. *J. Polym. Sci., Part B: Polym. Phys.* **1992**, *30*, 907–914.

(26) Budd, P. M.; Msayib, K. J.; Tattershall, C. E.; Ghanem, B. S.; Reynolds, K. J.; McKeown, N. B.; Fritsch, D. *J. Membr. Sci.* **2005**, *251*, 263–269.

(27) McKeown, N. B.; Budd, P. M.; Msayib, K. J.; Ghanem, B. S.; Kingston, H. J.; Tattershall, C. E.; Makhseed, S.; Reynolds, K. J.; Fritsch, D. *Chem.Eur. J.* **2005**, *11*, 2610–2620.

(28) Budd, P. M.; McKeown, N. B.; Ghanem, B. S.; Msayib, K. J.; Fritsch, D.; Starannikova, L.; Belov, N.; Sanfirova, O.; Yampolskii, Y.; Shantarovich, V. *J. Membr. Sci.* **2008**, *325*, 851–860.

(29) Ghanem, B. S.; McKeown, N. B.; Budd, P. M.; Al-Harbi, N. M.; Fritsch, D.; Heinrich, K.; Starannikova, L.; Tokarev, A.; Yampolskii, Y. *Macromolecules* **2009**, *42*, 7881–7888.

(30) Golemme, G.; Jansen, J. C.; Muoio, D.; Bruno, A.; Manes, R.; Buonomenna, M. G.; Choi, J.; Tsapatsis, M. In *Membr. Gas Sep.*; John Wiley & Sons Ltd., 2010; pp. 113–124.

(31) Sen, D.; Kalipcilar, H.; Yilmaz, L. *J. Membr. Sci.* **2007**, *303*, 194–203.

(32) Ahn, J.; Chung, W.-J.; Pinnau, I.; Guiver, M. D. *J. Membr. Sci.* **2008**, *314*, 123–133.

(33) Ahn, J.; Chung, W.-J.; Pinnau, I.; Song, J.; Du, N.; Robertson, G. P.; Guiver, M. D. *J. Membr. Sci.* **2010**, *346*, 280–287.

(34) Yang, T.; Xiao, Y.; Chung, T.-S. *Energy & Environmental Science* **2011**, *4*, 4171–4180.

(35) Walden, P. *Bull. Sci. Acad. Imp. Sci. St. Petersb.* **1914**, 405–422.

(36) Wilkes, J. S.; Levisky, J. A.; Wilson, R. A.; Hussey, C. L. *Inorg. Chem.* **1982**, *21*, 1263–1264.

(37) Galinski, M.; Lewandowski, A.; Stepniak, I. *Electrochim. Acta* **2006**, *51*, 5567–5580.

(38) Wasserscheid, P.; Welton, T.; Editors. *Ionic Liquids in Synthesis.*; Wiley-VCH Verlag GmbH & Co. KGaA, 2003; p. 364 pp.

(39) Welton, T. *Chem. Rev.* **1999**, *99*, 2071–2084.

(40) Bonhote, P.; Dias, A.-P.; Papageorgiou, N.; Kalyanasundaram, K.; Graetzel, M. *Inorg. Chem.* **1996**, *35*, 1168–1178.

(41) Fuller, J.; Carlin, R. T.; De Hugh C., L.; Haworth, D. *J. Chem. Soc., Chem. Commun.* **1994**, 299–300.

(42) Wilkes, J. S.; Zaworotko, M. J. *J. Chem. Soc., Chem. Commun.* **1992**, 965–967.

(43) Krossing, I.; Slattery, J. M.; Daguenet, C.; Dyson, P. J.; Oleinikova, A.; Weingärtner, H. *J. Am. Chem. Soc.* **2006**, *128*, 13427–13434.

(44) Wilkes, J. S. *Green Chem.* **2002**, *4*, 73–80.

(45) Castner, E. W.; Wishart, J. F.; Shirota, H. *Acc. Chem. Res.* **2007**, *40*, 1217–1227.

(46) Swatloski, R. P.; Spear, S. K.; Holbrey, J. D.; Rogers, R. D. *J. Am. Chem. Soc.* **2002**, *124*, 4974–4975.

(47) Hagiwara, R.; Matsumoto, K.; Nakamori, Y.; Tsuda, T.; Ito, Y.; Matsumoto, H.; Momota, K. *J. Electrochem. Soc.* **2003**, *150*, 195–199.

(48) Armand, M.; Endres, F.; MacFarlane, D. R.; Ohno, H.; Scrosati, B. *Nat. Mater.* **2009**, *8*, 621–9.

(49) Kawano, R.; Matsui, H.; Matsuyama, C.; Sato, A.; Susan, M. A. B. H.; Tanabe, N.; Watanabe, M. *J. Photochem. Photobiol., A* **2004**, *164*, 87–92.

(50) Brennecke, J. F.; Gurkan, B. E. *J. Phys. Chem. Lett.* **2010**, *1*, 3459–3464.

(51) Tang, J.; Radosz, M.; Shen, Y. *Macromolecules* **2008**, *41*, 493–496.

(52) Tokuda, H.; Hayamizu, K.; Ishii, K.; Susan, M. A. B. H.; Watanabe, M. *J. Phys. Chem. B* **2004**, *108*, 16593–16600.

(53) Seki, S.; Susan, M. A. B. H.; Kaneko, T.; Tokuda, H.; Noda, A.; Watanabe, M. *J. Phys. Chem. B* **2005**, *109*, 3886–3892.

(54) Tokuda, H.; Ishii, K.; Susan, M. A. B. H.; Tsuzuki, S.; Hayamizu, K.; Watanabe, M. *J. Phys. Chem. B* **2006**, *110*, 2833–2839.

(55) Tokuda, H.; Hayamizu, K.; Ishii, K.; Susan, M. A. B. H.; Watanabe, M. *J. Phys. Chem. B* **2005**, *109*, 6103–6110.

(56) Visser, A. E.; Swatloski, R. P.; Reichert, W. M.; Davis Jr., J. H.; Rogers, R. D.; Mayton, R.; Sheff, S.; Wierzbicki, A. *Chem. Commun.* **2001**, 135–136.

(57) Schuber, T. *Ionic Liquids Today* **2007**, *6*, 2–7.

(58) Pham, T. P. T.; Cho, C.-W.; Yun, Y.-S. *Water Res.* **2010**, *44*, 352–72.

(59) Swatloski, R. P.; Holbrey, J. D.; Rogers, R. D. *Green Chem.* **2003**, *5*, 361–363.

(60) Lin, H.; Freeman, B. D. *J. Mol. Struct.* **2005**, *739*, 57–74.

(61) Cussler, E. L. *J. Membr. Sci.* **1989**, *43*, 149–164.

(62) *Liquid Membranes: Theory and Applications.*; Noble, R. D.; Way, J. D., Eds.; ACS Sympos.; American Chemical Society: Washington DC, 1987; p. 196 pp.

(63) Blancard, L. A.; Hancu, D.; Beckman, E. J.; Brennecke, J. F. *Nature* **1999**, *399*, 28–29.

(64) Anthony, J. L.; Aki, S. N. V. K.; Maginn, E. J.; Brennecke, J. F. *Int. J. Environ. Tech. Manage.* **2004**, *4*, 105–115.

(65) Anderson, J. L.; Dixon, J. K.; Brennecke, J. F. *Acc. Chem. Res.* **2007**, *40*, 1208–1216.

(66) Muldoon, M. J.; Aki, S. N. V. K.; Anderson, J. L.; Dixon, J. K.; Brennecke, J. F. *J. Phys. Chem. B* **2007**, *111*, 9001–9009.

(67) Hert, D. G.; Anderson, J. L.; Aki, S. N. V. K.; Brennecke, J. F. *Chem. Commun.* **2005**, 2603–2605.

(68) Anthony, J. L.; Anderson, J. L.; Maginn, E. J.; Brennecke, J. F. *J. Phys. Chem. B* **2005**, *109*, 6366–6374.

(69) Cadena, C.; Anthony, J. L.; Shah, J. K.; Morrow, T. I.; Brennecke, J. F.; Maginn, E. J. *J. Am. Chem. Soc.* **2004**, *126*, 5300–5308.

(70) Bara, J. E.; Carlisle, T. K.; Gabriel, C. J.; Camper, D.; Finotello, A.; Gin, D. L.; Noble, R. D. *Ind. Eng. Chem. Res.* **2009**, *48*, 2739–2751.

(71) Carlisle, T. K.; Bara, J. E.; Gabriel, C. J.; Noble, R. D.; Gin, D. L. *Ind. Eng. Chem. Res.* **2008**, *47*, 7005–7012.

(72) Bara, J. E.; Gabriel, C. J.; Lessmann, S.; Carlisle, T. K.; Finotello, A.; Gin, D. L.; Noble, R. D. *Ind. Eng. Chem. Res.* **2007**, *46*, 5380–5386.

(73) Camper, D.; Bara, J. E.; Gin, D. L.; Noble, R. D. *Ind. Eng. Chem. Res.* **2008**, *47*, 8496–8498.

(74) Camper, D.; Bara, J. E.; Koval, C.; Noble, R. D. *Ind. Eng. Chem. Res.* **2006**, *45*, 6279–6283.

(75) Myers, C.; Pennline, H.; Luebke, D.; Ilconich, J.; Dixon, J. K.; Maginn, E. J.; Brennecke, J. F. *J. Membr. Sci.* **2008**, *322*, 28–31.

(76) Bates, E. D.; Mayton, R. D.; Ntai, I.; Davis Jr., J. H. *J. Am. Chem. Soc.* **2002**, *124*, 926–927.

(77) Jessop, P. G.; Heldebrant, D. J.; Li, X.; Eckert, C. A.; Liotta, C. L. *Nature* **2005**, *436*, 1102.

(78) Lozano, L. J.; Godinez, C.; De A. P., los R.; Hernandez-Fernandez, F. J.; Sanchez-Segado, S.; Alguacil, F. J. *J. Membr. Sci.* **2011**, *376*, 1–14.

(79) Scovazzo, P.; Kieft, J.; Finan, D. A.; Koval, C.; Dubois, D.; Noble, R. D. *J. Membr. Sci.* **2004**, *238*, 57–63.

(80) Scovazzo, P. *J. Membr. Sci.* **2009**, *343*, 199–211.

(81) Scovazzo, P.; Havard, D.; McShea, M.; Mixon, S.; Morgan, D. *J. Membr. Sci.* **2009**, *327*, 41–48.

(82) Bara, J. E.; Hatakeyama, E. S.; Gabriel, C. J.; Zeng, X.; Lessmann, S.; Gin, D. L.; Noble, R. D. *J. Membr. Sci.* **2008**, *316*, 186–191.

(83) Jansen, J. C.; Friess, K.; Clarizia, G.; Schauer, J.; Izak, P. *Macromolecules* **2011**, *44*, 39–45.

(84) Lu, J.; Yan, F.; Texter, J. *Prog. Polym. Sci.* **2009**, *34*, 431–448.

(85) MacFarlane, D. R.; Forsyth, M.; Howlett, P. C.; Pringle, J. M.; Sun, J.; Annat, G.; Neil, W.; Izgorodina, E. I. *Acc. Chem. Res.* **2007**, *40*, 1165–1173.

(86) Bates, F. S.; Fredrickson, G. H. *Physics Today* **1999**, 32–38.

(87) Hiemenz, P. C.; Lodge, T. P. *Polymer Chemistry*; 2nd ed.; CRC Press: New York, 2007.

(88) Snedden, P.; Cooper, A. I.; Scott, K.; Winterton, N. *Macromolecules* **2003**, *36*, 4549–4556.

(89) Winterton, N. *J. Mater. Chem.* **2006**, *16*, 4281–4293.

(90) Ueki, T.; Watanabe, M. *Macromolecules* **2008**, *41*, 3739–3749.

(91) Ueki, T.; Watanabe, M. *Chem. Lett.* **2006**, *35*, 964–965.

(92) Ueki, T.; Karino, T.; Kobayashi, Y.; Shibayama, M.; Watanabe, M. *J. Phys. Chem. B* **2007**, *111*, 4750–4754.

(93) Lee, H.-N.; Lodge, T. P. *J. Phys. Chem. Lett.* **2010**, *1*, 1962–1966.

(94) Lee, H.-N.; Newell, N.; Bai, Z.; Lodge, T. P. *Macromolecules* **2012**, *45*, 3627–3633.

(95) Ueki, T.; Watanabe, M. *Langmuir* **2007**, *23*, 988–990.

(96) Wang, H.; Gurau, G.; Rogers, R. D. *Chem. Soc. Rev.* **2012**, *41*, 1519–37.

(97) Remsing, R. C.; Swatloski, R. P.; Rogers, R. D.; Moyna, G. *Chem. Commun.* **2006**, 1271–1273.

(98) Qin, Y.; Lu, X.; Sun, N.; Rogers, R. D. *Green Chem.* **2010**, *12*, 968–971.

(99) Sun, N.; Rodriguez, H.; Rahman, M.; Rogers, R. D. *Chem. Commun.* **2011**, *47*, 1405–1421.

(100) Lan, W.; Liu, C.-F.; Yue, F.-X.; Sun, R.-C.; Kennedy, J. F. *Carbohydr. Polym.* **2011**, *86*, 672–677.

(101) Liu, Z.; Wang, H.; Li, Z.; Lu, X.; Zhang, X.; Zhang, S.; Zhou, K. *Mater. Chem. Phys.* **2011**, *128*, 220–227.

(102) Muhammad, N.; Man, Z.; Khalil, M. A. B.; Elsheikh, Y. A. *J. Appl. Sci.* **2010**, *10*, 1090–1096.

(103) Li, W.; Sun, N.; Stoner, B.; Jiang, X.; Lu, X.; Rogers, R. D. *Green Chem.* **2011**, *13*, 2038–2047.

(104) He, Y.; Li, Z.; Simone, P.; Lodge, T. P. *J. Am. Chem. Soc.* **2006**, *128*, 2745–2750.

(105) Meli, L.; Santiago, J. M.; Lodge, T. P. *Macromolecules* **2010**, *43*, 2018–2027.

(106) Meli, L.; Lodge, T. P. *Macromolecules* **2009**, *42*, 580–583.

(107) Ueki, T.; Watanabe, M.; Lodge, T. P. *Macromolecules* **2009**, *42*, 1315–1320.

(108) Lee, H.-N.; Bai, Z.; Newell, N.; Lodge, T. P. *Macromolecules* **2010**, *43*, 9522–9528.

(109) He, Y.; Lodge, T. P. *J. Am. Chem. Soc.* **2006**, *128*, 12666–12667.

(110) Bai, Z.; He, Y.; Lodge, T. P. *Langmuir* **2008**, *24*, 5284–5290.

(111) Bai, Z.; He, Y.; Young, N. P.; Lodge, T. P. *Macromolecules* **2008**, *41*, 6615–6617.

(112) Bai, Z.; Lodge, T. P. *J. Am. Chem. Soc.* **2010**, *132*, 16265–16270.

(113) Bai, Z.; Zhao, B.; Lodge, T. P. *J. Phys. Chem. B* **2012**, *116*, 8282–8289.

(114) Simone, P. M.; Lodge, T. P. *Macromolecules* **2008**, *41*, 1753–1759.

(115) Simone, P. M.; Lodge, T. P. *ACS Appl. Mater. Interfaces* **2009**, *1*, 2812–20.

(116) Virgili, J. M.; Nedoma, A. J.; Segalman, R. A.; Balsara, N. P. *Macromolecules* **2010**, *43*, 3750–3756.

(117) Hoarfrost, M. L.; Segalman, R. A. *Macromolecules* **2011**, *44*, 5281–5288.

(118) Susan, M. A. B. H.; Kaneko, T.; Noda, A.; Watanabe, M. *J. Am. Chem. Soc.* **2005**, *127*, 4976–4983.

(119) He, Y.; Lodge, T. P. *Chem. Commun.* **2007**, 2732–2734.

(120) Klingshirn, M. A.; Spear, S. K.; Subramanian, R.; Holbrey, J. D.; Huddleston, J. G.; Rogers, R. D. *Chem. Mater.* **2004**, *16*, 3091–3097.

(121) Neouze, M.-A.; Le Bideau, J.; Gaveau, P.; Bellayer, S.; Vioux, A. *Chem. Mater.* **2006**, *18*, 3931–3936.

(122) Katakabe, T.; Kaneko, T.; Watanabe, M.; Fukushima, T.; Aida, T. *J. Electrochem. Soc.* **2005**, *152*, A1913–A1916.

(123) Lee, J.; Aida, T. *Chem. Commun.* **2011**, *47*, 6757–62.

(124) Voss, B. A.; Bara, J. E.; Gin, D. L.; Noble, R. D. *Chem. Mater.* **2009**, *21*, 3027–3029.

(125) Cho, J. H.; Lee, J.; He, Y.; Kim, B. S.; Lodge, T. P.; Frisbie, C. D. *Adv. Mater.* **2008**, *20*, 686–690.

(126) Lee, J.; Panzer, M. J.; He, Y.; Lodge, T. P.; Frisbie, C. D. *J. Am. Chem. Soc.* **2007**, *129*, 4532–4533.

(127) Matsumoto, K.; Endo, T. *Macromolecules* **2009**, *42*, 4580–4584.

(128) Matsumoto, K.; Endo, T. *Macromolecules* **2008**, *41*, 6981–6986.

(129) Noro, A.; Matsushita, Y.; Lodge, T. P. *Macromolecules* **2008**, *41*, 5839–5844.

(130) Noro, A.; Matsushita, Y.; Lodge, T. P. *Macromolecules* **2009**, *42*, 5802–5810.

(131) Harner, J. M.; Hoagland, D. A. *J. Phys. Chem. B* **2010**, *114*, 3411–8.

(132) Lodge, T. P. *Science* **2008**, *321*, 50–51.

(133) He, Y.; Boswell, P. G.; Bühlmann, P.; Lodge, T. P.; Buehlmann, P. *J. Phys. Chem. B* **2007**, *111*, 4645–52.

(134) He, Y.; Lodge, T. P. *Macromolecules* **2008**, *41*, 167–174.

(135) Zhang, S.; Lee, K. H.; Sun, J.; Frisbie, C. D.; Lodge, T. P. *Macromolecules* **2011**, *44*, 8981–8989.

(136) Lee, K. H.; Zhang, S.; Gu, Y.; Lodge, T. P.; Frisbie, C. D. *Manuscript Submitted*.

(137) Yuan, J.; Antonietti, M. *Polymer* **2011**, *52*, 1469–1482.

(138) Ohno, H. *Macromol. Symp.* **2007**, *249-250*, 551–556.

(139) Ohno, H.; Yoshizawa, M.; Ogihara, W. *Electrochim. Acta* **2004**, *50*, 255–261.

(140) Ohno, H.; Ito, K. *Chem. Lett.* **1998**, 751–752.

(141) Yoshizawa, M.; Hirao, M.; Ito-Akita, K.; Ohno, H. *J. Mater. Chem.* **2001**, *11*, 1057–1062.

(142) Washiro, S.; Yoshizawa, M.; Nakajima, H.; Ohno, H. *Polymer* **2004**, *45*, 1577–1582.

(143) Nakajima, H.; Ohno, H. *Polymer* **2005**, *46*, 11499–11504.

(144) Tang, J.; Tang, H.; Sun, W.; Plancher, H.; Radosz, M.; Shen, Y. *Chem. Commun.* **2005**, 3325–3327.

(145) Hu, X.; Tang, J.; Blasig, A.; Shen, Y.; Radosz, M. *J. Membr. Sci.* **2006**, *281*, 130–138.

(146) Cong, H.; Radosz, M.; Towler, B. F.; Shen, Y. *Sep. Purif. Technol.* **2007**, *55*, 281–291.

(147) Tang, J.; Shen, Y.; Radosz, M.; Sun, W. *Ind. Eng. Chem. Res.* **2009**, *48*, 9113–9118.

(148) Green, M. D.; Long, T. E. *Polym. Rev.* **2009**, *49*, 291–314.

(149) Marcilla, R.; Mecerreyes, D.; Winroth, G.; Brovelli, S.; Rodriguez Maria del Mar, Y.; Cacialli, F. *Appl. Phys. Lett.* **2010**, *96*, 043308/1–043308/3.

(150) Yuan, J.; Mecerreyes, D.; Antonietti, M. *Prog. Polym. Sci.* ASAP.

(151) Mecerreyes, D. *Prog. Polym. Sci.* **2011**, *36*, 1629–1648.

(152) Ding, S.; Tang, H.; Radosz, M.; Shen, Y. *J. Polym. Sci., Part A: Polym. Chem.* **2004**, *42*, 5794–5801.

(153) Tang, H.; Tang, J.; Ding, S.; Radosz, M.; Shen, Y. *J. Polym. Sci., Part A: Polym. Chem.* **2005**, *43*, 1432–1443.

(154) Yan, F.; Texter, J. *Angew. Chem., Int. Ed.* **2007**, *46*, 2440–2443.

(155) Chen, H.; Choi, J.-H.; Cruz, D. S.; Winey, K. I.; Elabd, Y. A. *Macromolecules* **2009**, *42*, 4809–4816.

(156) Chen, H.; Elabd, Y. A. *Macromolecules* **2009**, *42*, 3368–3373.

(157) Stancik, C. M.; Lavoie, A. R.; Achurra, P. A.; Waymouth, R. M.; Gast, A. P. *Langmuir* **2004**, *20*, 8975–87.

(158) He, X.; Yang, W.; Pei, X. *Macromolecules* **2008**, *41*, 4615–4621.

(159) Tang, J.; Tang, H.; Sun, W.; Radosz, M.; Shen, Y. *J. Polym. Sci., Part A: Polym. Chem.* **2005**, *43*, 5477–5489.

(160) Bara, J. E.; Lessmann, S.; Gabriel, C. J.; Hatakeyama, E. S.; Noble, R. D.; Gin, D. L. *Ind. Eng. Chem. Res.* **2007**, *46*, 5397–5404.

(161) Bara, J. E.; Hatakeyama, E. S.; Gin, D. L.; Noble, R. D. *Polym. Adv. Technol.* **2008**, *19*, 1415–1420.

(162) Bara, J. E.; Noble, R. D.; Gin, D. L. *Ind. Eng. Chem. Res.* **2009**, *48*, 4607–4610.

(163) Bara, J. E.; Gabriel, C. J.; Hatakeyama, E. S.; Carlisle, T. K.; Lessmann, S.; Noble, R. D.; Gin, D. L. *J. Membr. Sci.* **2008**, *321*, 3–7.

(164) Simons, K.; Nijmeijer, K.; Bara, J. E.; Noble, R. D.; Wessling, M. *J. Membr. Sci.* **2010**, *360*, 202–209.

Chapter 2

Triblock Copolymer Ion Gels Based on Polymerized Ionic Liquids*

2.1 Introduction

Ionic liquids have exhibited great potential as gas separation media, largely due to their selective CO_2 solubility over other gases.[1–8] However, the fluid nature of ionic liquids prevent their direct use in membranes. As mentioned in Chapter 1, the pioneering work by Bara et al. focused on using cross-linked polymerized ionic liquid (PIL) membranes for CO_2-selective gas absorption and separation.[9–13] They have demonstrated that the separation performance can be tuned by modifying the polymer backbone, anion structure and incorporation of "free" ionic liquids. However, because most of the ionic liquids, if not all, are tethered to the polymer backbone, the mobility of the gas molecules in the PIL membranes is restricted, and therefore the gas permeability is relatively low. Previous research from the Lodge group showed that block copolymer ion gels containing moderate amount of triblock copolymer (5 – 20 wt%) exhibit high ionic conductivity close to the neat ionic liquid, indicating that the self-assembled polymeric network has minimal effect on mass transport.[14,15] In light of the advanced properties of

* Reproduced in part with permission from Gu. Y.; Lodge, T. P. *Macromolecules* **2011**, *44*, 1732–1736. Copyright 2012 American Chemical Society.

these two classes of materials, it is of great interest to combine PIL with ion gels for gas separation applications.

The work described in this chapter demonstrates the development of block copolymer ion gels based on polymerized ionic liquids, with special focus on their gas separation properties. The ion gel investigated here comprises [EMI][TFSA], a low-viscosity ionic liquid, and poly(styrene-*b*-1-[(2-acryloyloxy)ethyl]-3-butylimidazolium bis(trifluoro-methylsulfonyl)amide-*b*-styrene) (Scheme 2.2, denoted as SILS), an ABA triblock copolymer with a PIL mid-block.[16] The choice of this system was motivated by the following reasons. First, [EMI][TFSA] is a widely used ionic liquid in various applications. Both the physicochemical properties and the gas permeation properties of [EMI][TFSA] have been extensively studied.[8,17] Its low viscosity could also facilitate the diffusion of gas molecules through the ion gel membranes.[18] The acrylate-based PIL mid-block was chosen because of its relatively low glass transition temperature (ca. –9 °C), and its compatibility with [EMI][TFSA]. Moreover, previous studies on cross-linked PIL membranes have also shown that acrylate-based PILs have a better selectivity for CO_2 than the neat [EMI][TFSA].[9] Polystyrene was used as the end-block because of its incompatibility with [EMI][TFSA], so that the end-blocks can self-assemble to form physically cross-linked cores in the ionic liquid.

This chapter is organized as follows: we first describe the synthetic efforts to obtain a SILS triblock copolymer via a two-step sequential RAFT polymerization followed by two steps of post-polymerization reactions. The thermoreversible gelation behavior of SILS triblock copolymer in [EMI][TFSA] were investigated using rheological

measurements. The key research of this chapter was the gas separation studies on supported ion gel membranes. The procedure of preparing the gas separation membranes and performing gas permeation experiments is described. Then, the gas separation performance of the ion gel membranes are discussed and compared with the well-known Robeson plots.[19,20]

2.2 Experimental methods

Chemical and materials

All materials and chemical reagents were used as received unless otherwise noted. Styrene was purchased from Sigma-Aldrich and purified by filtration through an alumina column before use. 2,2'-Azobisisobutyronitrile (AIBN) was purified by recrystallization from methanol 3 times. Acryloyl chloride, 2-bromoethanol and 1-butylimidazole were also purchased from Sigma-Aldrich. Lithium bis(trifluoromethylsulfonyl)amide was purchased from 3M and 1-ethyl-3-methylimidazolium bromine ([EMI][Br]) was purchased from IoLiTec Inc. Poly(vinylidene fluoride) (PVDF) membranes (HVHP04700) were purchased from Millipore. CH_4, N_2 and CO_2 gas cylinders used in this study were all purchased from Minneapolis Oxygen Corporation. A polystyrene homopolymer (4kDa, PolyScience Inc.) was used as a reference material in DSC measurements.

Ionic liquid [EMI][TFSA] was synthesized via anion exchange reaction following a previous report.[21,22] Equal moles of [EMI][Br] (76.8 g, 0.402 mol) and LiTFSA (115.3 g, 0.402 mol) were mixed with 200 mL of water in a 1-liter round bottom flask. The

reaction mixture was stirred vigorously at 70 ℃ for 24 hours. The product, a hydrophobic ionic liquid, phase separated from the aqueous reaction mixture, and was collected using a separation funnel. Then, the ionic liquid was diluted with ca. 200 mL dichloromethane and washed 4 times with distilled water. The organic phase was passed through an alumina column to remove the yellowish color of the product. Most of the solvent was removed in a rotary evaporator and the residual amount of solvent was removed in a vacuum oven at 70 ℃ for 48 hours. The final product obtained was a slightly viscous, colorless liquid, with a total yield of 73%. ^{1}H-NMR spectrum compares well with that previously reported (Figure 2.1).

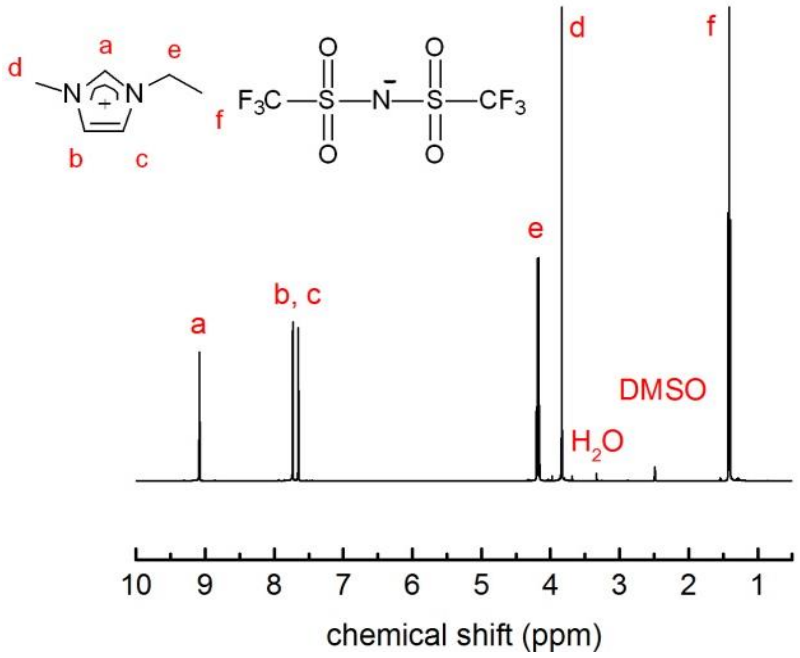

Figure 2.1 ^{1}H NMR spectrum (500 MHz, in DMSO-d_6) of [EMI][TFSA].

The difunctional chain transfer agent (CTA) *S,S'*-di(1-phenylethyl) trithiocarbonate was synthesized following a previously reported procedure (Scheme 2.1).[23] In a typical experiment, carbon disulfide (1.05 g, 13.8 mmol) was added to a suspension of cesium

Scheme 2.1 Synthesis of *S,S'*-di(1-phenylethyl)trithiocarbonate.

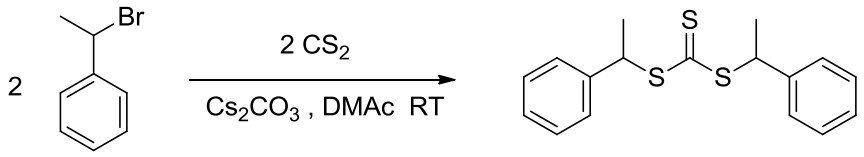

carbonate (4.86 g, 13.8 mmol) in *N*,*N*-dimethylacetamide (12 mL, DMAc). Then the reaction mixture was stirred vigorously at room temperature, while its color changed to blood red solution within 5 minutes. After stirring for 15 minutes, 1-bromoethyl benzene (2.55 g, 13.8 mmol) dissolved in DMAc (3 mL) was added to the mixture. The color of the reaction mixture immediately changed from red to pale yellow and the reaction was allowed to proceed for 26 hours. The reaction was quenched by pouring into ice water, followed by extraction with ethyl acetate (EtOAc). After the organic phase was dried by sodium sulfate, the crude product was obtained by removing EtOAc under vaccum. The product was purified with column chromatography using hexanes as the eluent (R_f = 0.15). The structure of the final product was confirmed using ^{1}H NMR spectroscopy (Figure 2.2).

Monomer and polymer synthesis

The synthesis of 2-bromoethyl acrylate (BrEA), a bromine-containing monomer, was adapted from previous reports.[9,24] 2-Bromoethanol (30.0 g, 240 mmol) was mixed with dry CH_2Cl_2 (200 mL) in a 500-mL Schlenk flask and immersed in an ice bath for at least 15 minutes. Then, acryloyl chloride (21.9 g, 242 mmol) and triethylamine (24.3 g, 240 mmol) were sequentially injected into the flask dropwise under stirring. The reaction mixture became a slurry after a few minutes. The ice bath was then removed and the

reaction was allowed to proceed overnight. After the insoluble by-product triethylamine chloride was removed by filtration, the filtrate solution was washed with NaCl aqueous solution three times and deionized (DI) water three times. The product was then dried with $MgSO_4$ for 1 hour. Solvent was removed using a rotary evaporator and the remaining product was purified through vacuum distillation (1750 mTorr, b.p. 72-74 ℃). The obtained product was a clear, colorless liquid with a total yield of 33.5 g, 78% yield. The synthesis was confirmed by ^{1}H-NMR spectroscopy (Figure 2.3).

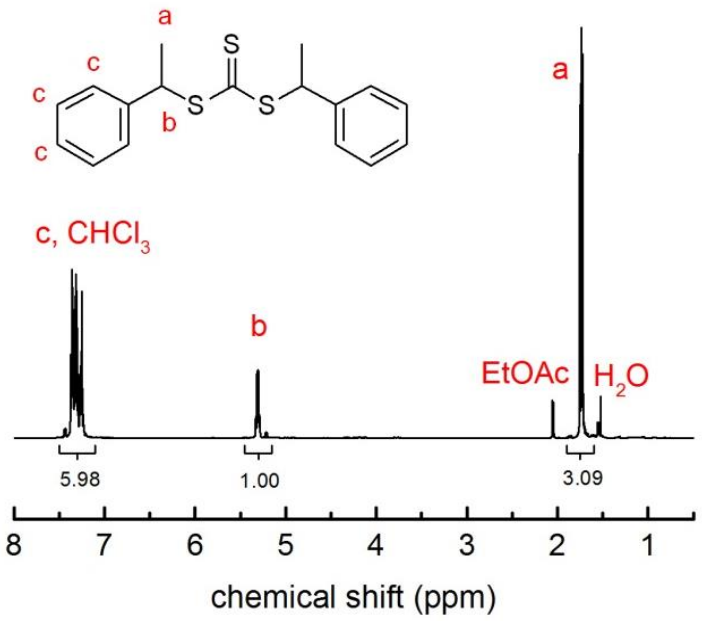

Figure 2.2 ^{1}H NMR spectrum (500 MHz, in $CDCl_3$) of *S,S'*-di(1-phenylethyl)trithiocarbonate, a difunctional chain transfer agent for RAFT polymerization

The PS-PIL-PS triblock copolymer was synthesized through a two-step sequential RAFT polymerization followed by two steps of post-polymerization reactions. Scheme 2.1 shows the synthetic procedure to obtain a PS-PIL-PS triblock copolymer. The first step was the preparation of a PS macro-CTA.[25] Purified styrene monomer (34.56 g, 332

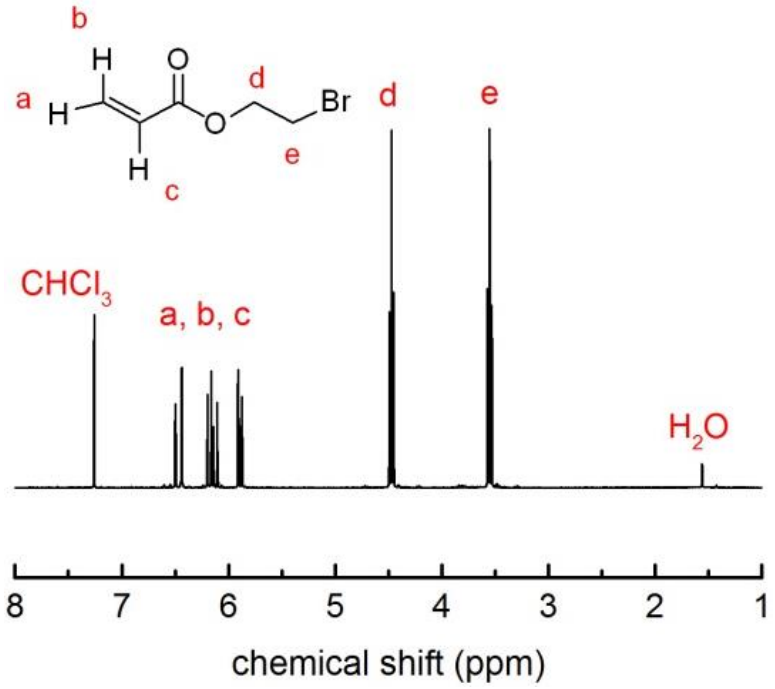

Figure 2.3 ^{1}H NMR spectra (500 MHz, in DMSO-d_6) of 2-bromoethyl acrylate (BrEA)

mmol) and the difunctional CTA (335.1 mg, 1.09 mmol) were mixed in a 100-mL Schlenk flask and bubbled with Argon for 30 mins. Then the reaction mixture was submersed in an oil bath at 100 ℃. After 20 hours, the reaction was quenched in liquid nitrogen. Crude product was precipitated in CH_3OH three times and then dried under vacuum at 80 ℃. The resulting PS had a molecular weight of 8 kDa and a dispersity of 1.05.

In the second step, BrEA (22.78 g, 127 mmol), AIBN (10.9 mg, 0.0665 mmol) and PS macro-CTA (1.20 g, 0.15 mmol) were dissolved in 2-butanone (50 mL), followed by argon bubbling for 1 hour. The polymerization was initiated by heating to 60 ℃ and was allowed to proceed for 15 hours of reaction before it was quenched in liquid nitrogen.

The polymer was then precipitated in hexanes three times and dried under vacuum. Both SEC (Figure 2.4 (a)) and ^{1}H-NMR (Figure 2.5) confirmed the growth of the poly(2-bromoethyl acrylate) (PBrEA) mid-block. The PS-PBrEA-PS had a total molecular weight of 98 kDa and a dispersity of 1.19.

Scheme 2.2 Synthetic route to PS-PIL-PS (4-252-4) triblock copolymer

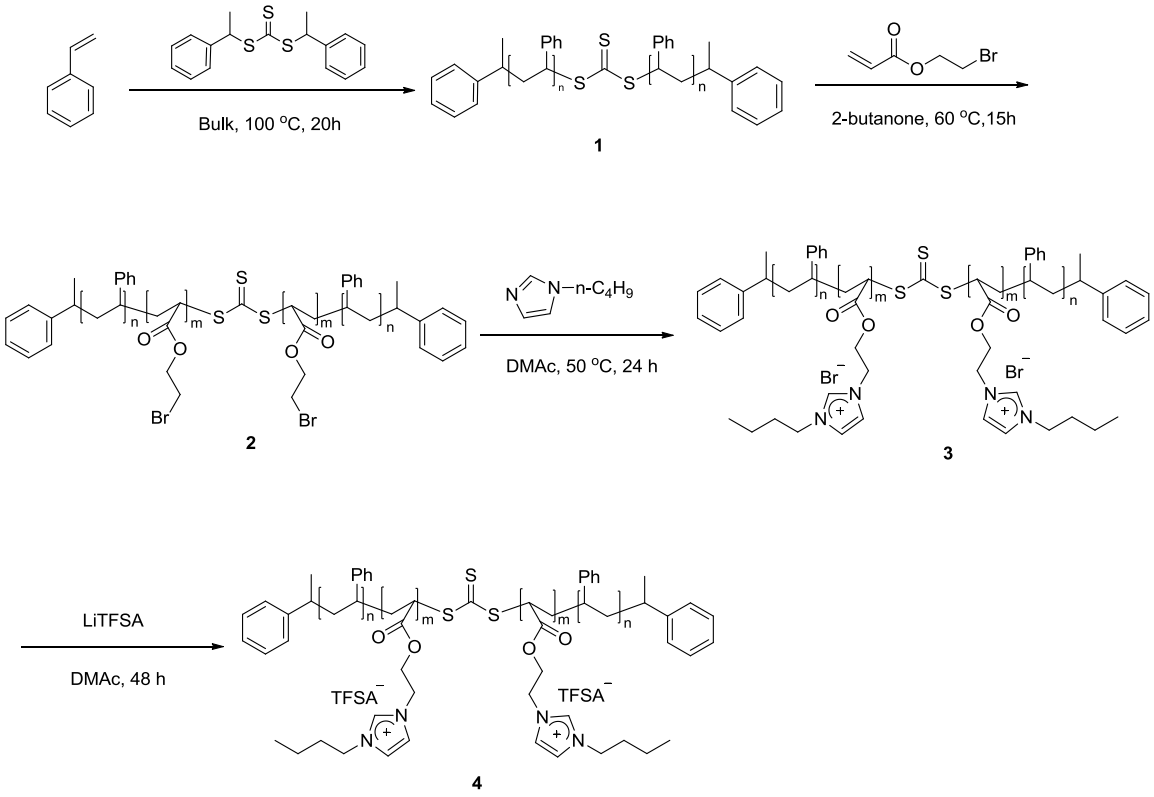

An excess amount of 1-butylimidazole (3.28 g, 26.4 mmol) and PS-PBrEA-PS (1.51 g) were then dissolved in *N*,*N*-dimethylacetamide (DMA) (20 mL) and the quarternization reaction was conducted at 50 ℃.[9,26] After 24 hours, the reaction was stopped and the reaction mixture was dialyzed in CH_3OH for 60 hours (solvent was refreshed every 12 hours) to remove residual reactants. The solvent was removed using a

rotary evaporator and then completely dried under vacuum at 80 ℃ overnight. The triblock copolymer with bromide anions was then reacted with an excess amount of LiTFSA to achieve anion exchange. The polymer (1.83 g) and LiTFSA (5.28 g) were dissolved in DMA (30 mL) and reacted at room temperature for 48 hours. The final product was precipitated in deionized water three times and dried under vacuum for 36 hours. The final product was characterized using ^{1}H NMR, SEC and elemental analysis. The polymer had a dispersity of 1.2 and a total molecular weight of 260 kg/mol. The composition of the SILS triblock copolymer was investigated using elemental analysis. Polymer samples were dried in a vacuum oven at room temperature for 24 hours before it was sent to Atlantic MicroLab Inc. for testing. ^{1}H NMR and elemental analysis results showed that the quarternization efficiency is higher than 93% (see Figure 2.5 and Table 2.1). Both elemental analysis and silver nitrate test have also confirmed a complete anion exchange from bromide to TFSA. The molecular characteristics of the polymers invlolved in the synthesis are listed in Table 2.2.

Table 2.1 Elemental analysis of PS-PIL-PS triblock copolymer

Polymer		**C**	**H**	**O**	**N**	**F**	**Br**
PS-PIL-PS	Calc. Value (%)	35.29	3.94	18.47	8.08	21.94	0
(4-252-4)	Exp. Value (%)	36.17	3.87	19.13	7.52	20.75	<det. limit

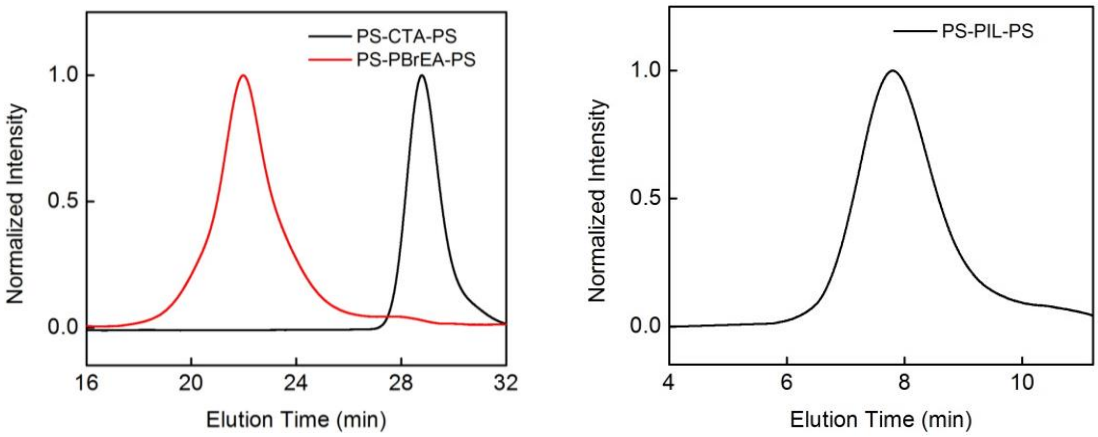

Figure 2.4 SEC traces of (a) PS macro-CTA (8kDa) and PS-PBrEA-PS (4-91-4) using THF as elution solvent; (b) PS-PIL-PS (4-252-4) using DMF (w/ 0.05M LiBr) as elution solvent. Total elution time is 40 min for THF (3 columns), and 13.33 min for DMF (1 column).

Table 2.2 Molecular characteristics of polymers synthesized in this study

Polymer	**$M_{n,\ PS}$ (kDa)[a]**	**$M_{n,\ PBrEA/PIL}$ (kDa)[b]**	**$M_{n,\ total}$ (kDa)**	**Đ**
PS-CTA-PS	4.0		8	1.05
PS-PBrEA-PS	4.0	91	99	1.2
PS-PIL-PS	4.0	252	260	1.2

[a] Molecular weight of PS was determined by SEC

[b] Molecular weight of mid-block was determined by ^{1}H NMR spectroscopy

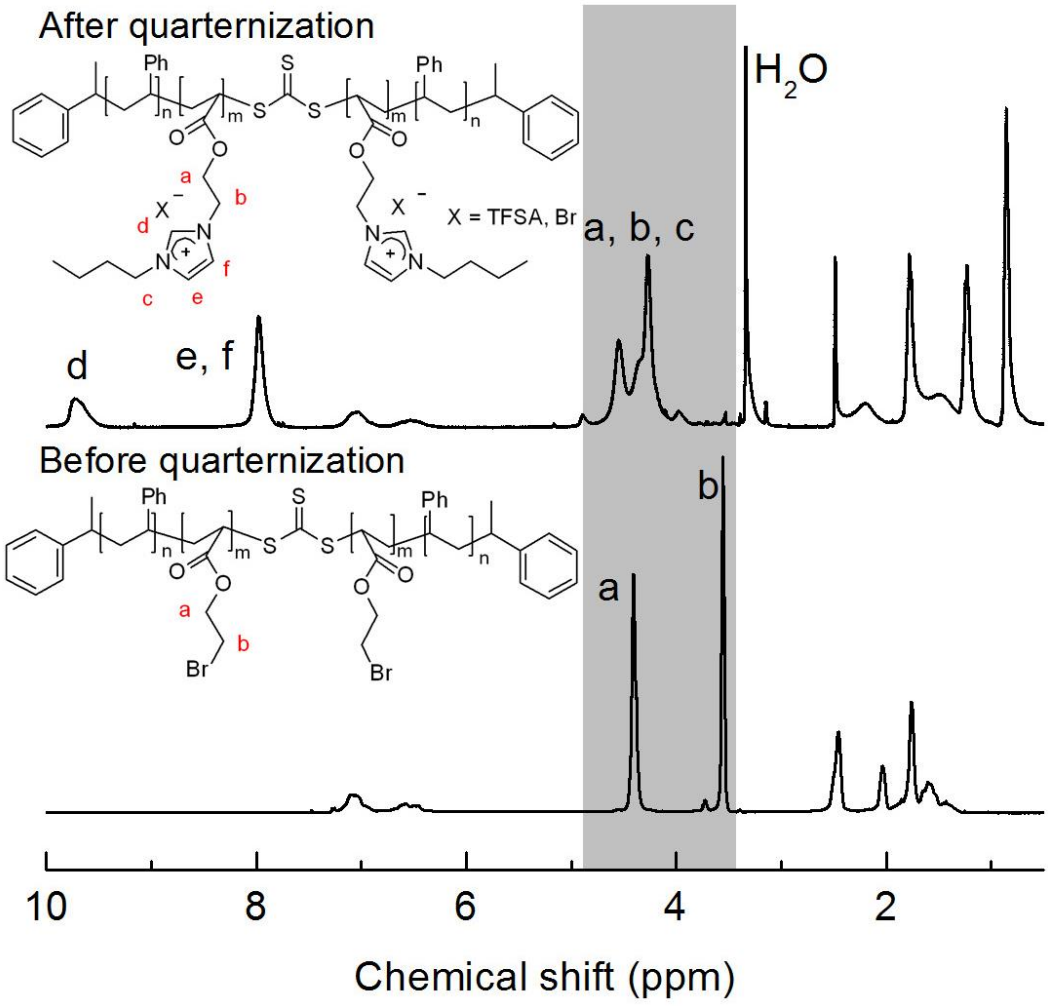

Figure 2.5 ^{1}H NMR spectra of PS-PIL-PS triblock copolymer before and after quarternization reaction.

Preparation of ion gel and supported ion gel membranes

Ion gels and supported ion gel membranes were prepared using a solvent casting method. The stock solution was prepared by dissolving PS-PIL-PS triblock copolymer and [EMI][TFSA] in tetrahydrofuran (THF). In the experiments, the ratio between ionic

liquid (IL) and triblock copolymer were kept at 85:15 (w:w) and the ratio between solvent and IL+polymer was 5:1. Most of the solvent was then removed by purging under N_2 overnight, and the residual solvent were removed under vacuum at ca. 70 ℃ for 48 hours. The ion gels were kept in a vacuum desiccator to avoid moisture.

The supported ion gel membranes were prepared in a home-made stainless steel container. A microporous PVDF membrane support wetted by THF was clamped at the bottom of the container. Typically, 1.8 g of prepared stock solution was then added into the container using a pipette. After complete solvent evaporation, the membrane was annealed at 90 ℃ for about 2 hours. Then the supported membrane was taken out of the container and transferred to a Teflon® cutting board, where a 25 mm diameter circular punch was used to cut out a sample membrane for gas permeation experiments. When the PVDF membrane pores are completely filled with ion gel, the white opaque membrane changes to a translucent membrane. A caliper was used to measure the membrane thickness, ca. 130 μm, which is close to the thickness of PVDF membranes.

Differential scanning calorimetry (DSC)

Thermal transitions of SILS triblock copolymer and a PS homopolymer (4 kDa) were measured using a Q1000 differential scanning calorimeter with liquid nitrogen cooling capacity. In a typical experiment, ca. 5 to 10 mg of sample was sealed in a hermetic aluminum pan, heated up to 150 ℃, and annealed for 5 min to remove any prior thermal history. The sample was then cooled to -130 ℃, and heated back up to 150 ℃ at a heating rate of 10 ℃/min. The DSC curve was taken from the second heating cycle.

Rheology

Rheological experiments were conducted on an ARES rheometer (Rheometric Scientific) using parallel plate geometry (50 mm diameter), with a gap of ca. 1 mm. In the experiments to determine the critical gelation concentration of SILS triblock copolymer in [EMI][TFSA], dynamic shear measurements (frequency sweeps) were performed at 25 ℃ on mixtures of SILS/[EMI][TFSA] with polymer weight fractions of 1, 4, 5, 10 wt%. Experimental temperature was controlled to within 0.5 ℃ of the set point with an environmental controller under a nitrogen atmosphere.

In temperature ramp experiments, the sample was equilibrated at 100 ℃ for ca. 10 minutes to remove any prior thermal history, and cooled down to 25 ℃ to start the measurement. It was then heated to 125 ℃ at 1 ℃/min with a shear rate of 0.3 rad/s and a strain of 3%. The modulus change of the ion gel was measured as a function of temperature.

To obtain the time temperature superposition (tTS) curve, the dynamic storage and loss moduli of the ion gel with 15 wt% PS-PIL-PS triblock copolymer were measured at 20 ℃ intervals between 20 ℃ and 100 ℃. The sample was thermally equilibrated for 15-20 minutes at each temperature and the gap was adjusted to compensate for the thermal expansion of the tool. Measurements were taken at a series of decreasing temperatures.

Size Exclusion Chromatography (SEC)

SEC was used to determine the molecular weight characteristics of the synthesized polymers. The experiments for PS-CTA-PS and PS-PBrEA-PS were performed on a SEC system composed of three Phenomenex Phenogel Columns with tetrahydrofuran (THF)

as the elution phase, and the PS-PIL-PS triblock copolymer was measured using a Waters Styragel HR4 column with *N*,*N*-dimethylformamide (DMF, w/ 0.05 M LiBr) as the elution phase. (Although the PS-PIL-PS triblock copolymer is soluble in THF, the SEC experiment cannot be conducted using THF because the polyelectrolytes will adhere to the packing materials in the column. Lithium salt was also added to DMF to prevent polyelectrolyte samples adhesion to the column.) Polymer samples were dissolved in HPLC grade THF or DMF at concentrations ranging from 1 – 8 mg/mL, and the solution was injected into the SEC using a 250 μL syringe. The flow rate was controlled at 1 mL/min via an Alltech 426 HPLC pump. After the column separation, the polymer solution was analyzed by a Wyatt Dawn DSP multi-angle light scattering detector and a Wyatt Technology Optilab DSP interferometric refractometer to obtain the molecular weight information. The dn/dc value of polystyrene was 0.192 in THF.

Gas permeation experiments and gas diffusion cell

The permeability of supported ion gel membranes were tested using a gas diffusion cell. Details concerning the cell construction can be found in a previous report.[27,28] As shown in Figure 2.6, the diffusion cell consists of two 15 cm^3 compartments separated by the membrane. In the experiments, a metal plug with a volume of 8.6 cm^3 was placed in the downstream compartment to reduce the experimental time. The membrane package, which is composed of the test membrane and a piece of metal mesh, was mounted between two stainless-steel disks and sealed with an O-ring. The effective membrane area was determined to be 3.15 cm^2 based on the open area of the disks. The entire membrane-disk assembly was then clamped between the two compartments. The pressures of both

upstream and downstream chambers were monitored using pressure transducers (Cole Palmer Model 97356-61), and recorded using a SuperLogics 8017 module.

In a pure gas experiment, both compartments were first flushed with the test gas (CO_2, N_2, or CH_4) for 1 hour to allow the membrane to become saturated with the gas. After flushing, about 30 psi (gauge pressure) of this gas was put into both compartments and the downstream was instantly vented to 0 (gauge pressure). Simultaneously, the whole cell was closed and data recording was started. In mixed gas experiments, the procedure was slightly different. First, both compartments were flushed with a background gas for 1 hour and then about 15 psi of this background gas was put into both compartments. Next, approximately 30 psi of the test gas was added to the upstream compartment. Immediately thereafter, the entire cell was sealed and data recording was started.

In both pure and mixed gas permeation experiments, the pressure difference between the two compartments was recorded as a function of time, and the permeability data were extracted using the following equations

$$\frac{1}{\beta}\ln\left(\frac{\Delta p_0}{\Delta p}\right) = P \cdot \frac{t}{l} \tag{2.1}$$

$$\beta = A\left(\frac{1}{V_{up}} + \frac{1}{V_{down}}\right) \tag{2.2}$$

where β is a geometric parameter determined by the diffusion cell; A is the membrane area and V_{up} and V_{down} are the volumes of the upstream and downstream compartments, respectively; Δp_0 and Δp are the pressure differences between the two compartments initially and at time t, respectively; P is the permeability and l is the membrane

thickness. By plotting left side of the equation, $\frac{1}{\beta}\ln\left(\frac{\Delta p_0}{\Delta p}\right)$ versus $\frac{t}{l}$, membrane permeability can be extracted from the slope from a linear fit. The permeability of ion gels is calculated by dividing the membrane permeability by porosity and tortuosity (3.1).

The membrane selectivity was then determined by permeability ratio of two different gases according to the following equation

$$\alpha_{i/j} = \frac{P_i}{P_j} \tag{2.3}$$

This equation can be used for both pure and mixed gas experiments.

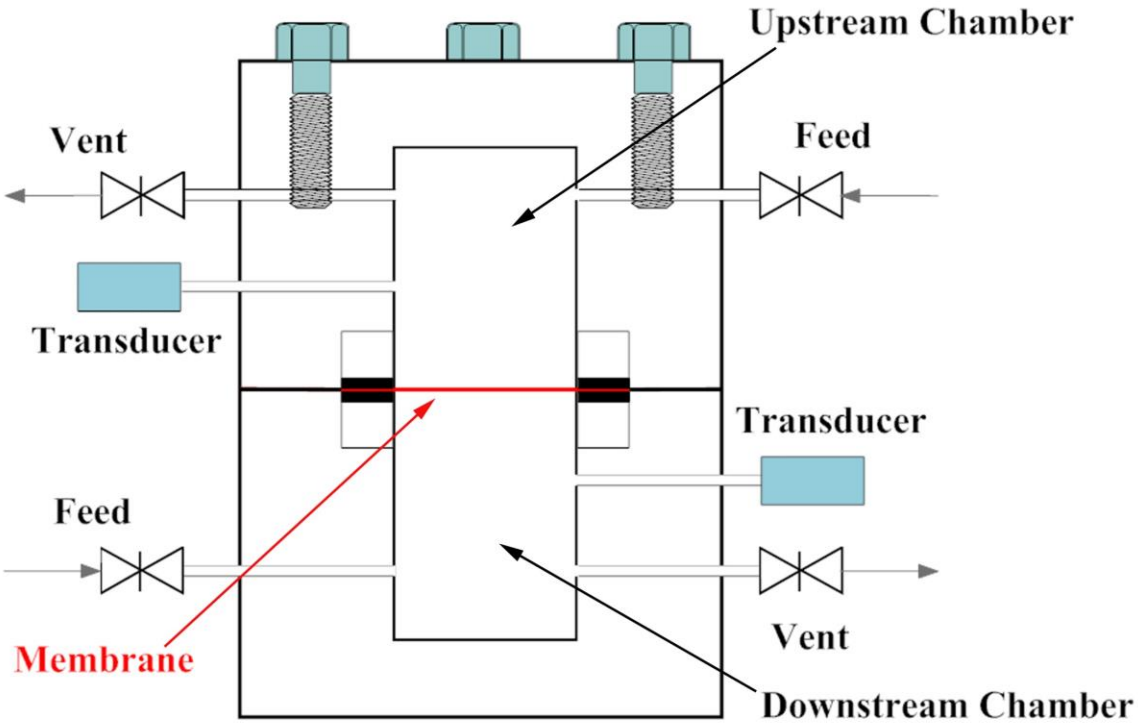

Figure 2.6 Gas diffusion cells: the membrane is clamped between two chambers of different pressures, and the pressure difference is measured over time (figure adapted from Refs 27, 28).

2.3 Results and Discussion

2.3.1 Gelation of SILS triblock copolymer in [EMI][TFSA]

To investigate the gelation behavior of the SILS triblock copolymer in [EMI][TFSA], mixtures of SILS and [EMI][TFSA] were prepared at a series of polymer concentrations from 1-10 wt%. As shown in Figure 2.7(a), the dynamic shear moduli of these mixtures were measured. The representative data displayed in this figure show a clear transition from the liquid-like behavior to the solid-like behavior upon increase in polymer concentration. At 1 wt%, the sample is clearly a liquid, as its storage modulus (G') is much smaller than its loss modulus (G''). Both G' and G'' exhibited different power law dependences on frequency: $G' \sim \omega^2$ and $G'' \sim \omega$, which are typical terminal rheological behavior of a viscous fluid. On the other hand, the 10 wt% mixture shows a solid-like rheological behavior as G' is higher than G'', and G' is independent of the shear frequency (ω). This is typical for a solid material.

The samples at 4 wt% showed intermediate behavior between a liquid and a solid. G' and G'' share similar values and have very close power law dependences on the frequency. This behavior represents the solid-liquid transition, which approximates the critical gelation concentration in this system. The rheological behavior also satisfied the well-known Winter-Chambon prediction about the critical gelation point,[29,30] where

$$G'(\omega) \approx G''(\omega) \sim \omega^n \tag{2.4}$$

Therefore, the loss tangent ($\tan\delta$) at the gelation point should be independent of frequency and have the value close to 1. As shown in Figure 2.7(b), $\tan\delta$ values for the 4

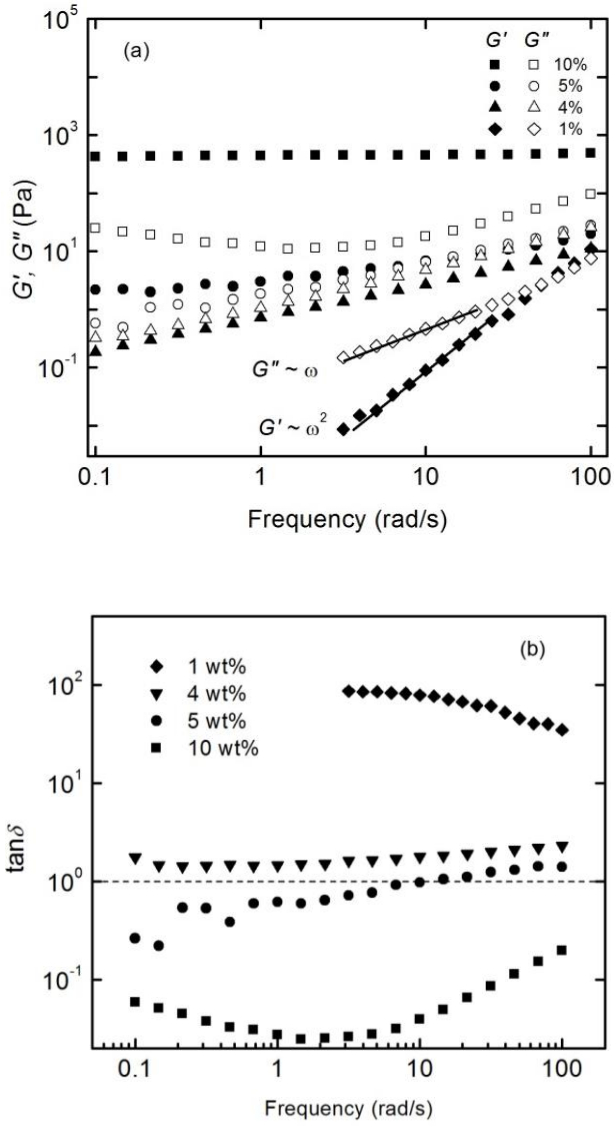

Figure 2.7 Dynamic shear experiments on SILS/[EMI][TFSA] mixtures at various concentrations: (a) storage and loss moduli; (b) loss tangent (tanδ)

wt% sample are almost parallel to the horizontal axis, thus confirming that the 4 wt% mixture of SILS and [EMI][TFSA] is very close to the gelation point. The critical gelation concentration found here is consistent with a previous report on an SOS/[BMI][PF_6] ion gel.[14]

After the critical gelation concentration was determined, a temperature ramp experiment was conducted on a 15 wt% SILS ion gel, which is the same gel used in gas separation studies discussed in the following section. The dynamic moduli *G′* and *G″* were measured at a frequency of 0.3 rad/s during a temperature ramp from 25 ℃ to 125 ℃ at a heating rate of 1 ℃/min. As shown in Figure 2.8, the intersection of the *G′* and *G″* curves indicates a critical gelation temperature at ca. 77 ℃, above which the gel will melt. This sol-gel transition is not unexpected according to the transient network theory.[15,31,32] Because the PS end-blocks are very short (less than 40 repeating units), the thermal dynamic penalty to pull the PS chains out of the micelle is relatively small. Moreover, the glass transition temperature (T_g) of a 4 kDa PS is only 80 ℃ (Figure 2.10), their higher segmental mobility above T_g makes PS easier to dissociate and diffuse into the surrounding ionic liquid, leading to the gel melting.[33] This thermoreversibility provides the possibility to process the ion gel at higher temperature and use it at room temperature.

To further understand the thermoreversible gelation behavior of 15 wt% SILS ion gel, the dynamic storage and loss moduli were measured over the temperature range from 20 to 100 °C. Figure 2.9 displays the obtained time temperature superposition (tTS) curves with reference to 100 ℃. We found that the longest relaxation time ($\tau_{1,\ gel}$) at the reference temperature was only 0.09 sec, indicating a very fast chain exchange between

the micellar cores formed by the short PS end-blocks. As the association strength is weak enough to allow observation of chain pullout on rheological measurements, the ion gel exhibits a terminal behavior at this temperature. This result is also consistent with the results displayed in Figure 2.8, as $G' < G''$ at 100 ℃.

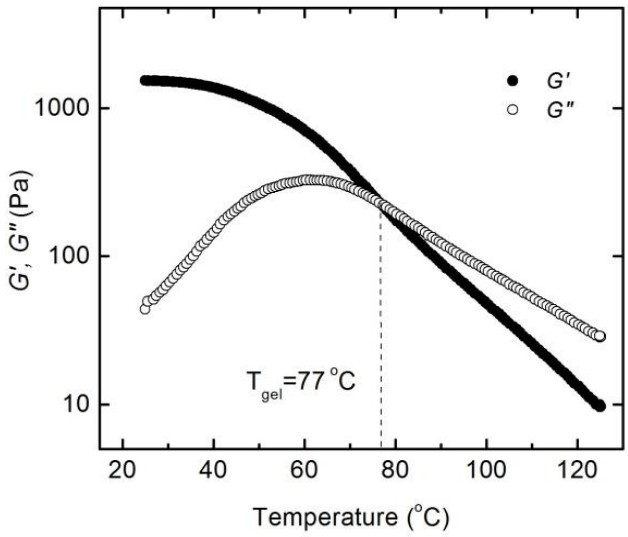

Figure 2.8 Temperature dependence of G' and G'' between 25 and 125 °C

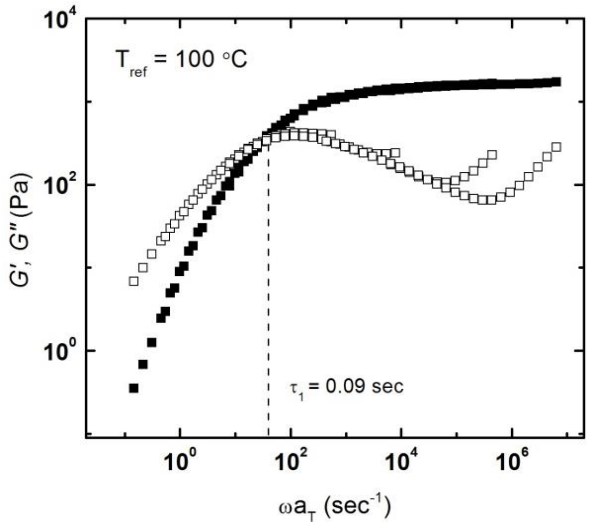

Figure 2.9 tTS master curves of dynamic storage (filled symbols) and loss moduli (open symbols) referenced to 100 °C for 15 wt% SILS/[EMI][TFSA] ion gel measured over 20 – 100 °C.

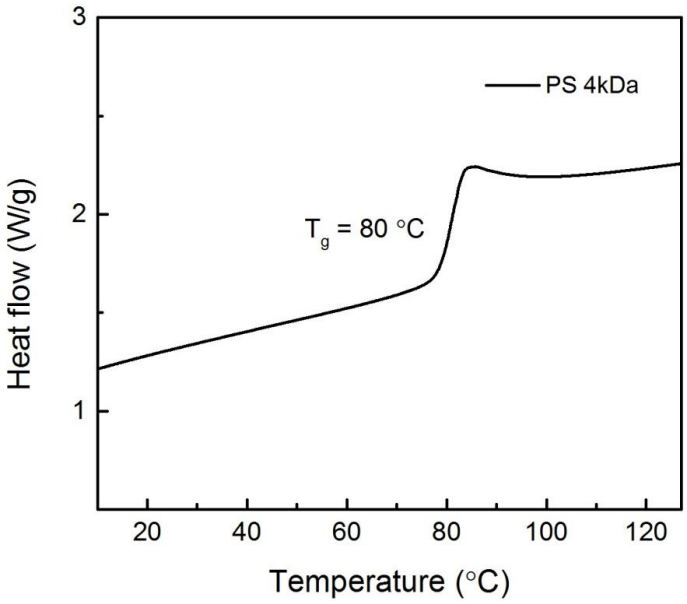

Figure 2.10 DSC curves of a PS homopolymer with a molecular weight of 4kDa.

2.3.2 Gas separation studies on supported ion gel membranes

Gas transport properties of ion gels were tested using a supported ion gel membrane prepared by filling a porous support. Interestingly, when the pores of PVDF support were completely filled with ion gels, the white and opaque PVDF membrane support turns into a translucent membrane (Figure 2.11). This change is due to the nearly matched refractive index of the glassy PVDF support ($\lambda \approx 1.420$) and [EMI][TFSA] ($\lambda \approx 1.425$). Both this transmittance change and the measurement of weight difference between "empty" and filled membranes were used to determine whether the membrane is completely filled with ion gels or not.

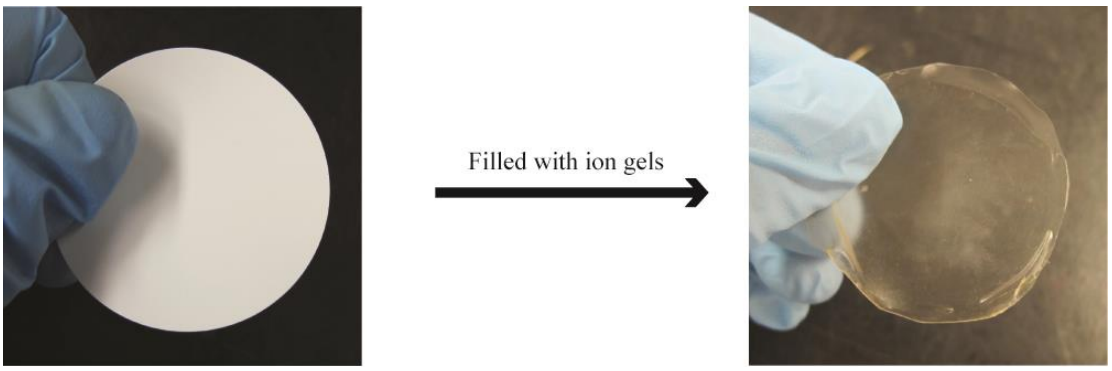

Figure 2.11 (Left) PVDF support without ion gel; (Right) supported ion gel membrane.

In the gas permeation tests, both pure gas and mixed gas permeation properties of the supported ion gel membrane were studied using the gas diffusion cell at room temperature with a pressure difference of approximately 30 psi (downstream at 1 atm). Table 2.3 shows the permeation results for two different gas pairs: CO_2/N_2 and CO_2/CH_4. The gas permeability of CO_2 was determined to be 985 barrers for the PIL gel containing 15 wt% of triblock copolymer, which is very close to the literature reported CO_2 permeability value of neat [EMI][TFSA] membranes. On the other hand, the permeability of N_2 and CH_4 were found to be ca. 25 barrers and 52 barrers, respectively. Interestingly, these observed values are significantly lower than those reported for neat [EMIM][TFSA]. In consequence, the block copolymer ion gel exhibits an ideal selectivity of 19 for CO_2/CH_4 and 39 for CO_2/N_2, both of which are higher than the reported values for neat [EMI][TFSA]. In a previous report by Bara et al., a cross-linked PIL membrane with the same polymer structure as the mid-block in this study was found to possess a higher selectivity than neat [EMI][TFSA] for both CO_2/N_2 and CO_2/CH_4,

consistent with the results here.[9] Their result suggested that the acrylate backbone of PIL helped improve the selectivity for CO_2 over other gases.

Table 2.3 Pure gas permeability and ideal selectivity of the ion gel

	Permeability (barrer)[a]			Ideal selectivity	
	CO_2	N_2	CH_4	CO_2/ N_2	CO_2/ CH_4
15% ion gel	980 ± 30	25 ± 2	52 ± 3	39	19
[EMIM][TFSA][b]	1000	44	90	21	11

[a] Permeability in barrers, units of 10^{-10} cm^3 (STP) cm/cm^2 sec cmHg;

[b] Permeability data of pure [EMI][TFSA] was from ref 4, 11

As noted earlier, the real selectivity of polymeric gas separation membranes is often lower than the ideal selectivity, due to the plasticization effect or competitive absorption.[34–39] This is also one of the major deficiencies of commercialized polymer gas separation membranes. However, at the current experimental pressure, by using this ion gel, we observe that the real selectivity is almost the same as the ideal selectivity. In Table 2.3, the permeability of each gas is essentially the same with and without the presence of another gas, which means that the mixed gas selectivity is essentially the same as the pure gas selectivity. This result is understandable because the selectivity in the ion gel is determined by differential solubility in the ionic liquid, which is not significantly affected when exposed to a gas mixture. It is also consistent with the previous reports studying mixed gas selectivity on a supported ionic liquid membrane (SILM).[40,41] In polymer membranes there can be a major selectivity decrease at high

pressure drops due to membrane plasticization. Future work in this area should also pay more attention to the ion gel membrane performance at higher pressures.

Table 2.4 Mixed gas selectivity and comparison with pure gas permeability

	Permeability (barrer) [a]				Real Selectivity	
	CO_2		N_2	CH_4		
	CO_2 (N_2)	CO_2(CH_4)	N_2(CO_2)	CH_4(CO_2)	CO_2/N_2	CO_2/CH_4
15% SILS gel	985 ± 30		25 ± 2	52 ± 3	40	20
	1030 ± 30	1040 ± 20	26 ± 2	51 ± 2		

[a] Data in the first row are pure gas results and the second row are mixed gas results. The mixed gas permeability was tested on a 50/50 mixture with a background gas (listed in brackets). Error bars are the standard deviation of three repetitive test for the same gas.

The gas separation properties of this new type of ion gel can be compared with existing polymeric gas separation membranes on a Robeson plot, i.e., a log-log plot of permeability vs. selectivity.[19,20] The empirical upper bound on the plot approximates the best permeability/selectivity combination for existing polymer membranes. As shown in Figure 2.12, the performance of the PIL gel lies above the upper bound for CO_2/N_2 and very close to the upper bound for CO_2/CH_4. This promising performance can be compared with recent reports of chemically cross-linked PIL and PIL-IL composite membranes reported by Bara et al. These PIL membranes generally show high selectivity for CO_2 but have very low permeability. By incorporating a certain amount of liquid (20 mol% free ionic liquids), the composite PIL membranes exhibit increased CO_2 permeability (ca. 50 barrers) with little sacrifice on the selectivity.

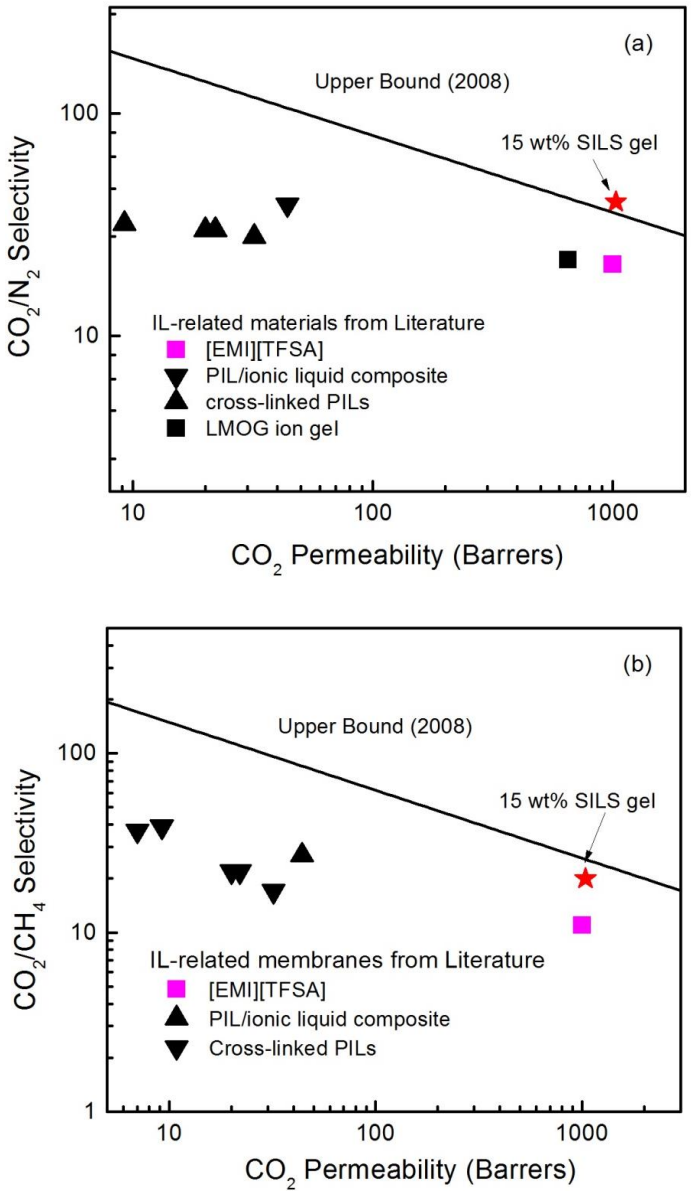

Figure 2.12 Robeson Plot comparison with upper bounds for various ionic liquid-related membranes: (a) CO_2/N_2; (b) CO_2/CH_4. Permeability data for these materials are from Ref 9-11, and 42. Data for Upper bound are from Ref 19 and 20.

Here, by further increasing the free ionic liquid fraction to 85 wt%, we found that the gas permeability has been significantly improved compared to these cross-linked PIL materials (ca. 50 times higher than the cross-linked PIL membranes and ca. 20 times higher than the composite materials). But the mechanical properties of ion gels are presumably much lower than the cross-linked PILs. The mechanical strength ion gels needs to be significantly improved before any further applications.

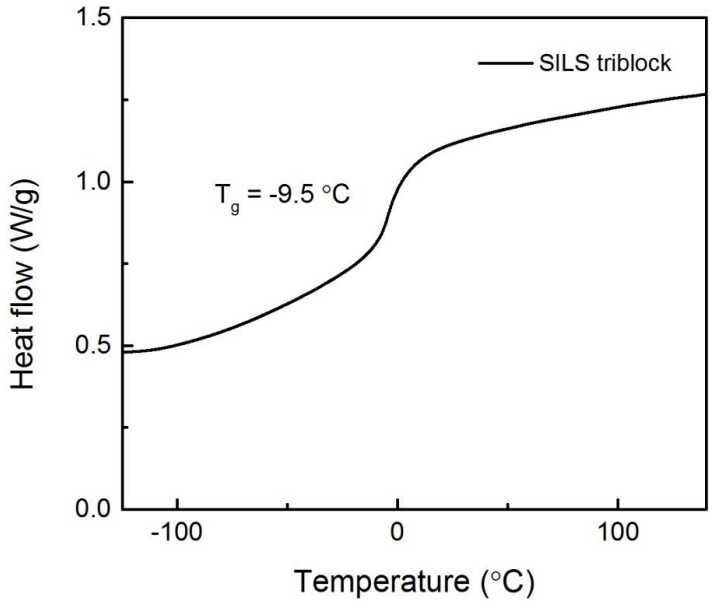

Figure 2.13 DSC curves of SILS (4-252-4) triblock copolymer. The glass transition on the curve corresponds to the T_g of the PIL mid-block.

The favorable transport properties of ion gels stem from the fact that the major component is free ionic liquid (85 wt%), and if we consider the swollen PIL in ionic liquid, the combined weight fraction of [EMI][TFSA] and swollen PIL mid-block is greater than 99 wt% in the system. The permeation of gas molecules through the ion gels are via the liquid mixture of [EMI][TFSA] and the solvated PIL mid-block. On the other

hand, DSC studies on the SILS triblock showed that the PIL mid-block has a very low glass transition temperature of ca. −9.5 ℃ (Figure 2.13). Therefore, the mobility of the gas molecules in the ion gels should not be significantly affected by the solvated mid-block. This also explained why the ion gel achieves a liquid-like permeability (close to that of the neat [EMI][TFSA]) in a solid-state material. By incorporating a PIL as the mid-block, the selectivity has also been increased by almost a factor of two over the corresponding pure ionic liquid. Recently, the idea of using a physical gel to achieve gas separation has also demonstrated using small molecules. Voss et al. reported the gelation of an ionic liquid using 12-hydroxystearic acid, a low-molecular weight gelator (LMOG).[42] Because only 1.5% of the gelators have been added, the local environment for gas permeation in the gel is not significantly affected. Therefore, this LMOG ion gel also exhibits excellent transport properties, close to the neat ionic liquid.

Here, we need to point out that this work is a proof-of-concept study to show the viability of using triblock copolymer ion gel as a gas separation material. The current supported ion gel membrane is still too thick for practical use. Therefore, the permeance of the ion gel membrane is limited by its thickness and the permeation efficiency is also reduced by using a support. Also, a gas separation membrane for industrial applications needs to be stable under a higher pressure drop (> 50 bar, CO_2/CH_4 separation), which cannot be achieved with the current membrane. In Chapter 4, we will describe a new strategy which can enhance the mechanical strength of block copolymer ion gels, while retaining their attractive diffusivity and solubility characteristics.

2.4 Conclusions

In this chapter, we have designed a new gas separation material with enhanced gas transport properties through gelation of PS-PIL-PS in an ionic liquid, [EMI][TFSA]. This represents a new way of combining the advanced gas separation properties of ionic liquid with the mechanical strength of block copolymers. We have investigated the rheological properties of these ion gels as well as their gas separation properties.

The synthesis of PS-PIL-PS triblock copolymer was achieved through sequential RAFT polymerization followed by post-polymerization reactions. The SILS triblock copolymer can form an ion gel in [EMI][TFSA] with as low as 4 wt% polymer. The thermoreversible nature of the ion gel offers the advantage of solvent-free processing in practical applications. More importantly, this new class of material exhibits both high permeability and high real selectivity for CO_2/N_2 and CO_2/CH_4 gas pairs, thus exhibiting great promise for future gas separation membranes.

2.5 References

(1) Noble, R. D.; Gin, D. L. *J. Membr. Sci.* **2011**, *369*, 1–4.

(2) Gin, D. L.; Noble, R. D. *Science* **2011**, *332*, 674–676.

(3) Brennecke, J. F.; Gurkan, B. E. *J. Phys. Chem. Lett.* **2010**, *1*, 3459–3464.

(4) Bara, J. E.; Carlisle, T. K.; Gabriel, C. J.; Camper, D.; Finotello, A.; Gin, D. L.; Noble, R. D. *Ind. Eng. Chem. Res.* **2009**, *48*, 2739–2751.

(5) Anderson, J. L.; Dixon, J. K.; Brennecke, J. F. *Acc. Chem. Res.* **2007**, *40*, 1208–1216.

(6) Camper, D.; Bara, J. E.; Gin, D. L.; Noble, R. D. *Ind. Eng. Chem. Res.* **2008**, *47*, 8496–8498.

(7) Camper, D.; Bara, J. E.; Koval, C.; Noble, R. D. *Ind. Eng. Chem. Res.* **2006**, *45*, 6279–6283.

(8) Camper, D.; Becker, C.; Koval, C.; Noble, R. D. *Ind. Eng. Chem. Res.* **2006**, *45*, 445–450.

(9) Bara, J. E.; Lessmann, S.; Gabriel, C. J.; Hatakeyama, E. S.; Noble, R. D.; Gin, D. L. *Ind. Eng. Chem. Res.* **2007**, *46*, 5397–5404.

(10) Bara, J. E.; Hatakeyama, E. S.; Gabriel, C. J.; Zeng, X.; Lessmann, S.; Gin, D. L.; Noble, R. D. *J. Membr. Sci.* **2008**, *316*, 186–191.

(11) Bara, J. E.; Hatakeyama, E. S.; Gin, D. L.; Noble, R. D. *Polym. Adv. Technol.* **2008**, *19*, 1415–1420.

(12) Bara, J. E.; Noble, R. D.; Gin, D. L. *Ind. Eng. Chem. Res.* **2009**, *48*, 4607–4610.

(13) Bara, J. E.; Camper, D. E.; Gin, D. L.; Noble, R. D. *Acc. Chem. Res.* **2010**, *43*, 152–159.

(14) He, Y.; Boswell, P. G.; Bühlmann, P.; Lodge, T. P.; Buehlmann, P. *J. Phys. Chem. B* **2007**, *111*, 4645–52.

(15) Zhang, S.; Lee, K. H.; Sun, J.; Frisbie, C. D.; Lodge, T. P. *Macromolecules* **2011**, *44*, 8981–8989.

(16) Gu, Y.; Lodge, T. P. *Macromolecules* **2011**, *44*, 1732–1736.

(17) Scovazzo, P.; Havard, D.; McShea, M.; Mixon, S.; Morgan, D. *J. Membr. Sci.* **2009**, *327*, 41–48.

(18) Morgan, D.; Ferguson, L.; Scovazzo, P. *Ind. Eng. Chem. Res.* **2005**, *44*, 4815–4823.

(19) Robeson, L. M. *J. Membr. Sci.* **1991**, *62*, 165–185.

(20) Robeson, L. M. *J. Membr. Sci.* **2008**, *320*, 390–400.

(21) Bonhote, P.; Dias, A.-P.; Papageorgiou, N.; Kalyanasundaram, K.; Graetzel, M. *Inorg. Chem.* **1996**, *35*, 1168–1178.

(22) Bai, Z.; Lodge, T. P. *J. Am. Chem. Soc.* **2010**, *132*, 16265–16270.

(23) Aoyagi, N.; Ochiai, B.; Mori, H.; Endo, T. *Synlett* **2006**, 636–638.

(24) Ding, S.; Tang, H.; Radosz, M.; Shen, Y. *J. Polym. Sci., Part A: Polym. Chem.* **2004**, *42*, 5794–5801.

(25) Mayadunne, R. T. A.; Rizzardo, E.; Chiefari, J.; Krstina, J.; Moad, G.; Postma, A.; Thang, S. H. *Macromolecules* **2000**, *33*, 243–245.

(26) Stancik, C. M.; Lavoie, A. R.; Achurra, P. A.; Waymouth, R. M.; Gast, A. P. *Langmuir* **2004**, *20*, 8975–87.

(27) Yang, C.; Nuxoll, E. E.; Cussler, E. L. *AIChE J.* **2001**, *47*, 295–302.

(28) Phillip, W. A. Block Copolymer Membranes for Selective Separations. Ph.D. Thesis, University of Minnesota, Twin Cities, 2009, p. 202.

(29) Chambon, F.; Petrovic, Z. S.; MacKnight, W. J.; Winter, H. H. *Macromolecules* **1986**, *19*, 2146–2149.

(30) Winter, H. H.; Chambon, F. *J. Rheo.* **1986**, *30*, 367–382.

(31) Tanaka, F.; Edwards, S. F. *Macromolecules* **1992**, *25*, 1516–1523.

(32) He, Y.; Lodge, T. P. *Macromolecules* **2008**, *41*, 167–174.

(33) Hiemenz, P. C.; Lodge, T. P. *Polymer Chemistry*; 2nd ed.; CRC Press: New York, 2007.

(34) Wind, J. D.; Staudt-Bickel, C.; Paul, D. R.; Koros, W. J. *Ind. Eng. Chem. Res.* **2002**, *41*, 6139–6148.

(35) Visser, T.; Koops, G. H.; Wessling, M. *J. Membr. Sci.* **2005**, *252*, 265–277.

(36) Baker, R. W.; Lokhandwala, K. *Ind. Eng. Chem. Res.* **2008**, *47*, 2109–2121.

(37) Wind, J. D.; Paul, D. R.; Koros, W. J. *J. Membr. Sci.* **2004**, *228*, 227–236.

(38) Koros, W. J.; Fleming, G. K.; Jordan, S. M.; Kim, T. H.; Hoehn, H. H. *Prog. Polym. Sci.* **1988**, *13*, 339–401.

(39) Donohue, M. D.; Minhas, B. S.; Lee, S. Y. *J. Membr. Sci.* **1989**, *42*, 197–214.

(40) Neves, L. A.; Crespo, J. G.; Coelhoso, I. M. *J. Membr. Sci.* **2010**, *357*, 160–170.

(41) Baltus, R. E.; Counce, R. M.; Culbertson, B. H.; Luo, H.; DePaoli, D. W.; Dai, S.; Duckworth, D. C. *Sep. Sci. Technol.* **2005**, *40*, 525–541.

(42) Voss, B. A.; Bara, J. E.; Gin, D. L.; Noble, R. D. *Chem. Mater.* **2009**, *21*, 3027–3029.

Chapter 3

CO_2 Separation using Triblock Copolymer Ion Gels*

3.1 Introduction

CO_2 separation from other light gases (e.g., N_2, CH_4 and H_2) is an important technology widely used in applications such as natural gas sweetening, carbon capture from coal-fire power plant exhausts and hydrogen production.[1–7] Currently, five major technologies have been proposed and developed for CO_2 separation: amine-based absorption, physical solvent absorption, cryogenic distillation, membrane separation and pressure-swing adsorption.[8,9] Among these, membrane separation can be economically advantageous over the other more energy-intensive methods, especially in small and medium-scale separations, such as gas wells in remote areas and off-shore oil platforms.[10–13]

A high-performance gas separation material requires both high permeability and high selectivity; however, it is hard to achieve both at the same time. As mentioned in Chapter 2, gas permeation through a dense polymer membrane follows a solution-diffusion mechanism.[14–16] The permeability is thereby determined by the product of gas solubility and diffusivity. On the other hand, the selectivity, α, is determined by the permeability

* Reproduced in part from with permission from Gu, Y.; Cussler, E. L.; Lodge, T. P. *Journal of Membrane Science* **2012**, *423-424*, 20-26. Copyright 2012 Elsevier.

ratio of two gases on the same membrane, which, in turn, is also determined by the product of solubility ratio and diffusivity ratio.

$$P = S \times D \tag{3.1}$$

$$\alpha_{i/j} = \frac{P_i}{P_j} = \frac{S_i}{S_j} \times \frac{D_i}{D_j} \tag{3.2}$$

The particular ratio that contributes more to the selectivity of a membrane is determined by the gas pairs involved. For a polymeric CO_2 separation membrane, separation efficiency is determined by the diffusivity and the diffusivity ratio, which strongly depends on the stiffness of the polymer.[17–19] However, there is a general trade-off relationship between the selectivity and permeability of these membranes: the more permeable polymers are generally less selective, and *vice versa*.[10] This is because the polymers with higher selectivity usually have less free volume and higher glass transition temperature, which leads to a low gas permeability.[20–22]

Recently, ionic liquids have also been widely explored as new CO_2 separation media,[23–25] for four primary reasons: (*i*) ionic liquids generally show a highly preferential solubility for CO_2 over other gases such as N_2 and CH_4, which enhances the S_i/S_j term in eq 1; (*ii*) compared with conventional liquid membranes, the non-volatile nature of ionic liquids prevents solvent loss due to evaporation; (*iii*) gas solubility and selectivity can be easily tuned by changing the anion or cation in the ionic liquid, or by incorporating certain functional groups; (*iv*) as liquids, the transport rates are high. [26–37] Supported ionic liquid membranes (SILMs) have demonstrated the viability of using ionic liquid as an alternative for CO_2 separation.[31]

From an applications perspective, it is desirable to develop solid-state materials which combine the appealing properties of ionic liquids with a solid-like structure.[38–42] To achieve this goal, efforts have been made using either low-molecular weight gelators,[43] or compatible macromolecules, such as chemically-crosslinked polymerized ionic liquids (PIL).[44–48] In Chapter 2, we have also demonstrated that an ABA-triblock copolymer ion gel with a PIL mid-block can be used in CO_2 separations.[49] Gas permeation studies showed that this ion gel has both high permeability and favorable selectivity for CO_2/N_2 and CO_2/CH_4 gas pairs, which exceeded the famous "upper bound" on the respective Robeson plots. This excellent separation performance makes ion gels a promising class of material in future gas separation membranes.

This chapter is an extension of the previous work to explore the application of triblock copolymer ion gels for CO_2 separations. The gas separation performance of two block copolymer ion gel systems were examined for CO_2/N_2 and CO_2/CH_4 gas pairs. The ion gels were formed by self-assembly of 10-15 wt% poly(styrene-*b*-ethylene oxide-*b*-styrene) (SOS) and poly(styrene-*b*-methyl methacrylate-*b*-styrene) (SMS) triblock copolymers in the ionic liquid 1-ethyl-3-methylimidazolium bis(trifluoromethyl-sulfonyl)amide ([EMI][TFSA]), via association of the insoluble polystyrene end-blocks. As poly(ethylene oxide) (PEO) and poly(methyl methacrylate) (PMMA) are more commonly used polymers, the synthesis of the copolymers are much easier to achieve. Both ion gels show liquid-like gas permeability but different selectivity for the same gas pair. These two systems are compared with the previous results on SILS gels to explore the effect of mid-block identity on gas separation performance. Furthermore, we

employed a pressure-decay method to analyze the effect of polymer type on gas separation by measuring the gas solubility of mid-block homopolymer/IL mixtures. The materials design consideration of the block copolymer ion gels are also discussed at the end of the chapter.

3.2 Experimental Methods

Chemicals and Materials

All reagents were used as received unless otherwise noted. Lithium bis(trifluoromethylsulphonyl)amide (LiTFSA) was purchased from 3M and 1-ethyl-3-methylimidazolium bromide ([EMI][Br]) was purchased from IoLiTec Inc. Poly(ethylene oxide) (PEO, M_n = 35 kDa, $Đ$ = 1.04) was purchased from Sigma-Aldrich and purified by precipitation in hexanes 4 times. Poly(methyl methacrylate) (PMMA, M_n = 100 kDa, $Đ$ = 1.10) was previously synthesized by Ilan Zeroni. The SMS (18-86-18) and SOS(3-35-3) triblock copolymers, provided by Sipei Zhang, were previously synthesized via atom transfer radical polymerization (ATRP) and reversible addition-fragmentation chain transfer polymerization (RAFT), respectively. The numbers in parentheses indicate the number-average block molecular weights in kDa. The synthetic details of the SMS triblock copolymer was described in a previous report.[50] PS-PIL-PS (4-252-4) was used as a reference material for comparing the gas separation performances. The synthesis and characterization details for SILS were described in Chapter 2. Table 1 lists the molecular characteristics of all these polymers.

A poly(vinylidene fluoride) (PVDF) membrane support (product# HVHP04700) was purchased from Millipore. This hydrophobic membrane has a nominal porosity of 75% and pore size of 0.45 microns. Gas cylinders of CO_2 (99.99% purity), CH_4 (99.95% purity) and N_2 (99.99% purity) used in this study were purchased from Minneapolis Oxygen Corporation.

Polymer synthesis and characterization

The synthetic details of SOS(3-35-3) triblock copolymer is provided here. It was synthesized via RAFT using the 35kDa PEO homopolymer as the precursor (Scheme 3.1). The chain transfer agent (CTA), (*S*)-1-dodecyl-(*S'*)-(α, α'-dimethyl-α"-acetic acid) trithiocarbonate, was synthesized by Dr. Chun Liu following a previously reported procedure.[51]

Scheme 3.1 Synthetic route to SOS triblock copolymer

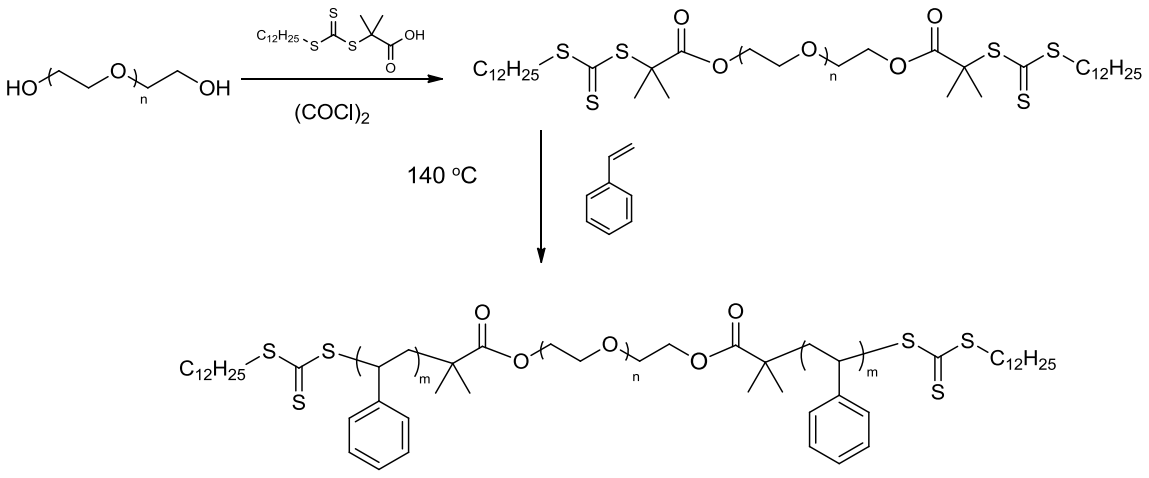

First, the chain transfer agent was attached to the PEO precursor on both ends. CTA (1.60 g, 4.40 mmol) was mixed with excess oxalyl chloride (4.4 mL) in 10 mL of dry CH_2Cl_2 under argon atmosphere and stirred at room temperature for 2 hours. Excess reactants were then removed under vacuum and the CTA was redissolved in 50 mL of CH_2Cl_2. Subsequently, purified PEO (15.1 g, 0.43 mmol) and another 60 mL of CH_2Cl_2 was added to the solution followed by argon bubbling for 30 minutes. The reaction was allowed to proceed for 36 hours, after which the mixture was precipitated in hexanes 4 times to obtain the PEO macroinitiaor (CTA-PEO-CTA). In the second step, CTA-PEO-CTA was used to grow polystyrene end-blocks. CTA-PEO-CTA (7.52g, 0.215 mmol) and purified styrene (10.35g, 0.100 mol) were mixed in a 250-mL Schlenk flask, degassed via three freeze-pump-thaw cycles, and heated in an oil bath at 70 ℃ to obtain a homogeneous solution. The solution was then heated to 140 ℃ and polymerization was allowed to proceed for 28 minutes, followed by quenching with liquid N_2. The reaction mixture was diluted in ca. 100 mL of CH_2Cl_2 and precipitated into n-hexane four times. The product was then collected and dried in a vacuum oven at 50 ℃ for 24 hr. Each step of synthesis was characterized using the ^1H NMR spectroscopy (Figure 3.1) and the molecular weight characteritics was analyzed using SEC (Figure 3.2).

(a) CTA-PEO-CTA

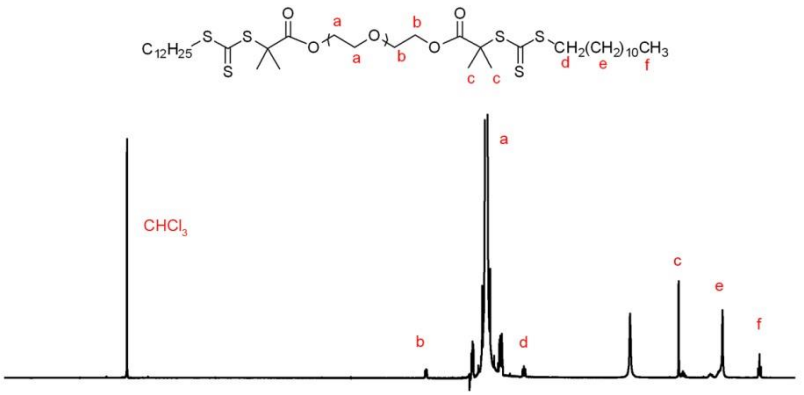

(b) PS-PEO-PS (3-35-3)

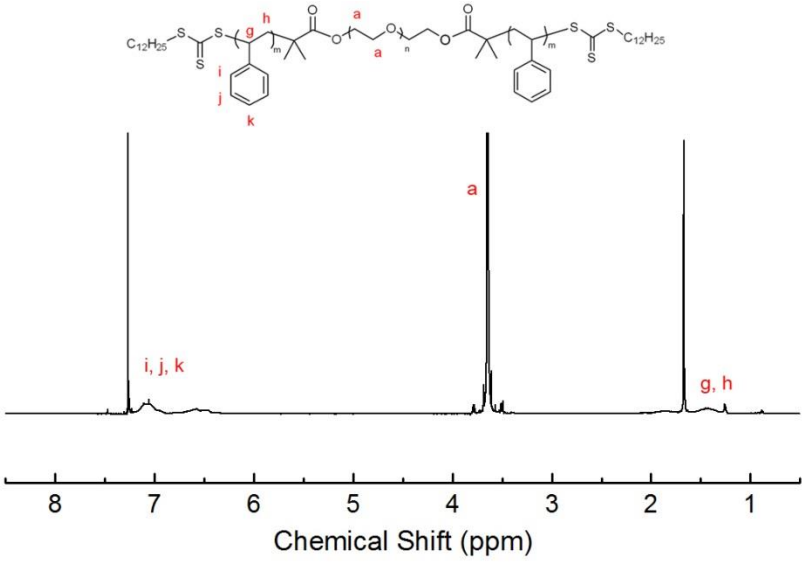

Figure 3.1 ^{1}H NMR spectra (500 MHz, in $CDCl_3$) of (a) CTA-PEO-CTA, and (b) PS-PEO-PS (3-35-3) triblock copolymer.

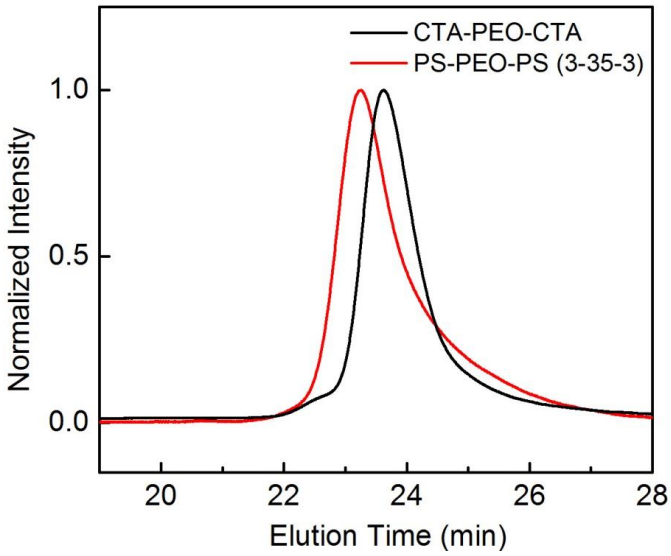

Figure 3.2 SEC traces of PEO macroinitiator and PS-PEO-PS (3-35-3)

Table 3.1 Molecular characteristics of polymers used in this study[a]

Materials	Code	Molecular Weight (kDa)	Dispersity
PS-PMMA-PS	SMS	18-86-18	1.21
PS-PEO-PS	SOS	3-35-3	1.03
PS-PIL-PS	SILS	4-252-4	1.21
PEO		35	1.04
PMMA		100	1.10

[a] Molecular weights were determined by a combination of size exclusion chromatography (SEC) and ^{1}H NMR spectroscopy; the molecular weights of the homopolymers were determined by SEC with a light scattering detector (Wyatt Dawn).

Sample preparation: ionic liquids and supported ion gel membranes

The [EMI][TFSA] used in this study was prepared through an anion exchange reaction between [EMI][Br] and LiTFSA following the same procedure described in Chapter 2.[52] The ionic liquid was stored in a vacuum desiccator to avoid water absorption. [EMI][TFSA]/homopolymer mixtures for solubility tests were prepared using a solvent-casting method. Polymer and ionic liquids were mixed at the desired weight ratio and dissolved in methylene chloride. After most of the solvent were removed under N_2 purge, the sample was placed in a desiccator under dynamic vacuum and stirred overnight.

Stock solutions for membrane casting were prepared by dissolving the triblock copolymers and [EMI][TFSA] at a desired weight ratio in a cosolvent. Tetrahydrofuran was used as the cosolvent for SMS ion gels, and actone was used for SOS. The weight ratio of cosolvent to IL + polymer was kept at roughly 5:1. The solution was then filtered through a 0.45 micron poly(tetrafluoroethylene) filter before use. The supported ion gel membranes were prepared by filling a porous PVDF support with ion gels using a solvent-casting method using a home-made stainless steel container. A porous PVDF membrane support wetted by the cosolvent was clamped at the bottom of the container. After ca. 1.8 g of stock solution was added into the container, a nitrogen purge was used to accelerate solvent evaporation. After most of the cosolvent evaporated, the membranes were placed in a vacuum oven at 40 ℃ for 1 day and then annealed at 90 ℃ for 2 hours. The membranes were transferred to a Teflon cutting board and cut into circular samples with 25 mm diameter. The membrane thickness, about 130 μm and close to that of the

membrane support, was measured with calipers. The detailed procedures for membrane preparation and a description of the gas diffusion cell can be found in Chapter 2.

Gas permeation and gas solubility measurements

Gas permeation properties of the supported ion gel membranes were measured using a stainless steel gas diffusion cell with two 15 cm^3 compartments separated by the membrane. Typical experiments for both pure and mixed gas experiments were conducted at room temperature with a pressure difference of 2 atm and repeated 3 times Details for experimental procedures and data processing methods were described in Chapter 2.

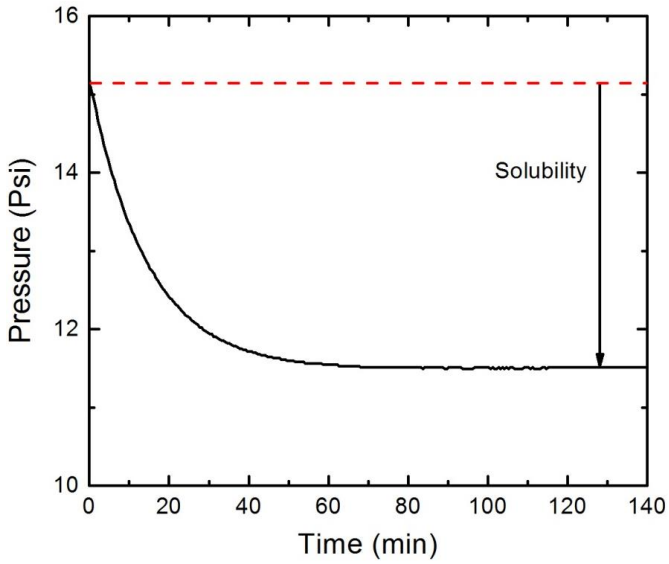

Figure 3.3 Typical raw data for a solubility test (CO_2 in neat [EMI][TFSA]): total pressure decay shows the gas solubility in the liquid.

Measurements of gas solubility in [EMI][TFSA] and [EMI][TFSA]/homopolymer solutions were conducted using the same gas diffusion cell but through a different method. First, these IL and IL/polymer samples were stirred in a vacuum desiccator for

over 24 hours to remove dissolved gas. Approximately 5 g of liquid sample was then placed in the bottom of the cell together with a stir bar. Before the experiments started, the sample in the cell was flushed with test gas at 15 psi for 2 hours to allow the liquid samples to saturate. An additional 15 psi of test gas was quickly charged into the diffusion cell and then the cell was sealed immediately. Simultaneously, data collection was started and pressure drop was measured over time. Typically, equilibrium can be reached after approximately 2 hours and the total amount of gas absorbed into the sample is used to calculate gas solubility. Figure 3.3 shows the typical raw data of a pressure decay experiment.

3.3 Results and discussions

3.3.1 Gas permeation properties

In this study, the gas permeation properties of SMS ion gel were measured at two polymer concentrations of 10 wt% and 15 wt%, and SOS ion gel measured at 15 wt%. Table 3.2 shows all the permeation results of these block copolymer ion gels, and the previously reported data of neat [EMI][TFSA] and 15 wt% SILS gel are included for comparison. All these ion gels exhibited good gas transport properties, with $P_{CO2} > 700$ barrers, similar to the value for the SILS gel. More interestingly, the gas permeability of both N_2 and CH_4 were found to be strongly dependent on the polymer midblock. For example, 15 wt% SMS ion gel shows a N_2 permeability of 35 barrers and CH_4 permeability of 66 barrers, so the ideal selectivity is 24 for CO_2/N_2 and 13 for CO_2/CH_4 (Figure 2). The 10 wt% samples were found to be of slightly higher permeability and

similar selectivity. These selectivity results of SMS gels are close to the reported values of neat [EMI][TFSA]. On the other hand, the 15 wt% SOS ion gel shows a very different performance: 17 barrers for N_2 and 32 barrers for CH_4, both of which are much lower than the permeability of neat [EMI][TFSA]. In consequence, the SOS gel was found to have higher ideal selectivity than neat [EMI][TFSA] for both CO_2/N_2 and CO_2/CH_4 gas pairs, similar to the SILS gel. In these cases, ion gels possess a superior gas separation performance when the polymer mid-blocks are PEO or PIL. This midblock effect will be discussed later in more detail.

Table 3.2 Pure gas permeation properties of ionic liquids and ion gels

Material	Pure gas permeability (barrers)			Ideal selectivity	
	CO_2	N_2	CH_4	CO_2/N_2	CO_2/CH_4
[EMI][TFSA][a]	1000	44	90	22	11
10 wt% SMS	870	40	76	22	11
15 wt% SMS	840	35	66	24	13
15 wt% SOS	710	17	32	42	22
15 wt% SILS[a]	980	25	52	39	19

[a] Data of [EMI][TFSA] and 15 % SILS ion gel are from Ref 46 and Chapter 2

Table 3.3 Mixed gas permeation properties of 15 wt% ion gels[a]

Materials	Mixed gas permeability (barrers)				Mixed gas selectivity	
	$CO_2(N_2)$	$CO_2(CH_4)$	$N_2(CO_2)$	$CH_4(CO_2)$	CO_2/N_2	CO_2/CH_4
15 wt% SMS	820	840	37	69	22	12
15 wt% SOS	740	730	19	35	39	21
15 wt% SILS[b]	1030	1040	26	51	40	20

[a] The mixed gas permeability is measured in a 50/50 mixture with a background gas (listed in brackets)

[b] Data of SILS ion gel are from Chapter 2

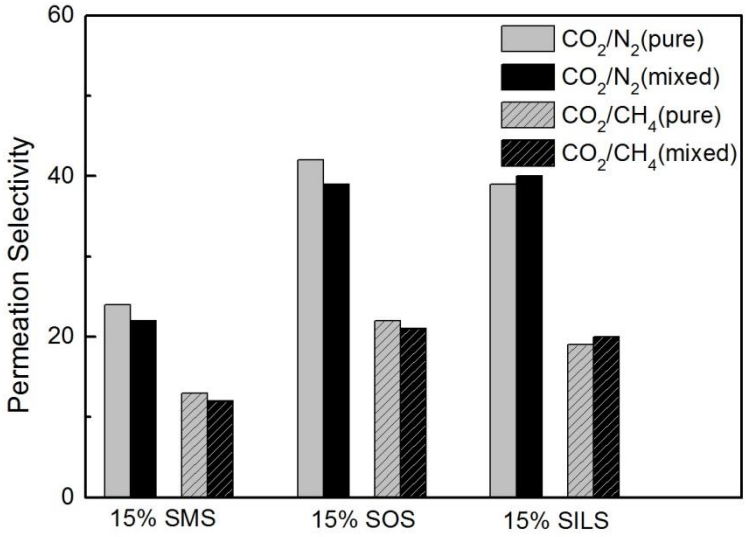

Figure 3.4 Pure and mixed gas selectivity for CO_2/N_2 and CO_2/CH_4 gas pairs of three different ion gel systems: SMS, SILS and SOS (polymer concentrations are 15 wt%)

While these ideal selectivities are significant, polymeric CO_2 separation membranes may suffer significant selectivity loss under mixed gas operations.[53–58] This is thought to be due both to the plasticization caused by dissolved CO_2 in the polymer, which decreases the diffusivity ratio, and to competitive absorption between CO_2 and other gases, which decreases the solubility ratio.[57,59] However, as is shown in Table 3.3, the permeability data from mixed gas experiments on these SILMs are almost the same as those in pure gas experiments: the ideal selectivity is essentially the same as mixed gas selectivity at 30 psi. The reason why there is no selectivity loss is straightforward to understand: because the gels have liquid-like properties, their selectivity stems not from an altered ratio of diffusivities, but principally from the solubility ratio of ionic liquids, which is not significantly affected when the gels are exposed to a gas mixture at low pressures. Similar results have also been observed in membranes based on pure ionic liquids.[60]

It is necessary to point out that block copolymer ion gels may not be able to avoid selectivity losses in mixed gas operation at higher pressures. Brennecke and co-workers have discovered that the presence of CO_2 may enhance the solubility of a less soluble gas such as O_2 and CH_4 in an imidazolium-based ionic liquid.[61] However, we have not found any literature report studying this effect on [EMI][TFSA]. A more recent work by Simons et al. also showed that polymerized ionic liquids with pendant imidazolium cations may effectively resist the plasticization due to the reversible swelling of the polymers by CO_2.[62] Therefore, the future researcher should also examine the gas separation performance of ion gels at higher pressure drops.

3.3.2 Gas solubility studies

Block copolymer ion gels are formed by self-assembly of ABA-triblock copolymers in an ionic liquid that can selectively dissolve the mid-block B. In both SMS and SOS ion gels, the insoluble polystyrene (PS) end-blocks aggregate into glassy polymer cores interconnected by the mid-blocks (PEO, PMMA) swollen in ionic liquid.[63] From the viewpoint of gas permeation, the diffusivity of gas molecules in glassy polymer cores (~10^{-10} cm^2sec^{-1}) is approximately four orders of magnitude lower than in ionic liquids (~10^{-6} cm^2sec^{-1}).[60,64] Therefore, an ion gel can be considered as a network structure composed of glassy crosslinks (PS cores), which mainly provide the mechanical support to ion gels, and polymer mid-block/ionic liquid mixture, which provide the permeation path for gas molecules.[65]

As mentioned earlier, the gas separation performance of ion gel, specifically the selectivity α, is found to be strongly dependent on mid-block identity. Since the gas permeation phase in ion gel is the mid-block/[EMI][TFSA] mixture, it is important to understand the effect of different homopolymers on the gas solubility in IL solutions. To our knowledge, although there has been extensive research on gas solubility in neat ionic liquids, there have been few reports concerning the influence that polymers can exert on IL gas solubility. Here, we report the gas solubility of PEO/[EMI][TFSA] (13.2 wt%) and PMMA/[EMI][TFSA] (11.2 wt%), in comparison with neat [EMI][TFSA]. The homopolymer weight fractions are specifically chosen to match the mid-block concentrations in 15 wt% ion gels. All the gas solubility measurements were conducted via a pressure decay method.

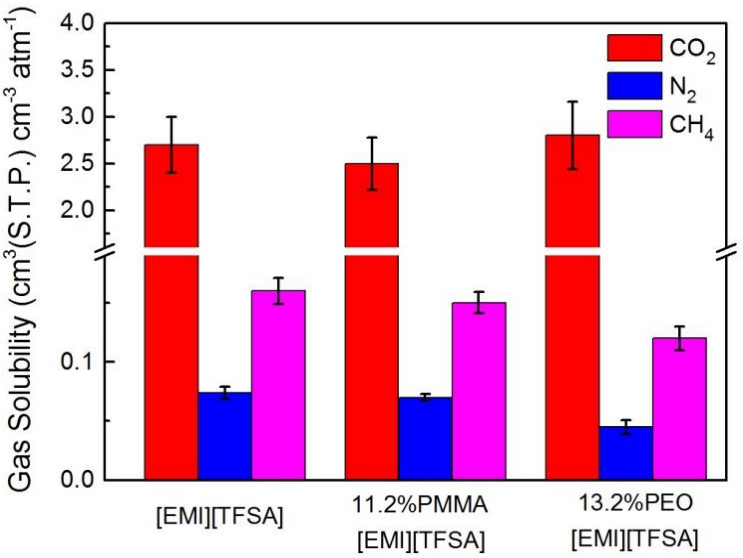

Figure 3.5 Gas solubility of CO_2, N_2 and CH_4 in [EMI][TFSA] and mixtures of [EMI][TFSA] with PMMA and PEO homopolymers, respectively

Figure 3.5 shows the gas solubility of CO_2, N_2, and CH_4 in neat [EMI][TFSA] and homopolymer/[EMI][TFSA] mixtures. The CO_2, N_2 and CH_4 solubilities are found to be 2.6, 0.074 and 0.16 cm^3 (S.T.P.) cm^{-3} atm^{-1} in neat [EMI][TFSA], respectively, which are consistent with values in a previous report.[66] Moreover, CO_2 solubility in IL solutions is found to be not significantly affected when blended with PEO or PMMA homopolymers. However, for PEO/[EMI][TFSA] solutions both the N_2 and CH_4 solubilities are lower than in neat [EMI][TFSA], while the solubility of CO_2 is unchanged. Consequently, the ideal solubility ratio (S_i/S_j in equation 3.2) is increased by 70% for CO_2/N_2 and 45% for CO_2/CH_4 gas pair when [EMI][TFSA] is blended with PEO. In contrast, the N_2 and CH_4 solubility in PMMA/[EMI][TFSA] solution are very close to those of neat [EMI][TFSA], which leads to a solubility ratio essentially the same as neat [EMI][TFSA] for both gas pairs. This important result clearly shows that for IL/polymer mixtures, the gas solubility

as well as solubility ratio is strongly dependent on the type of polymer added. The fact that PEO can enhance the separation performance of ILs is not unexpected, as PEO itself has been known to exhibit both good CO_2 solubility and higher solubility selectivities for CO_2/CH_4 and CO_2/N_2.[8] Additionally, oligomers and polymers of ethylene oxide have also been previously incorporated into IL or IL-related composite materials to increase CO_2 uptake.[67,68]

As can be seen in Figure 3.6, PEO/[EMI][TFSA] exhibits a much higher solubility ratio than both neat [EMI][TFSA] and the PMMA/[EMI][TFSA] mixture. Moreover, this solubility ratio difference also qualitatively agrees with the selectivity difference in their corresponding block copolymer ion gels, which supports the inference that midblock/IL mixture constitutes the gas permeation phase in an ion gel. It also shows that the gas separation performance of ion gels can be readily altered by using different polymers.

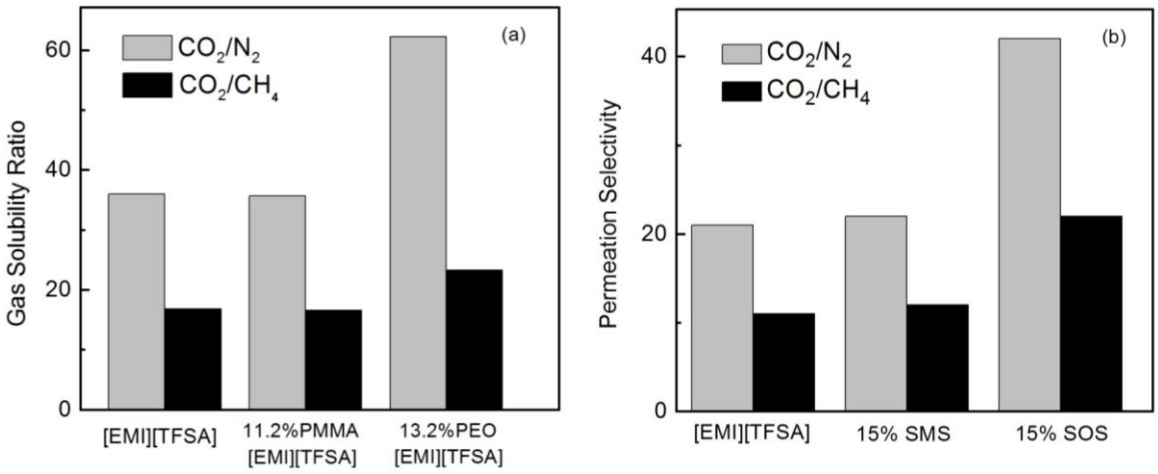

Figure 3.6 (a) Gas solubility ratio for CO_2/N_2 and CO_2/CH_4 gas pairs in [EMI][TFSA], blends of [EMI][TFSA] with PMMA and PEO homopolymers., and (b) pure gas selectivity of [EMI][TFSA] and corresponding 15 wt% ion gel systems.

3.3.3 Robeson plot comparison and materials design consideration

The gas separation properties of ion gels can be compared with other existing membranes on a Robeson plot,[17,19] a widely used metric to evaluate gas separation membrane performance. On this chart, the real selectivity of a gas pair is plotted against permeability of the more permeable gas on a log-log scale. The empirical "upper bound" on this plot, which shows the well-known flux/selectivity tradeoff in membrane separations, approximates the best selectivity/permeability combination of existing polymer membranes.[20] As shown in Figure 3.7, the separation performance of the 15 wt% ion gels are all located in the high permeability region (CO_2 permeability > 700 barrers) on both the CO_2/N_2 and CO_2/CH_4 plots. Specifically, the performances of the SOS and SILS gels are located above the upper bound for CO_2/N_2 and close to the upper bound for CO_2/CH_4. These promising results highlight the future potential of ion gels in CO_2 separations.

The favorable separation performance of ion gels can be compared with a previous report of chemically cross-linked PIL composite materials, also shown in Figure 3.7.[46] By incorporating 20% of free IL into a crosslinked PIL matrix, this composite material achieved an enhanced CO_2 separation of ~50 barrers with a CO_2/CH_4 selectivity of 39 and CO_2/N_2 selectivity of 32. As block copolymer ion gels contain more than 85% free IL in the system, the CO_2 permeability is therefore more than one order of magnitude higher than the PIL composites. However, presumably these physically crosslinked ion gels are not as robust as the chemically crosslinked materials.

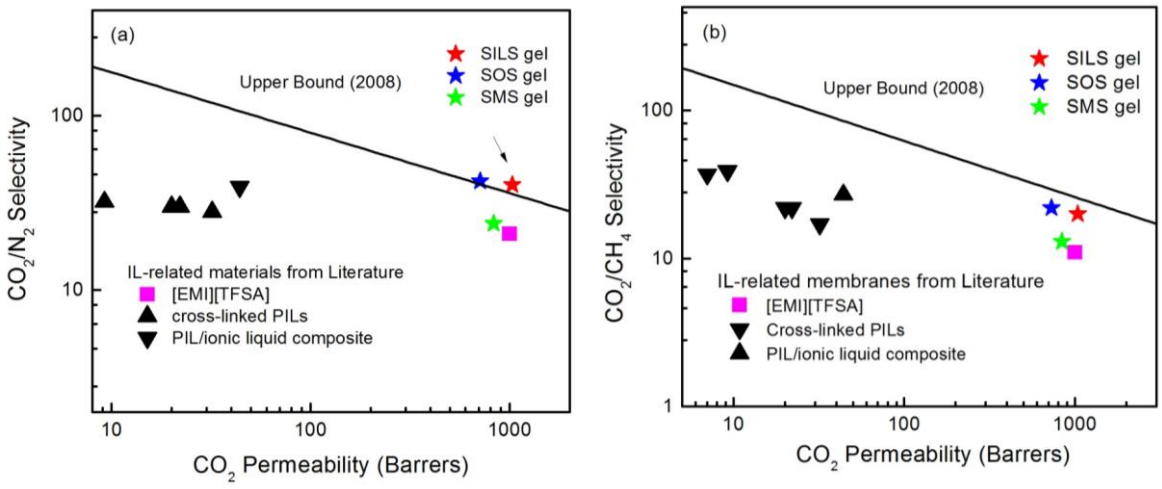

Figure 3.7 Comparison of gas separation performance for various ionic liquid-related separation materials on Robeson Plot (a) CO_2/N_2, and (b) CO_2/CH_4. Data for the materials except ion gels are from Refs 44-46. Upper bounds are adapted from original Robeson Plots (Refs. 17, 19).

Through comparison with other materials on Robeson plots, we have demonstrated the viability of using block copolymer ion gels as high-performance selective materials in CO_2 separation. The good separation properties of ion gels can be attributed to two primary reasons. First, by using PEO and PIL as the mid-block, the selectivity of ion gels have been increased by a factor of 2 over the corresponding neat ionic liquid [EMI][TFSA]. This mid-block effect is confirmed by our gas solubility measurements. Second, the rapid gas transport properties of ion gel is due to the fact that these gels contain a very high fraction of free ionic liquids (≥ 85%), and if we consider the gas permeation phase to be composed of dissolved mid-block in IL, the combined weight fraction is even higher than 95%. By incorporating high fractions of IL into the materials,

these gels exhibit liquid-like gas transport properties in solid-state materials. In a very recent report, a similar strategy using poly(vinylidene fluoride-*co*-hexafluoropropylene) (PVDF-HFP), a fluoroelastomer, was employed to develop a physically cross-linked ion gel for gas separation. As only 20 wt% copolymer was added to solidify the ionic liquids, this achieved a CO_2 permeability of ca. 550 barrers, similar to the results in this study.

So far, this proof-of-concept study with ion gels has successfully shown promising performance for gas separation applications. One of the limiting factors here is the thickness of the membrane. However, this may not be a significant disadvantage due to the high permeability. To explore this point in more detail, we can compare the mass transfer resistance in the membrane with that in the adjacent gas. If we assume that the membrane had a thickness of 100 nm and a permeability of 1000 barrers, then the resistance after unit conversion is this thickness divided by this permeability, or about 1 s/cm. The resistance in the gas is also due to a boundary layer thickness, typically about 0.1 cm, divided by a diffusion coefficient, about 0.1 cm^2/s, or about 1 s/cm. If the gas pressure is higher, the gas diffusion will be lower and the gas phase resistance will be higher still. Thus there may be little advantage to making still more permeable membranes, because this higher permeability will be eclipsed by the resistance from this boundary layer, which is also known as the concentration polarization.

The membranes developed here would benefit from greater mechanical strength. Because the storage moduli of these gels are only several kilopascals, they will be very hard to operate at industrially used pressures (> 50 bars). Therefore, it is highly desirable

to develop a material with greater mechanical strength, while keeping the attractive gas transport properties of ion gels.

3.4 Conclusions

In this chapter, gas separation performance of two ion gel systems with CO_2/N_2 and CO_2/CH_4 gas pairs were tested using supported ion gel membranes. Due to the high free ionic liuqid concentration in the system, both SMS and SOS ion gels show very high CO_2 permeability. Moreover, the SOS gel exhibits a much higher selectivity for both gas pairs than both the SMS gel and neat [EMI][TFSA], indicating that the gas separation performance of ion gels can be significantly influenced by the mid-block identity. This midblock effect is further confirmed by gas solubility experiments on homopolymer/[EMI][TFSA] solutions. Added PEO is found to significantly increase the solubility ratio of IL solutions for both gas pairs. Robeson plot comparisons indicate promising separation performance of ion gels when compared with other IL-based materials, and the current "upper bound" for both CO_2/N_2 and CO_2/CH_4. Therefore, this class of material shows potential for future applications in membrane separation of CO_2 from other gases.

3.5 Reference

(1) Schrag, D. P. *Science* **2007**, *315*, 812–813.

(2) Chu, S. *Science* **2009**, *325*, 1599.

(3) Hammond, G. P.; Akwe, S. S. O. *Int. J. Energ. Res.* **2007**, *31*, 1180–1201.

(4) Luby, P.; Susta, M. R. *Power* **2007**, *151*, 40,42,44–48,50.

(5) *Membrane Separations Technology: Principles and Applications*; Noble, R. D.; Stern, S. A., Eds.; 2nd Ed.; Elsevier, 1995; p. 718 pp.

(6) Baker, R. W. *Ind. Eng. Chem. Res.* **2002**, *41*, 1393–1411.

(7) Baker, R. W.; Lokhandwala, K. *Ind. Eng. Chem. Res.* **2008**, *47*, 2109–2121.

(8) Lin, H.; Freeman, B. D. *J. Mol. Struct.* **2005**, *739*, 57–74.

(9) Rochelle, G. T. *Science* **2009**, *325*, 1652–1654.

(10) Freeman, B. D.; Pinnau, I. *ACS Symp. Ser.* **1999**, *733*, 1–27.

(11) Spillman, R. W. *Chem. Eng. Prog.* **1989**, *85*, 41–62.

(12) Balat, H.; Oz, C. *Energy Exploration & Exploitation* **2007**, *25*, 357–392.

(13) Babcock, R. E.; Spillman, R. W.; Goddin, C. S.; Cooley, T. E. *Energy Progress* **1988**, *8*, 135–142.

(14) Koros, W. J.; Fleming, G. K.; Jordan, S. M.; Kim, T. H.; Hoehn, H. H. *Prog. Polym. Sci.* **1988**, *13*, 339–401.

(15) Gin, D. L.; Noble, R. D. *Science* **2011**, *332*, 674–676.

(16) Koros, W. J.; Fleming, G. K. *J. Membr. Sci.* **1993**, *83*, 1–80.

(17) Robeson, L. M. *J. Membr. Sci.* **1991**, *62*, 165–185.

(18) Robeson, L. M.; Smith, C. D.; Langsam, M. *J. Membr. Sci.* **1997**, *132*, 33–54.

(19) Robeson, L. M. *J. Membr. Sci.* **2008**, *320*, 390–400.

(20) Freeman, B. D. *Macromolecules* **1999**, *32*, 375–380.

(21) Stern, S. A.; Shah, V. M.; Hardy, B. J. *Journal of Polymer Science, Part B: Polymer Physics* **1987**, *25*, 1263–1298.

(22) Stern, S. A. *J. Membr. Sci.* **1994**, *94*, 1–65.

(23) Baltus, R. E.; Counce, R. M.; Culbertson, B. H.; Luo, H.; DePaoli, D. W.; Dai, S.; Duckworth, D. C. *Sep. Sci. Technol.* **2005**, *40*, 525–541.

(24) Baltus, R. E.; Culbertson, B. H.; Dai, S.; Luo, H.; DePaoli, D. W. *J. Phys. Chem. B* **2004**, *108*, 721–727.

(25) Neves, L. A.; Crespo, J. G.; Coelhoso, I. M. *J. Membr. Sci.* **2010**, *357*, 160–170.

(26) Wasserscheid, P.; Welton, T.; Editors. *Ionic Liquids in Synthesis.*; Wiley-VCH Verlag GmbH & Co. KGaA, 2003; p. 364 pp.

(27) Welton, T. *Chem. Rev.* **1999**, *99*, 2071–2084.

(28) Earle, M. J.; Seddon, K. R. *Pure Appl. Chem.* **2000**, *72*, 1391–1398.

(29) Brennecke, J. F.; Gurkan, B. E. *J. Phys. Chem. Lett.* **2010**, *1*, 3459–3464.

(30) Anderson, J. L.; Dixon, J. K.; Brennecke, J. F. *Acc. Chem. Res.* **2007**, *40*, 1208–1216.

(31) Scovazzo, P.; Kieft, J.; Finan, D. A.; Koval, C.; Dubois, D.; Noble, R. D. *J. Membr. Sci.* **2004**, *238*, 57–63.

(32) Bara, J. E.; Camper, D. E.; Gin, D. L.; Noble, R. D. *Acc. Chem. Res.* **2010**, *43*, 152–159.

(33) Lozano, L. J.; Godinez, C.; De A. P., los R.; Hernandez-Fernandez, F. J.; Sanchez-Segado, S.; Alguacil, F. J. *J. Membr. Sci.* **2011**, *376*, 1–14.

(34) Bates, E. D.; Mayton, R. D.; Ntai, I.; Davis Jr., J. H. *J. Am. Chem. Soc.* **2002**, *124*, 926–927.

(35) Camper, D.; Bara, J. E.; Koval, C.; Noble, R. D. *Ind. Eng. Chem. Res.* **2006**, *45*, 6279–6283.

(36) Carlisle, T. K.; Bara, J. E.; Gabriel, C. J.; Noble, R. D.; Gin, D. L. *Ind. Eng. Chem. Res.* **2008**, *47*, 7005–7012.

(37) Smith, G. D.; Borodin, O.; Li, L.; Kim, H.; Liu, Q.; Bara, J. E.; Gin, D. L.; Nobel, R. *Phys. Chem. Chem. Phys.* **2008**, *10*, 6301–6312.

(38) Ueki, T.; Watanabe, M. *Macromolecules* **2008**, *41*, 3739–3749.

(39) Lodge, T. P. *Science* **2008**, *321*, 50–51.

(40) Lu, J.; Yan, F.; Texter, J. *Prog. Polym. Sci.* **2009**, *34*, 431–448.

(41) Yuan, J.; Antonietti, M. *Polymer* **2011**, *52*, 1469–1482.

(42) He, Y.; Li, Z.; Simone, P.; Lodge, T. P. *J. Am. Chem. Soc.* **2006**, *128*, 2745–2750.

(43) Voss, B. A.; Bara, J. E.; Gin, D. L.; Noble, R. D. *Chem. Mater.* **2009**, *21*, 3027–3029.

(44) Bara, J. E.; Lessmann, S.; Gabriel, C. J.; Hatakeyama, E. S.; Noble, R. D.; Gin, D. L. *Ind. Eng. Chem. Res.* **2007**, *46*, 5397–5404.

(45) Bara, J. E.; Gabriel, C. J.; Hatakeyama, E. S.; Carlisle, T. K.; Lessmann, S.; Noble, R. D.; Gin, D. L. *J. Membr. Sci.* **2008**, *321*, 3–7.

(46) Bara, J. E.; Hatakeyama, E. S.; Gin, D. L.; Noble, R. D. *Polym. Adv. Technol.* **2008**, *19*, 1415–1420.

(47) Bara, J. E.; Noble, R. D.; Gin, D. L. *Ind. Eng. Chem. Res.* **2009**, *48*, 4607–4610.

(48) Jansen, J. C.; Friess, K.; Clarizia, G.; Schauer, J.; Izak, P. *Macromolecules* **2011**, *44*, 39–45.

(49) Gu, Y.; Lodge, T. P. *Macromolecules* **2011**, *44*, 1732–1736.

(50) Zhang, S.; Lee, K. H.; Frisbie, C. D.; Lodge, T. P. *Macromolecules* **2011**, *44*, 940–949.

(51) Mayadunne, R. T. A.; Rizzardo, E.; Chiefari, J.; Krstina, J.; Moad, G.; Postma, A.; Thang, S. H. *Macromolecules* **2000**, *33*, 243–245.

(52) Bai, Z.; Lodge, T. P. *J. Am. Chem. Soc.* **2010**, *132*, 16265–16270.

(53) Visser, T.; Koops, G. H.; Wessling, M. *J. Membr. Sci.* **2005**, *252*, 265–277.

(54) Donohue, M. D.; Minhas, B. S.; Lee, S. Y. *J. Membr. Sci.* **1989**, *42*, 197–214.

(55) Wind, J. D.; Staudt-Bickel, C.; Paul, D. R.; Koros, W. J. *Ind. Eng. Chem. Res.* **2002**, *41*, 6139–6148.

(56) Neyertz, S.; Brown, D.; Pandiyan, S.; Van N. F. A., der V. *Macromolecules* **2010**, *43*, 7813–7827.

(57) Wind, J. D.; Paul, D. R.; Koros, W. J. *J. Membr. Sci.* **2004**, *228*, 227–236.

(58) Puleo, A. C.; Muruganandam, N.; Paul, D. R. *Journal of Polymer Science, Part B: Polymer Physics* **1989**, *27*, 2385–2406.

(59) Vu, D. Q.; Koros, W. J.; Miller, S. J. *Ind. Eng. Chem. Res.* **2002**, *41*, 367–380.

(60) Scovazzo, P.; Havard, D.; McShea, M.; Mixon, S.; Morgan, D. *J. Membr. Sci.* **2009**, *327*, 41–48.

(61) Hert, D. G.; Anderson, J. L.; Aki, S. N. V. K.; Brennecke, J. F. *Chem. Commun.* **2005**, 2603–2605.

(62) Simons, K.; Nijmeijer, K.; Bara, J. E.; Noble, R. D.; Wessling, M. *J. Membr. Sci.* **2010**, *360*, 202–209.

(63) He, Y.; Lodge, T. P. *Macromolecules* **2008**, *41*, 167–174.

(64) Shiflett, M. B.; Yokozeki, A. *Ind. Eng. Chem. Res.* **2005**, *44*, 4453–4464.

(65) Zhang, S.; Lee, K. H.; Sun, J.; Frisbie, C. D.; Lodge, T. P. *Macromolecules* **2011**, *44*, 8981–8989.

(66) Bara, J. E.; Carlisle, T. K.; Gabriel, C. J.; Camper, D.; Finotello, A.; Gin, D. L.; Noble, R. D. *Ind. Eng. Chem. Res.* **2009**, *48*, 2739–2751.

(67) Bara, J. E.; Gabriel, C. J.; Lessmann, S.; Carlisle, T. K.; Finotello, A.; Gin, D. L.; Noble, R. D. *Ind. Eng. Chem. Res.* **2007**, *46*, 5380–5386.

(68) Hu, X.; Tang, J.; Blasig, A.; Shen, Y.; Radosz, M. *J. Membr. Sci.* **2006**, *281*, 130–138.

Chapter 4

Toughness Enhancement of Triblock Copolymer Ion Gels via End-Block Crosslinking*

4.1 Introduction

In the preceding chapters, the block copolymer ion gels studied as CO_2 separation media were exclusively physically cross-linked systems. While these physical gels exhibit remarkable gas separation performance, they are considered as "soft materials". The stability of supported ion gel membranes is still relatively low, which limits their viability in industrial applications. Moreover, the effective membrane thickness is limited by the thickness of the PVDF support, and the actual membrane performance is also decreased due to the tortuosity of the porous support. Often, the pressure drop that a supported ion gel membrane can withstand is lower than the requirement of industrial application, such as natural gas processing (CO_2/CH_4 separation, ca. 50 atm).[1,2] Therefore, it is highly desirable to enhance the mechanical properties of block copolymer ion gels without affecting their mass transport properties. In this chapter, a strategy using

* This project is conducted in collaboration with Dr. Sipei Zhang. This chapter is reproduced in part with permission from Gu, Y.; Zhang, S.; Martinetti, L.; Lee, K. H.; McIntosh, L. D.; Frisbie, C. D.; Lodge, T. P. *J. Am. Chem. Soc.* **2013**, *135*, 9652–9655. Copyright 2013 American Chemical Society.

chemical crosslinking to enhance the mechanical properties of ion gel is demonstrated. Through just one step of chemical cross-linking of the polystyrene cores, the mechanical strength of block copolymer ion gels can be significantly enhanced without affecting the gas separation performance.

Before explaining this strategy in more detail, it is necessary to briefly discuss the difference between physically and chemically cross-linked ion gels. Depending on the nature of cross-linking junctions in the network, ion gels can be divided into physical and chemical gels. Physical gels utilize weak interactions such as phase separation, hydrogen bonding and crystallization to achieve gelation,[3–7] while chemical gels are connected by covalent bonding.[8–10] Due to the reversible nature of these non-covalent interactions, physically cross-linked ion gels provide flexibility in material processing and device production.[11,12] The mechanical and rheological properties of physical gels are also sensitive to external stimuli such as temperature change and light, which enabled further applications including electrochemical sensors and self-healing materials.[13,14] On the other hand, chemical gels are usually prepared by reaction of monomers or macromers with cross-linkable functionalities. Once the cross-linking reaction is completed, the gel structure cannot be tuned without breaking covalent bonds. Recent studies of chemically cross-linked ion gels have shown very promising results in terms of mechanical properties and ionic conductivity. For instance, Shibayama and co-workers successfully demonstrated that tetra-functional poly(ethylene glycol)-based ion gels exhibit superior toughness and high break strength (ca. 20 MPa under compression test) by adding only 3-6 wt% of polymer, and the ionic conductivity is very close to that of the pure ionic

liquid.[15–17] The advanced mechanical strength of this material is attributed to its well-defined homogeneous network structure. Additional examples including epoxy-based ion gels also show enhanced modulus at higher polymer concentrations.[18,19] However, because the gel network is "permanently" locked by the covalent bonds, chemical gels lack the tunable structure as well as processing flexibility. The key motivation of this project is to combine the reversibility of physically cross-linked ion gels with the high mechanical strength of chemical cross-linking. Such materials are anticipated to have advantages in various applications where ion gels have already shown great promises, such as gas separation and plastic electronics.

Herein we demonstrate a novel type of block copolymer ion gel with chemically cross-linkable end-blocks. This ion gel is prepared through self-assembly of poly[(styrene-*r*-vinylbenzyl azide)-*b*-ethylene oxide-*b*-(styrene-*r*-vinylbenzyl azide)] (SOS-N_3) and [EMI][TFSA]. The azide functionality was chosen to achieve chemical crosslinking as it has been previously demonstrated as a facile process. Pioneered by Bang, Hawker and coworkers, the self-cross-linking reaction of poly(vinylbenzyl azide) (PVBA) has been successfully applied to the crosslinking of polystyrene phases in various polymer systems, such as block copolymer thin-films and nanoparticle suspensions.[20–24] Narrowly distributed PVBA blocks can be synthesized through RAFT polymerization, which allows the incorporation into ABA-triblock copolymer ion gels. The cross-linkable ion gel is structurally similar to the previously studied SOS ion gel, with the only difference being that ca. 28% of the styrene units have a pendant azide functionality.[25] In such a system, the poly(styrene-*r*-vinylbenzyl azide) end-blocks will

first form physically cross-linked cores due to the incompatibility with [EMI][TFSA], whereby the azide groups in the cores can be chemically cross-linked by annealing at elevated temperatures. This is the first time both physical and chemical cross-linking is realized in the same ion gel system. A significant enhancement in toughness and ultimate strength has been achieved after thermal cross-linking, while the ionic conductivity and gas permeability remain the same. The thermo-reversibility of the ion gel before chemical cross-linking and the cross-linking reaction kinetics were also investigated.

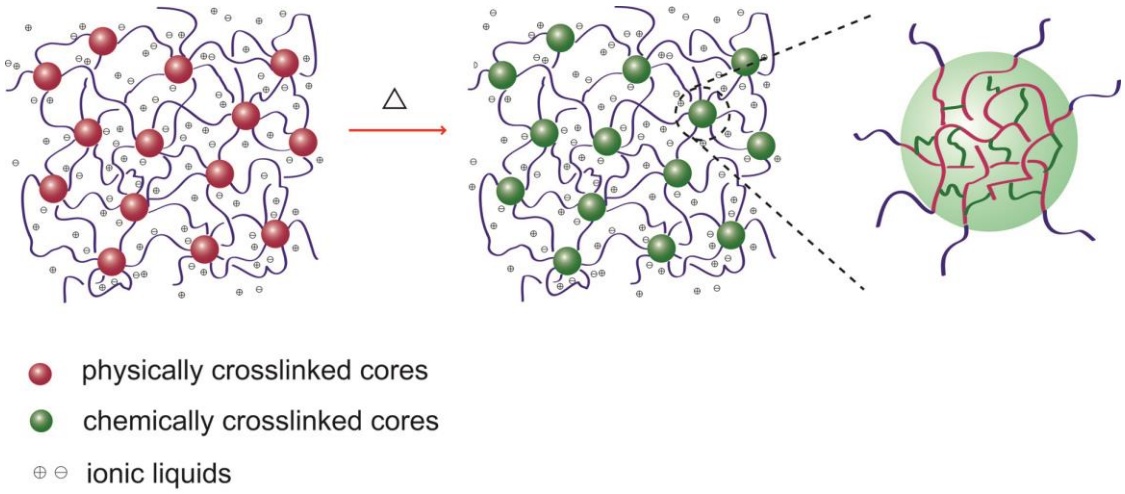

Figure 4.1 Sequential block copolymer self-assembly and chemical cross-linking of SOS-N_3 ion gels

This chapter is organized as follows. First, we describe the synthesis and characterization of the SOS and SOS-N_3 triblock copolymers. Then we discuss the cross-linking kinetics of PS-N_3, and the linear viscoelastic properties of ion gel before, during and after the cross-linking reaction. Tensile properties, gas separation performance and ionic conductivity of the SOS-N_3 ion gel were studied through comparison with the previously studied SOS/[EMI][TFSA] ion gel. Results of the comparison demonstrates

that one-step of chemical cross-linking of the cores can yield a much tougher ion gel, while the mass transport properties such as ionic conductivity and gas permeation are not affected.

4.2 Experimental methods

Chemical and materials

All reagents were used as received unless otherwise noted. Poly(ethylene oxide) (PEO) precursor (M_n = 35kDa, $Đ$ = 1.04) was purchased from Sigma-Aldrich and precipitated in hexanes 4 times. Styrene and 4-vinylbenzyl chloride (VBC) were passed through activated alumina columns prior to use. Oxalyl chloride, methyl acrylate, *n*-propylamine, tri(2-carboxyethyl)phosphine hydrochloride (TCEP) and sodium azide (NaN_3) were also purchased from Sigma-Aldrich. The chain transfer agent (CTA), (*S*)-1-dodecyl-(*S'*)-(α, α'-dimethyl-α"-acetic acid) trithiocarbonate, was synthesized by Dr. Chun Liu following a previously reported procedure.[26]

Polymer synthesis

SOS and SOS-N_3: The SOS(3.4-35-3.4) triblock copolymer was synthesized via RAFT polymerization from a PEO precursor following a reported procedure.[27] The SOS-N_3 triblock copolymer was synthesized using a combination of reversible addition-fragmentation chain transfer (RAFT) polymerization and post-polymerization reaction (see Scheme 4.1). First, the chain transfer agent (CTA), (*S*)-1-dodecyl-(*S'*)-(α, α'-dimethyl-α"-acetic acid) trithiocarbonate, was attached to a PEO precursor on both ends

following a previously established procedure.[27] In this reaction, CTA (1.62 g, 4.4 mmol) was mixed with excess oxalyl chloride (7.0 mL) in 10 mL of dry CH_2Cl_2 under argon atmosphere and stirred at room temperature for 2 hours. Excess reagents were then removed under vacuum and the CTA was redissolved in 50 mL of CH_2Cl_2. Subsequently, purified PEO (16.0 g, 0.45 mmol) and CH_2Cl_2 (60 mL) was added to the solution followed by argon bubbling for 30 minutes. The reaction was allowed to proceed for 36 hours, after which the mixture was precipitated in hexanes 4 times to obtain PEO end-capped with CTA.

Then, the CTA-PEO-CTA was used to copolymerize styrene and VBC (molar ratio 4:1) into the endblocks. CTA-PEO-CTA (10.01 g, 0.286 mmol), purified styrene (10.98 g, 0.106 mol) and VBC (4.03 g, 0.0264 mol) were mixed in a 250-mL Schlenk flask, degassed via three freeze-pump-thaw cycles, and heated in an oil bath at 70 ℃ to obtain a homogeneous solution. The solution was then heated to 140 ℃ and polymerization was allowed to proceed for 67 minutes, followed by quenching with liquid N_2. The reaction mixture was diluted in ca. 200 mL of CH_2Cl_2 and precipitated into n-hexane four times. The product was then collected and dried in a vacuum oven at 50 ℃ for two days. The trithiocarbonate end-groups of SOS-Cl were removed to prevent side reaction between NaN_3 and the thiol groups in the next step. SOS-Cl (9.60 g, 0.225 mmol) was dissolved in dry tetrahydrofuran (ca. 150 mL) in a Schlenk flask at 60 ℃ followed by bubbling with argon for 10 minutes. Subsequently, TCEP (150 mg, 5.25×10^{-4} mol) and n-propylamine (4.0 mL, 0.049 mol) were added into the flask and the reaction was allowed to proceed at room temperature for 2 hours. Methyl acrylate (9.0 mL, 0.099 mol) was injected into the

reaction flask and the mixture was stirred overnight at room temperature for the reaction to go to complete. The contents were precipitated into hexanes and the collected precipitate was dissolved again in CH_2Cl_2 and passed through a basic alumina column. Excess solvent was then removed under vacuum, and the concentrated solution was precipitated in pentane twice.

After removal of the CTA end-groups, the SOS-Cl polymer was reacted with NaN_3 to install the desired azide functionality. SOS-Cl (8.00g, 1.85×10^{-4} mol) and NaN_3 (1.25g, 0.0192 mol) were dissolved in *N*,*N*-dimethylformamide (ca. 500mL) at 60 ℃ and the reaction was stopped after stirring for 40 hours. Deionized water (ca. 5mL) was added to quench the reaction. Most of the DMF was removed using a rotary evaporator. The contents were dissolved in CH_2Cl_2 and washed with NaCl aqueous solution 3 times, followed by addition of $MgSO_4$ to dry the organic phase. Crude polymer product was obtained by precipitation in diethyl ether. Residual sodium salt was removed by dissolving the precipitate in CH_2Cl_2 and filtering the solution. The final product was obtained by precipitation in n-pentane twice. The first, second and fourth steps of the synthesis were followed by ^{1}H-NMR (Figure 4.2) and the third step was confirmed via UV-Vis spectroscopy (Figure 4.4). The dispersity (*Đ*) of the polymers was measured using size exclusion chromatography (SEC, Figure 4.3) and the molecular weights were determined by ^{1}H-NMR integration. Molecular characteristics of all polymers are listed in Table 4.1.

Scheme 4.1 Synthetic route to SOS-N_3 triblock copolymer

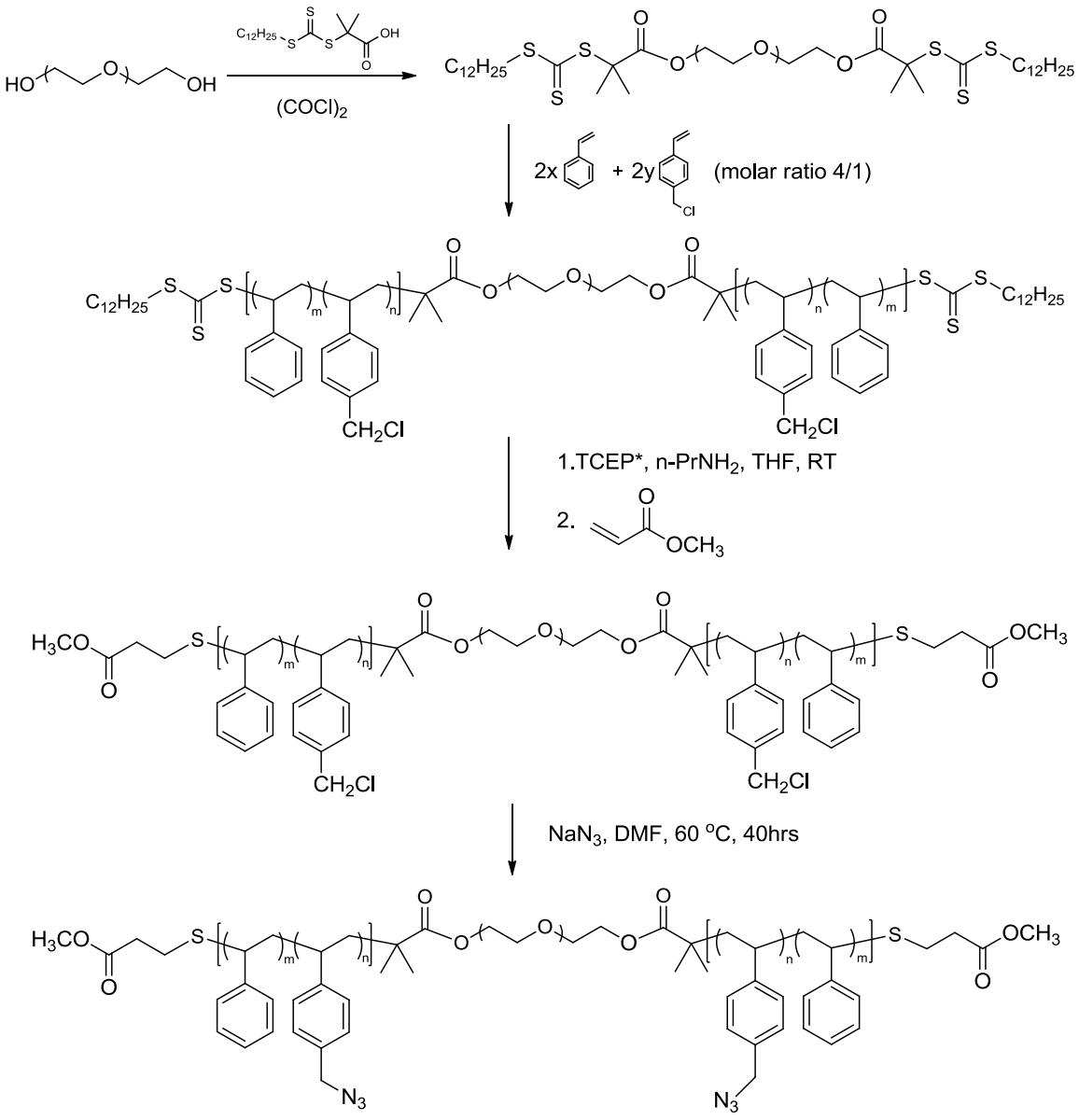

* TCEP: tri(2-carboxylethyl)phosphine hydrochloride

Table 4.1 Molecular characteristics of polymers used in this study

Polymer	$M_{n,\ PVBC/PVBA}$ (kDa)[c]	$N_{PVBC/PVBA}$	$M_{n,\ PS}$ (kDa)[c]	N_{PS}	$M_{n,\ PEO}$ (kDa)	$Đ$
SOS-N_3(3.8-35-3.8)	1.4	9	2.4	23	35	1.12
SOS-Cl no CTA	1.4	9	2.4	23	35	1.11
SOS-Cl	1.4	9	2.4	23	35	1.07
CTA-PEO-CTA					35	1.10
SOS(2.8-35-2.8)[a]			2.8	27	35	1.05
SOS(3.4-35-3.4)[b]			3.4	33	35	1.08
PS-N_3	2.7	18	6.2	60		1.43
PS-*r*-PBVC	2.7	18	6.2	60		1.15

[a] Reported in ref 25, used in comparison of ion gel shear rheology and ionic conductivity.

[b] Reported in ref 12, used in ion gels for comparison of extensional rheology.

[c] M_n determined by ^{1}H-NMR. PVBA: poly(vinylbenzyl azide). PVBC: poly(vinylbenzyl chloride).

(a) CTA-PEO-CTA

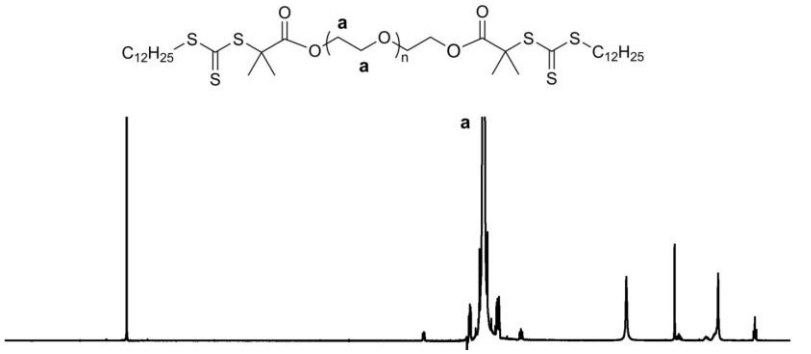

(b) SOS-Cl

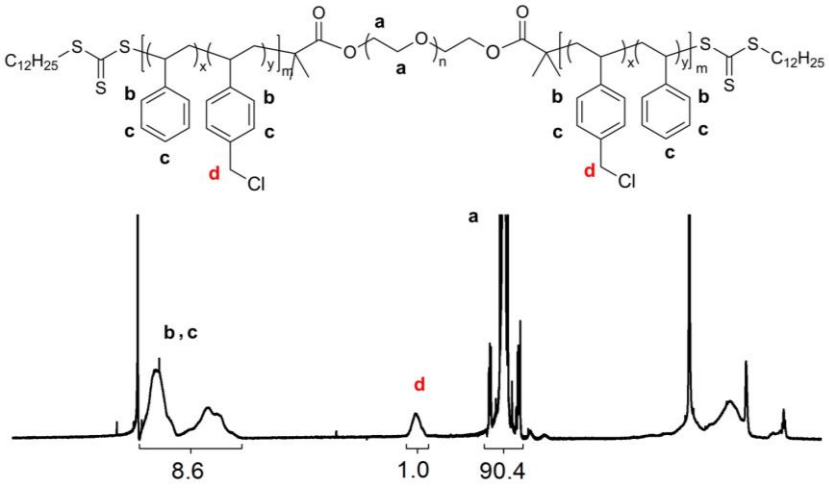

(c) SOS-N_3

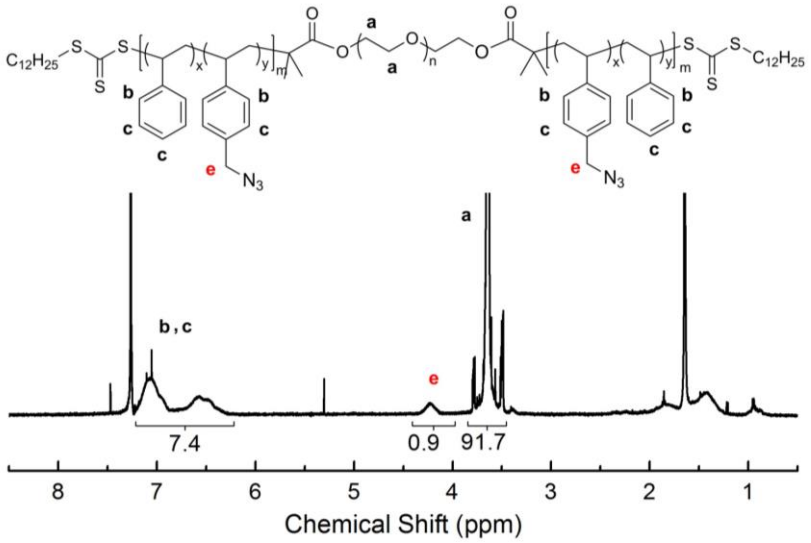

Figure 4.2. ^{1}H NMR spectra (500 MHz, in $CDCl_3$) of (a) CTA-PEO-CTA, (b) SOS-Cl, and (c) SOS-N_3

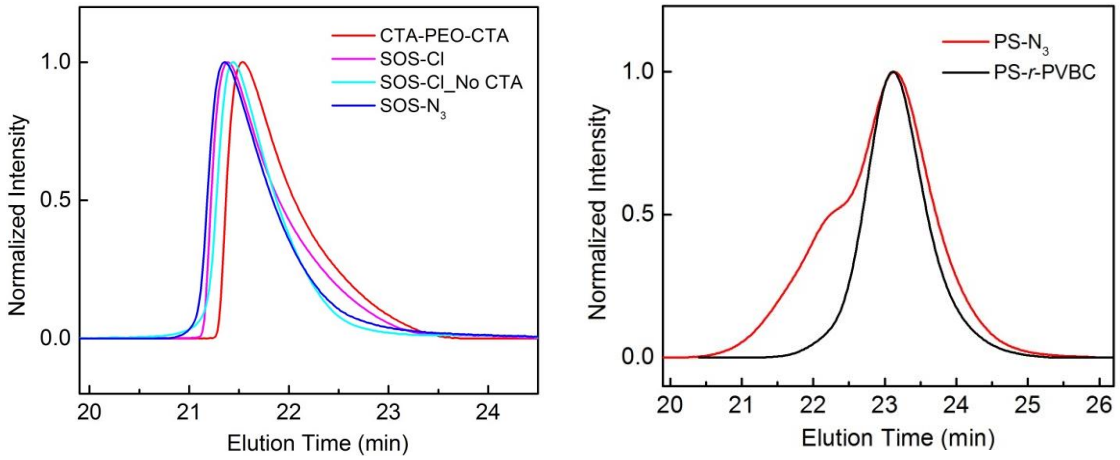

Figure 4.3 SEC traces of (a) all polymers involved in the synthesis of SOS-N_3, and (b) PS-*r*-PVBC and PS-N_3

.

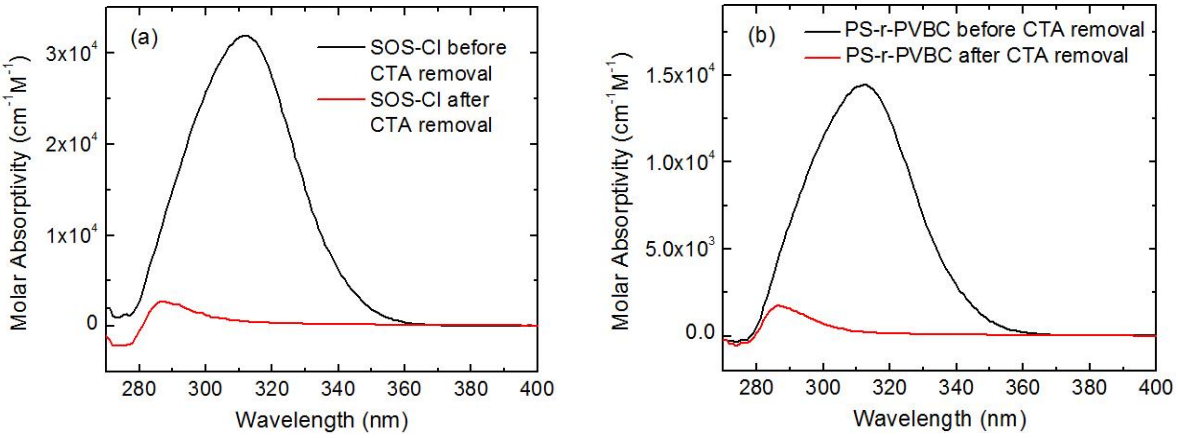

Figure 4.4 UV-Vis spectra of (a) SOS-Cl and (b) PS-*r*-PVBC before and after CTA removal

Scheme 4.2. Synthetic route to PS-N_3

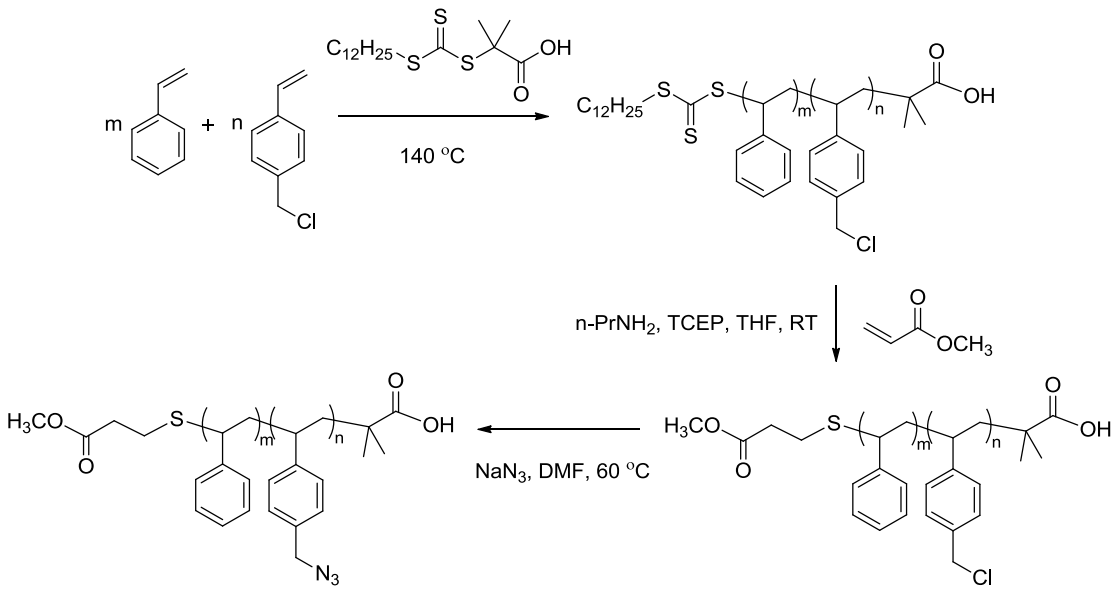

Synthesis of PS-N_3: CTA (0.374 g, 1.03×10^{-3} mol), styrene (6.25 g, 0.041 mol) and VBC (17.04 g, 0.164 mol) were mixed in a Schlenk flask and bubbled with Argon for 30 minutes. The polymerization then proceeded in bulk at 140 °C for 50 min. The contents were quenched with liquid N_2 and dissolved in CH_2Cl_2 (ca. 50 mL). The solution was then precipitated with methanol (ca. 500 mL) three times, and the product was dried in a vacuum oven at 70 °C overnight. The CTA end-groups was then removed to prevent reaction of the thiol groups with NaN_3 in the next step. PS-*r*-PVBC (4.00 g, 4.44×10^{-4} mol) and dry THF (HPLC grade, ca. 55 mL) was mixed in a round-bottom flask and bubbled with Ar for ca. 10 min, while *n*-propylamine (3.7 mL, 0.0449 mol) and TCEP (150 mg, 5.25×10^{-4} mol) were added. The flask was then sealed and the reaction proceeded at room temperature for 2 hours, followed by injection of methyl acrylate (ca. 8 mL). The mixture was stirred overnight for the reaction to go to completion. The

contents were precipitated into methanol twice. The product was dried in a vacuum oven at ca. 60 °C for 2 days. In the third step, PS-*r*-PVBC (after CTA removal) was reacted with NaN_3 to obtain PS-N_3. PS-*r*-PVBC (1.40 g, 1.56×10^{-4} mol) and DMF (ca. 150 mL) were mixed in a round-bottom flask and stirred until all polymer was dissolved. Then, NaN_3 (0.93 g, 0.0143 mol) was added and reaction was allowed to proceed at 60 °C for 40 h. Deionized water (ca. 5 mL) was used to quench the reaction. Excess DMF was removed using a rotary evaporator, and the contents were dissolved in CH_2Cl_2, followed by precipitation into methanol twice. The final product was dried in a vacuum oven at ca. 60 °C for 2 days. The first and third steps were verified with ^{1}H-NMR spectroscopy (Figure 4.5). The second step was confirmed with UV-Vis spectroscopy (Figure 4.4). The dispersity (*Đ*) of the polymers was measured using SEC, and all molecular characteristics are listed in Table 4.1. The SEC trace of the PS-N_3 appears bimodal (Figure 4.3), which is likely due to chain coupling due to incomplete removal of the CTA.

Crosslinking kinetics study

PS-N_3 (ca. 0.1g) was placed in 1-mL ampules under dynamic vacuum for at least 3 hours before these ampules were flame-sealed. Samples were heated on a pre-heated metal block at certain temperatures for different amounts of time. After cooling back to room temperature, ampules were broken and solid polymer samples within were put into CH_2Cl_2 and vigorously stirred for at least 6 hours to determine whether the chemical crosslinking experiment has happened.

(a) PS-*r*-PVBC

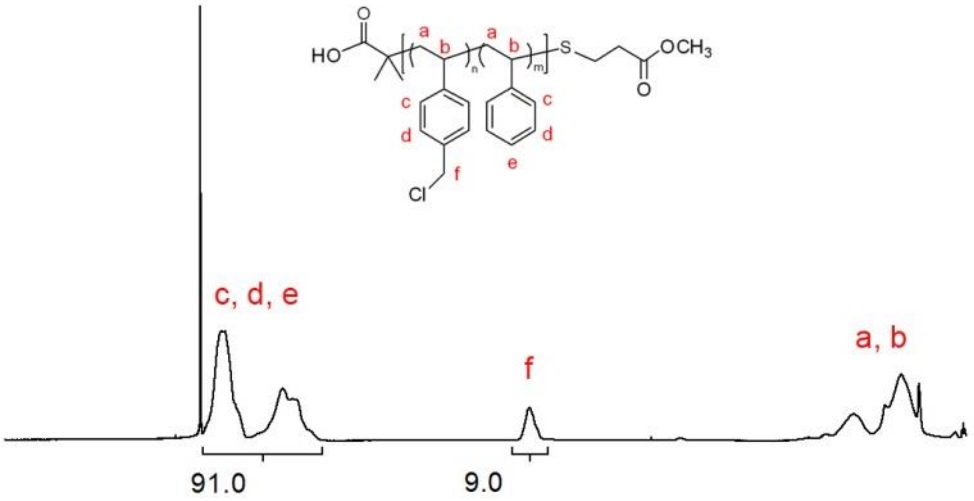

(b) PS-N_3

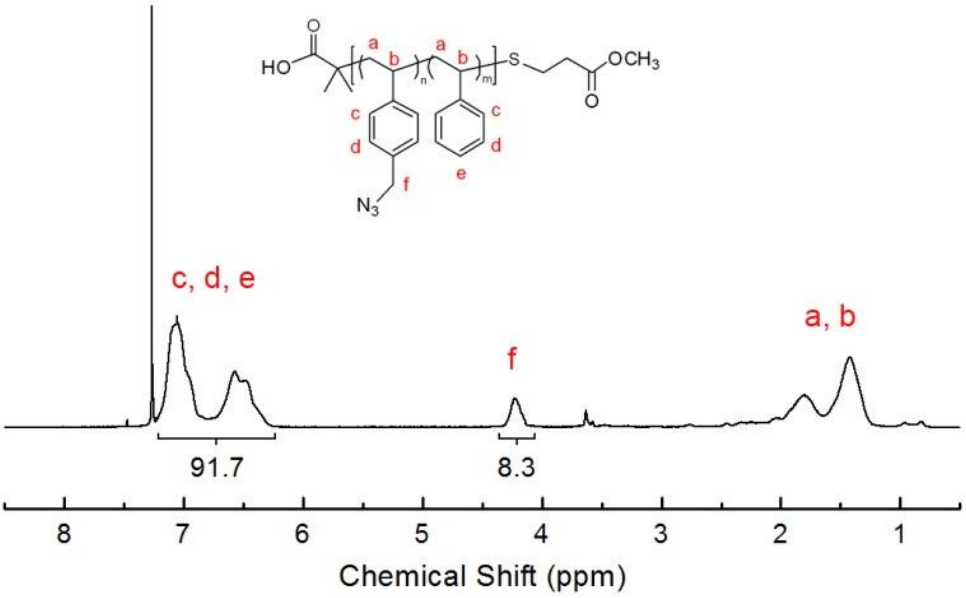

Figure 4.5 ^{1}H NMR spectra (500 MHz, in $CDCl_3$) of (a) PS-*r*-PVBC and (b) PS-N_3 random copolymers

Ionic liquid and ion gels preparation

Ionic liquid [EMI][TFSA] was synthesized via an anion exchange reaction following a previously reported procedure.[9] It was dried under vacuum at 70 ℃ and stored in glovebox or vacuum desiccator to avoid moisture absorption. The ion gels were prepared using a solvent casting method. Stock solutions to prepare ion gels were prepared by mixing weighed amounts of polymer with [EMI][TFSA] in CH_2Cl_2. After 2 hours of stirring, the solution was purged under N_2 flow overnight to remove most of the solvent. The residual solvent was completely removed by keeping the sample in a vacuum oven at ca. 45 ℃ for 2 days.

Samples for extensional rheology were first cast into a petri dish following the same procedure as above. Then the samples were annealed at ca. 100 ℃ for 2 hours to obtain smooth films. Cross-linked samples were prepared by further annealing at ca. 200 ℃ for 45 minutes to ensure complete cross-linking reaction. To avoid moisture effects, all the ion gel samples were kept in a desiccator under vaccum.

Rheology

Shear rheological measurements were conducted on ARES rheometer (Rheometric Scientific) using parallel plate geometry. Depending on the modulus, both 50 and 25 mm diameter plates were employed with a gap spacing of ca. 1 mm. In temperature ramp experiments, the sample was equilibrated at 100 ℃ for ca. 10 minutes to remove any prior thermal history, and cooled down to 25 ℃ to start the frequency sweep measurement. It was then heated to 100 ℃ at 1 ℃/min with a shear rate of 0.3 rad/s and a strain of 5%. After holding at 100 ℃ for 10 min, it was cooled back to 30 ℃ under the

same conditions as heating. To obtain time temperature superposition curves (tTS) before chemical crosslinking (temperature ≤ 100 °C), the sample was thermally equilibrated for 15-20 minutes at each temperature and the gap was adjusted to compensate the thermal expansion of the tool. Strain sweep experiments were first conducted to determine the linear viscoelastic regimes at each temperature, and then the dynamic shear moduli were measured. Temperatures were controlled to within 0.4 ℃ of the set point with an environmental control circulator under a nitrogen atmosphere. Measurements were taken at a series of decreasing temperatures. The frequency strain sweep experiments were set at 10 rad/s.

In cross-linking kinetics studies, one set of experiments were frequency sweeps performed at 100 ℃ after holding at a higher temperature for a certain amount of time. Specifically, the sample was heated up to the desired temperature using a temperature ramp, with a heating rate of 10 ℃/min. It was then annealed at that temperature for 10 min and cooled down to 100 ℃ with the same ramp rate. Then, frequency sweeps were conducted at the same conditions described above. In another experiment, the cross-linking kinetics was examined using a time sweep experiment at 200 ℃ (as shown in the Figure 4.10). An ion gel sample was first heated to 200 ℃ using a temperature ramp with a heating rate of 10 ℃/min. Subsequently, the modulus change was measured as a function of time, with a strain of 3% and frequency of 10 rad/s..

Extensional rheological measurements were performed on an ARES-G2 rheometer (TA Instruments) using an extensional viscosity fixture, with the help from Luca Martinetti. Samples were cut with a rectangular punch (width = 4.5 mm) and carefully

lifted out of the petri dish. As shown in Figure 4.6(a), the samples were then loaded onto the fixture between the drums (length = 13 mm). The thickness of each sample was measured using a caliper, being approximately 0.7 mm. Tests were conducted at 40 ℃, and the temperature was controlled to within 0.2 ℃ of the set point using an environmental temperature controller under a nitrogen atmosphere. The sample was stretched at a constant deformation rate, and the instrument measures the resulting extensional stress/viscosity until the sample breaks.

As shown in Figure 4.6(b), compressional rheological measurements were conducted on a RSA-G2 rheometer (TA instruments) using a parallel plate fixtures under a nitrogen atmosphere. Large amplitude compressional tests were conducted on 8 mm parallel plates at 40 ℃. Cylindrical ion gel samples (diameter = 2 mm, thickness = 2 mm) were

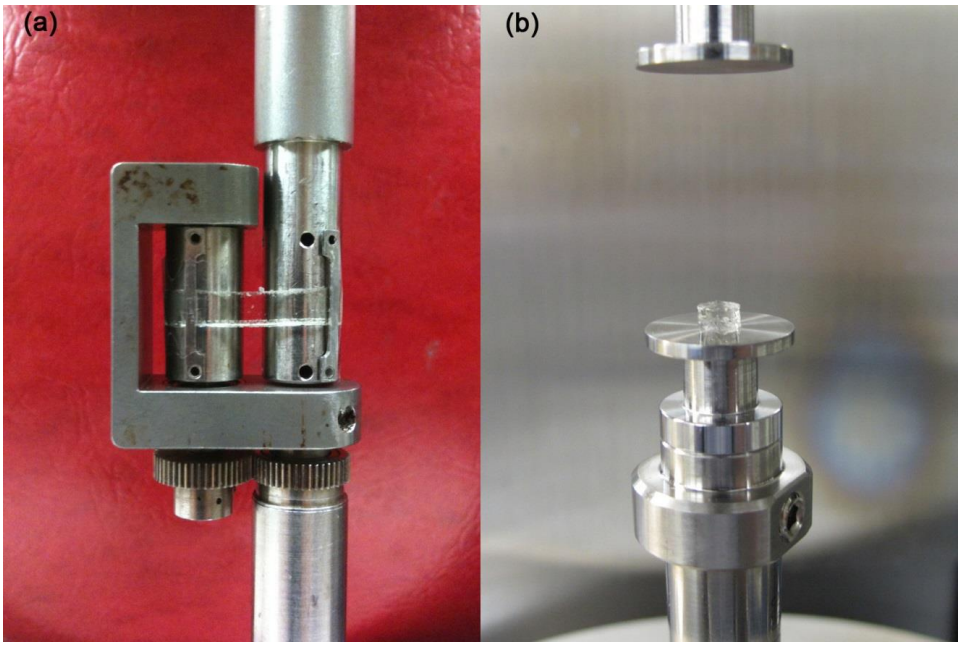

Figure 4.6. Photo of ion gel samples loaded on rheometers: (a) extension viscosity fixture, (b) parallel plate compressional fixture.

prepared using a cylinder mold. The sample was compressed at a constant strain rate, and the resulting compressional stress and viscosity was measured by the rheometer.

Impedance spectroscopy

Impedance measurements were performed by Dr. Sipei Zhang with a homemade cell using a Solartron 1255B frequency response analyzer connected to a Solartron SI 1287 electrochemical interface. Frequency sweeps were conducted from 1 – 106 Hz with AC amplitude of 10 mV. The cell is composed of a Teflon spacer with an inner diameter of 4 mm and a thickness of 2 mm sandwiched between two platinum coated stainless steel electrodes. Temperatures were controlled to within 0.5 ℃ of the set point with a thermostated water bath. The samples were thermally equilibrated for 30 min prior to the measurements. Measurements were performed at a series of increasing temperatures. Ionic conductivity was determined from the high frequency plateau of the real part of the complex conductivity.

Small-angle X-ray scattering (SAXS)

Small-angle X-ray scattering (SAXS) experiments were performed at the DuPont-Northwestern-Dow collaborative access team (DND-CAT) beamline at the Advanced Photon Source, Argonne National Laboratories by Lucas McIntosh. The ion gel samples were first prepared by solvent casting, while the thermal cross-linked ion gel sample was prepared by heating to 200 ℃ for 45 minutes to ensure complete cross-linking. Samples were sealed in DSC pans with a rubber O-ring. Both samples were pre-annealed at 80 ℃ for 2 hours in vacuum oven and exposed to X-ray irradiation at room temperature. Two-dimensional scattering patterns were recorded by a Mar-CCD area detector, and then

azimuthally integrated to give one-dimensional scattering data in the form of intensity (I) versus wave vector (q). The X-ray wavelength was 0.7293 Å, and the sample-to-detector distance was 5.68 m.

Fourier transform infrared (FTIR) spectroscopy

FTIR experiments were conducted on a Nicolet iS5 FT-IR spectrometer (Thermo Scientific) to monitor the crosslinking of the azide groups. Ion gel samples for IR spectroscopy were prepared using a solvent casting method: a premixed stock solution of [EMI][TFSA], SOS-N_3 triblock copolymer and CH_2Cl_2 was drop casted on a polished NaCl salt plate. A thin layer of ion gel film with ca. 60 μm thickness formed after the sample was purged under N_2 flow for 2 hours. The residual solvents were then removed under vacuum at 60 ℃ for 24 hours. Thermally cross-linked samples were prepared by further annealing at a desired temperature (e.g. 200 ℃) for a certain amount of time. IR spectra of ion gels before and after cross-linking were collected in the wavenumber range of 600-4000 cm^{-1} at room temperature.

Gas separation studies

Gas permeation properties of ion gels were measured using the previously mentioned gas diffusion cell. The supported ion gel membranes before cross-linking were prepared using the solvent casting method.[28,29] To achieve chemical cross-linking in the support, the un-cross-linked ion gel membrane was clamped between a flat stainless steel plate and a glass slide, and then the membrane was annealed at 140 ℃ for 16 hours in a vacuum oven to ensure a complete cross-linking reaction. The gas separation performance of ion gels before and after crosslinking were both measured using the same

methods as in the previous chapters (see Chapter 2 for detailed procedures). All of the measurements were taken at 25 ℃ using a circulating water bath as the temperature controller.

The maximum pressure that the tested membrane samples can withstand (burst pressure) was measured by incrementally increasing the pressure difference in the gas diffusion cell until failure. The downstream chamber was open to the atmosphere to ensure a constant pressure. The test starts at 20 Psi and increased ca. 15 psi every two minutes until failure. The failure point was defined as the moment there is a sharp decrease of the upstream chamber pressure (see Figure 4.18).

4.3 Results and discussion

4.3.1 Viscoelastic properties before chemical cross-linking

Before investigating the influence of chemical cross-linking on gel properties, the linear viscoelasticity of the SOS-N_3 ion gel was measured in its physically cross-linked state. The dynamic storage (G') and loss (G'') moduli for the ion gel with 10 wt% SOS-N_3 were measured over the temperature range from 30 to 100 °C. Previous studies in the literature reported that azide cross-linking in PS-N_3 thin films can be achieved at a temperature of 250 °C.[20] Because the temperature range explored here is much lower, the gel is expected to behave as a physically cross-linked transient network, and gelation is based solely on the incompatibility between the end-blocks and [EMI][TFSA]. The loss tangent (tan δ) spectra were shifted horizontally using tTS (not shown), and the same shift factors were applied to the dynamic moduli to obtain master curves as a function of

reduced frequency (squares and circles), as shown in Figure 4.7. The tTS master curve for an SOS/[EMI][TFSA] ion gel with 10 wt% SOS(2.8-35-2.8) reported previously are also shown for comparison (solid lines).[25] The curves for both gels are shifted to a reference temperature of 40 °C.

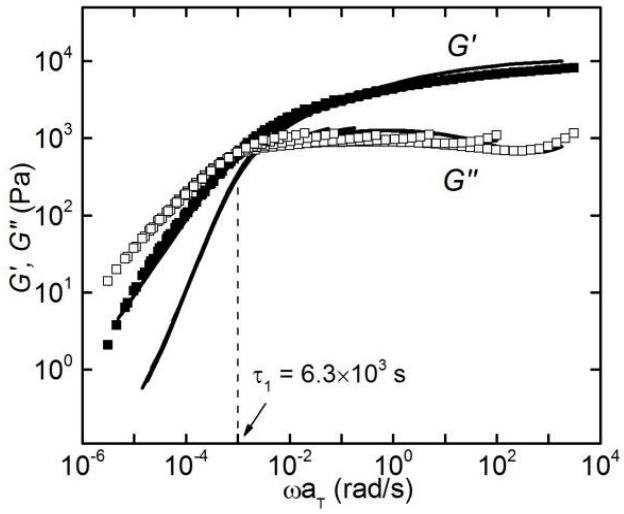

Figure 4.7. tTS master curves of dynamic storage and loss moduli referenced to 40 °C for ion gels with 10 wt% SOS-N_3(3.8-35-3.8) and 10 wt% SOS(2.8-35-2.8) measured over 30 – 100 °C. Symbols and lines represent moduli for the SOS-N_3(3.8-35-3.8) and SOS(2.8-35-2.8) gel, respectively.

For the 10 wt% SOS-N_3 gel above 70 °C, the association strength of the end-blocks is weak enough for the measurement to access the time scale of reversible chain pull-out from the micelle cores, and thus terminal flow behavior is observed, as evidenced by the crossover between G' and G''.[30–33] The longest relaxation time ($\tau_{1,gel}$) at 40 °C is 6.3×10^3 sec, as determined by the crossover frequency at which G' and G'' values are equal. This is slightly higher than that of the SOS (2.8-35-2.8) gel, which is 2.5×10^3 sec at 40 °C.

This small difference in $\tau_{1,gel}$ could be due to the combination of a slightly higher degree of polymerization for the end-blocks of SOS-N_3 and a slightly different interaction parameter (χ) between the end-blocks and the ionic liquid induced by the azide groups in the end-blocks.

The plateau modulus (G_N) of the SOS-N_3 gel can be determined as the value of G' at the frequency where the corresponding curve of tan δ has a minimum, and was found to be 7.8 kPa. According to linear viscoelastic theory, the plateau modulus can be expressed as:

$$G_N = \frac{cfRT}{M_x} \qquad \text{(Eq 4.1)}$$

where c is the concentration of the block copolymer in w/v, f is the fraction of elastically effective mid-blocks inside the copolymer, R is the ideal gas constant, and M_x is the number average molecular weight between cross-links.[34] We estimate $M_x = M_{e,\,PEO}/w_{PEO}$, where $M_{e,\,PEO}$ is the entanglement molecular weight of melt PEO, which is 1.6 kDa at 140 °C, and w_{PEO} is the weight fraction of PEO in the gel.[35] Assuming all PEO chains bridge two cross-linking cores instead of looping back to the same one ($f = 1$), the value of G_N at 30 °C (the temperature at which the measured plateau modulus was extracted) was predicted to be 2.5×10^4 Pa. The ratio of the observed value to the ideal value of G' gives a bridging fraction of 31%, which is similar to that calculated for the SOS(2.8-35-2.8) gel (29%), and agrees well with other reported transient gel systems.[36–38]

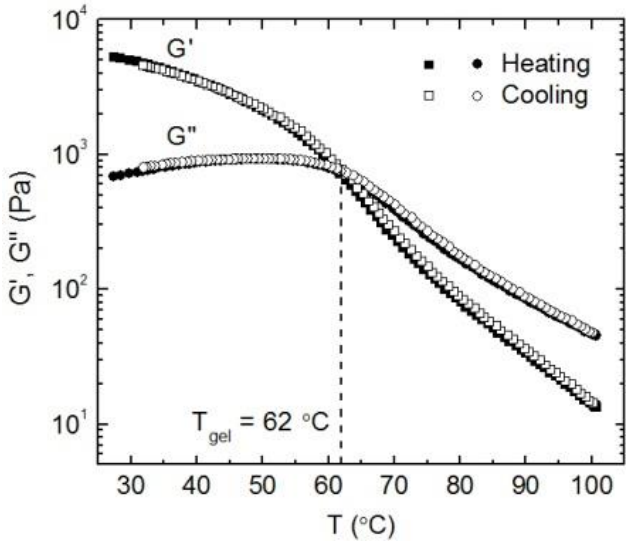

Figure 4.8 Temperature ramps of an ion gel with 10 wt% SOS-N_3(3.8-35-3.8). Storage moduli are shown as square and loss moduli are shown as circles.

To further confirm that no chemical cross-linking happens below 100 °C, temperature ramps were conducted on the ion gel with 10 wt% SOS-N_3. Figure 4.8 shows the temperature dependence of G' and G'' upon heating and cooling. The traces overlap very well, suggesting that the gel is fully thermoreversible over the temperature range of 30 – 100 °C. A gelation temperature of 62 °C was extracted, as determined by the crossover where G' and G'' values are equal. The thermoreversibility of SOS-N_3 ion gels also enables solvent-free processing at moderately elevated temperature without inducing thermal cross-linking, which can find potential applications in patterning of ion gel in electrochemical devices.

4.3.2 Cross-linking kinetics

As mentioned, the cross-linking reaction of the azide group can be achieved via

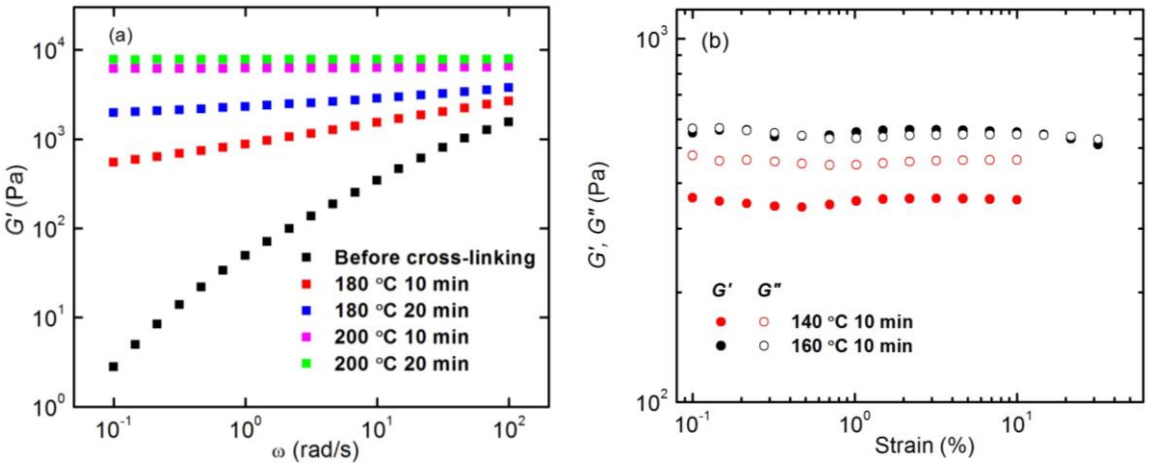

Figure 4.9 Dynamic storage moduli of ion gel with 10 wt% SOS-N_3(3.8-35-3.8) (a) before chemical cross-linking and after holding at the 180 °C and 200 °C (frequency sweep); (b) after holding at the 140 °C and 160 °C (strain sweep)

either UV irradiation (λ = 254 nm) or heating (250 °C).[20] In this report, we focused on the thermal cross-linking method. As far as we know, no detailed information on the cross-linking kinetics has been reported. Therefore, we utilize the synthesized PS-N_3 as a model system for investigation. Table 4.2 summarizes the results for cross-linking kinetic studies performed on PS-N_3 random copolymer samples sealed under vacuum and heated at different times at the three temperatures. At 140 °C, the sample heated for 10 min appeared to be completely insoluble in CH_2Cl_2, a good solvent for all components of the gel before chemical cross-linking, indicating that the gel had been chemically cross-linked. The same result was observed for samples heated for 5 and 10 min at 160 °C, and all three samples at 180 °C.

Table 4.2 Cross-linking Kinetics for PS-N_3.

T (°C)	2 min	5 min	10 min
140	-	SS	I
160	SS	I	I
180	I	I	I

SS: slightly soluble. I: insoluble.

Because the molar concentration of azide groups in PS-N_3 (23%) is similar to that in SOS-N_3 (28%) (Table 4.1), the local concentrations of azide groups in PS-N_3 and the micellar cores of the gel should be similar as well. Therefore, it was expected that the kinetics of chemical cross-linking for PS-N_3 reflects that of the gel. However, frequency sweep experiments at 100 °C revealed that the cross-linking reaction is much slower in the ion gel (please note that physical gel at 100 °C shows a liquid-like behavior, while a chemical gel should have a solid-like behavior). After annealing the gel at 140 °C and 160 °C for 10 minutes, we obtained a gel of equally solid-like and liquid-like properties (Figure 4.9(b)). It was not until the same sample was held at 180 °C for an additional 10 min did it show solid-like behavior versus shear rate at 100 °C, suggesting that chemical cross-linking has proceeded to a measurable extent, as displayed in Figure 4.9(a). This timeframe is significantly longer than the PS-N_3 polymer, as holding at 140 °C for 10 min

was sufficient to complete chemical crosslinking.

To further examine the extent of crosslinking under controlled conditions, the sample was further annealed at for another three 10 min intervals at 180 °C, 200 °C and 200 °C, respectively. Frequency sweep experiments for G' and G'' at 100 °C were conducted after each time interval. Generally, G' of the ion gel sample keeps increasing while G'' keeps decreasing, indicating that the cross-linking reaction is still proceeding. The gel is undergoing a conversion from physical cross-linking to chemical cross-linking Finally, G' becomes independent of frequency, and G'' is too small to be measured below 20 rad/s., which suggests that the gel was completely chemically cross-linked.

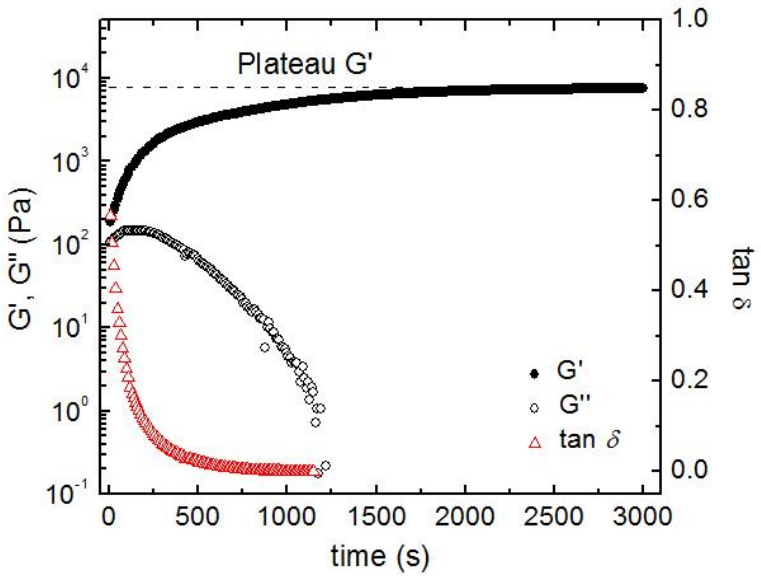

Figure 4.10 Dynamic storage and loss moduli of ion gel with 10 wt% SOS-N_3(3.8-35-3.8) as a function of time at 200 °C.

In another experiment, a 10 wt% SOS-N_3 physical gel was first equilibrated at 110 °C to ensure it was in the liquid state, followed by rapidly heating from 110 °C to 200 °C. Then the ion gel modulus was monitored as a function of time at this temperature. The

time it takes for chemical cross-linking to go to completion was determined by the point at which the storage modulus reaches a plateau. Figure 4.10 shows the result of the time sweep at 200 °C. The storage modulus reached a plateau after ca. 35 min, indicating that complete chemical cross-linking is achieved. It is also necessary to point out that the time it takes to reach the gel point, where $\tan\delta = 1$, is only about 5 min. This means that the cross-linked network structure can be rapidly formed within only a few minutes while annealing for longer time can help improving the mechanical strength.

Both of the above experiments suggest that the cross-linking kinetics for the gel is much slower than that for a pure PS-N_3 "homopolymer". One possible reason is solvent penetration into the micelle cores at elevated temperatures. Additionally, in the case of the gel, end-block chain exchange between different micelle cores happens constantly at 200 °C, making it different from the scenario of the random copolymer, where the only diffusive contribution comes from the motion of the PS-N_3 chains. Given the ignorance of the mechanism of the poly(vinylbenzyl azide) cross-linking reaction by itself, this process is even more complicated in a physically cross-linked gel.

4.3.3 Mechanical properties after chemical cross-linking

From Figure 4.10, it can be seen that the plateau in G' after chemical cross-linking is approximately 8 kPa, which is similar to the value before chemical cross-linking (7.8 kPa). This similarity in stiffness is reasonable, since the modulus is mainly determined by the number density of elastically effective mid-blocks, which is not expected to vary significantly upon chemical cross-linking of the cores. It is necessary to point out that after chemical crosslinking, G'' is substantially decreased and G' changes from highly

frequency dependent (Figure 4.7) to completely frequency independent (Figure 4.9). This is due to the reduced stress relaxation mode in ion gel, as chain pullout from micelle cores is prevented by chemical cross-linking within PS-N_3 domains.

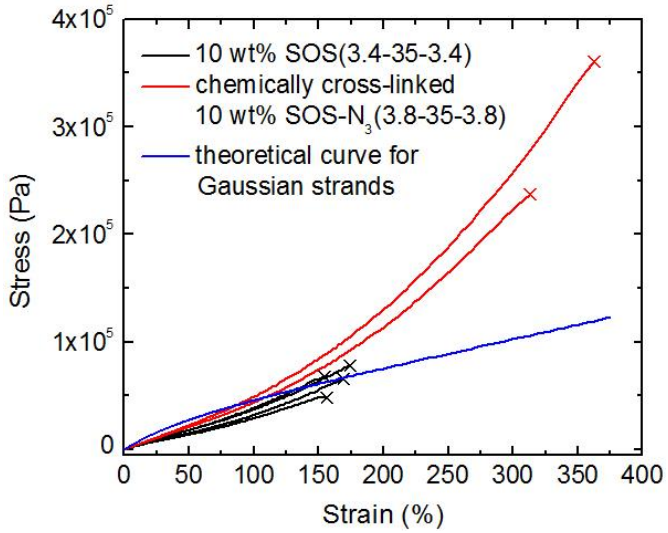

Figure 4.11 Stress-strain relationships for ion gels with 10 wt% SOS(3.4-35-3.4) and 10 wt% SOS-N_3 after chemical cross-linking measured at 40 °C.

However, the nonlinear mechanical properties are improved significantly after chemical crosslinking. Figure 4.11 compares the stress-strain relationships of gels with 10 wt% SOS(3.4-35-3.4), and 10 wt% SOS-N_3 after chemical cross-linking at 40 °C (the 10 wt% SOS-N_3 gels before cross-linking were too deformable to be reproducibly mounted in the extensional fixture). From the stress-strain curves, it is clear that for chemically cross-linked gels, both percent elongation and tensile strength are significantly higher than the physical gels. Figures 4.12 and 4.13 compare the extracted average values of percent elongation, tensile strength, and toughness of the two gels. The mechanical properties for the gel with 10 wt% SOS-N_3 are improved substantially after chemical

crosslinking, with values more than 2, 4, and 8 times higher for percent elongation, tensile strength, and toughness, respectively. These considerable differences in extensional properties likely stem from a change in failure mechanism. In physically cross-linked SOS ion gel, PS chains can be pulled out of the micellar cores under large strains, leading to gel failure.[37] In contrast, the PS-N_3 end-blocks in the chemically cross-linked SOS-N_3 ion gel cannot be pulled out from the cross-linked cores. As the chain pull-out is restricted, mid-block chains in a chemical gel can be stretched to a much higher extent and gel failure is very likely due to bond rupture in PEO mid-blocks.[34]

The tensile stress of the two gels can be compared to that predicted from rubber elasticity assuming the mid-blocks are Gaussian strands:

$$\sigma_e = \frac{\nu k_B T}{V}\left(\lambda - \frac{1}{\lambda^2}\right) = \frac{cfRT}{M_x}\left(\lambda - \frac{1}{\lambda^2}\right) \tag{4.2}$$

where ν is the number density of elastically effective mid-blocks, k_B is Boltzmann's constant, V is the volume of the gel, λ is the extension ratio ($\lambda = \varepsilon + 1$, where ε is strain), c is the concentration of the block copolymer in w/v, f is the fraction of elastically effective mid-blocks inside the copolymer, and M_x is the average molecular weight between crosslinks.[25,34] Assuming a bridging fraction of 100%, the calculated values of tensile stress are plotted in Figure 4.11 (blue curve). For the gel with 10 wt% SOS(3.4-35-3.4), the theoretical values are higher than the experimental results up to 120% strain, mainly because in the actual gel, the bridging fraction is less than 100%. The same trend can be observed for the gel with 10 wt% SOS-N_3 at lower strains (< 70%). This is consistent with the bridging fraction of 35% determined from the value of G_N in the

linear regime. At strains greater than 150%, where the physically cross-linked ion gels with 10 wt% SOS(3.4-35-3.4) start to break, the measured stress of the chemically cross-linked ion gel with 10 wt% SOS-N_3 deviates significantly from that of a random coil prediction. Such a deviation is not unexpected because the Gaussian assumption is not valid here. At large deformations, the mid-block PEO chains are stretched to a significant extent so that the Gaussian distribution no longer be applies.[34]

Similar results have been observed in the extensional study of chemically cross-linked natural rubber, where experimental data at large extensions also significantly exceeded model prediction based on Gaussian networks.[34,39] Additionally, [EMI][TFSA] is a good solvent for PEO, and the mid-blocks are "anchored" by the end-blocks after chemical cross-linking, so it is likely that mid-blocks would not assume a Gaussian conformation even without external forces. This may add more complexity to understanding the current system.

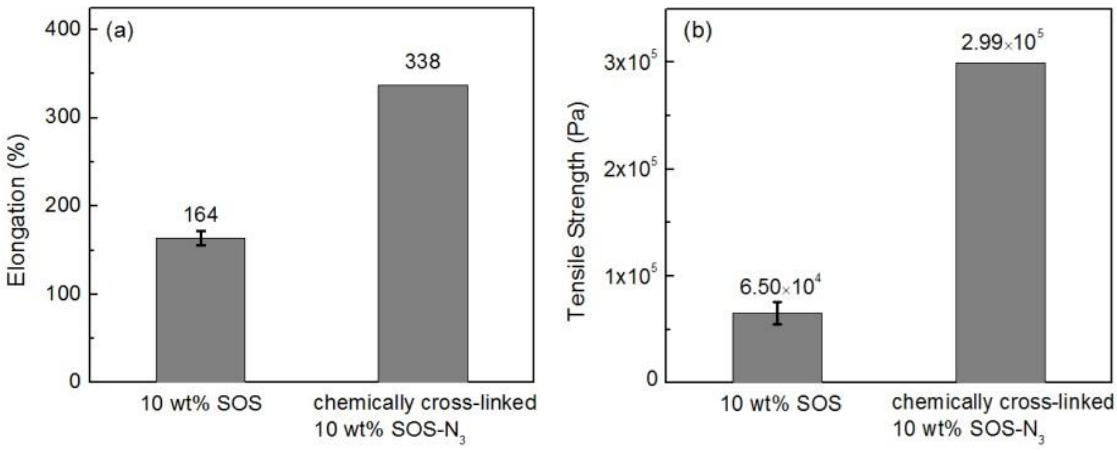

Figure 4.12 Average (a) percent elongation and (b) tensile strength of ion gels with 10 wt% SOS(3.4-35-3.4) and 10 wt% SOS-N_3 after chemical cross-linking measured at 40 °C.

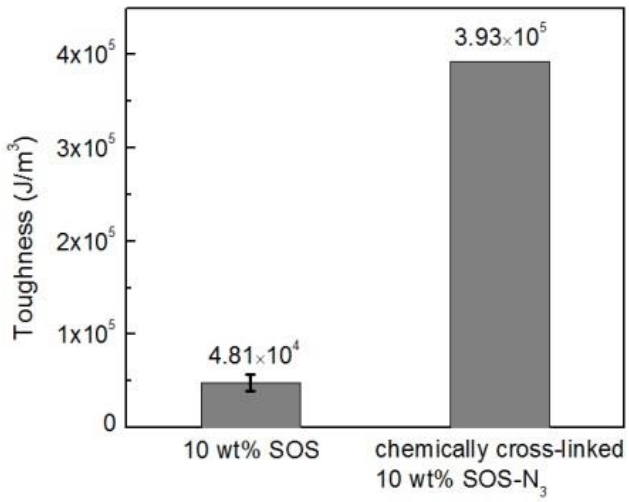

Figure 4.13 Average toughness of ion gels with 10 wt% SOS(3.4-35-3.4) and 10 wt% SOS-N_3 after chemical cross-linking measured at 40 °C.

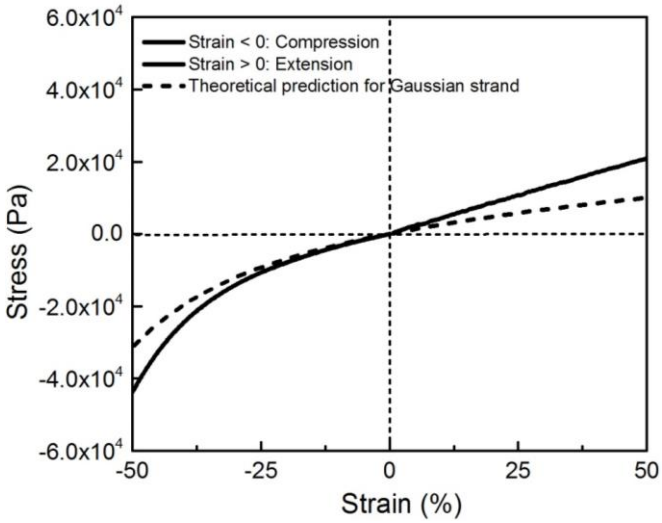

Figure 4.14 Stress-strain curves (compression and extension) of 10 wt% SOS-N_3 ion gel after chemical cross-linking measured at 40 °C. The curve is compared to model prediction for the Gaussian strands (assuming bridging fraction = 31%) for uniaxial compression and extension.

Figure 4.14 shows the stress-strain curve for a combination of uniaxial compression and extension of the cross-linked 10 wt% SOS-N_3 ion gel (black) from 50% compressive strain to 50% extensional strain. The curve is also compared to the same model prediction from rubber elasticity (red) as in Eq 4.2 by assuming that the mid-blocks are Gaussian strands and the bridging fraction is 35% (based on shear experiment). At strains higher than 20%, the experimental data starts to substantially deviate from the Gaussian model prediction. This deviation is reasonable because the Gaussian assumption cannot be applied at a higher deformation, which is similar to the uniaxial extension experiments.

4.3.4 Small-angle X-ray scattering

Small-angle X-ray scattering (SAXS) measurements were performed to investigate a morphology change of the ion gels. Figure 4.15 shows the SAXS profiles of the 10 wt% SOS-N_3 ion gels before and after chemical cross-linking. Because the polymer concentration is relatively low in the gel and the SOS-N_3 polymers have very long PEO mid-blocks (ca. 800 repeating units), the Percus-Yevick disordered hard sphere model is used to fit the scattering profiles.[40–43] This hard-sphere model assumes a dense core of the PS-N_3 domains, with radius R_c, which is surrounded by an outer shell of dissolved PEO chains defining an effective hard-core radius, R_{HS}. The microstructure of the gel is assumed as a liquid with interacting hard spheres, at a volume fraction ϕ. The scattering intensity I is expressed as the product of a constant K, the number of scattering units, N, the form factor, $P(q)$, and the structure factor, $S(q)$.

$$I = KNP(q)S(q) \qquad \text{(Eq 4.3)}$$

The scattering data were fitted using an averaged expression for $P(q)$ with a interfacial thickness d_0 and incorporates dispersity of the core size. The average aggregation number, N_{agg}, of the PS-N_3 cores are calculated using the core size based on the following equation, with assumption that there is no solvent penetration into the cores and the density of PS-N_3 is equivalent to that of polystyrene (ρ = 1.05 g/cm^3)

$$\frac{4\pi R_c^3}{3} = \frac{M_{n,PS-N_3} N_{agg}}{N_A \rho_{PS-N_3}} \qquad \text{(Eq 4.4)}$$

Average core-to-core distances, d_{nn}, are calculated based on the following equations, using the fitting result of equivalent hard sphere radius R_{HS} and volume fraction of the hard spheres ϕ.[44] The close packing volume fraction of the cores ϕ_{CP} is assumed to be 0.64.

$$\frac{2R_{HS}}{d_{nn}} = \left(\frac{\phi}{\phi_{CP}}\right)^{1/3} \qquad \text{(Eq4.5)}$$

$$\phi_{CP} = 0.64$$

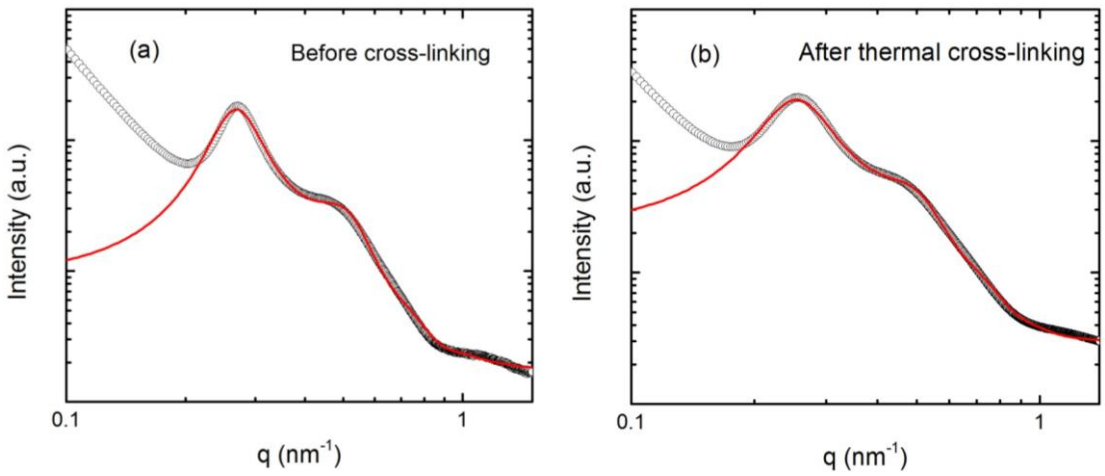

Figure 4.15 1D SAXS profiles of 10 wt% SOS-N_3 ion gels (a) before cross-linking and (b) after thermal cross-linking. SAXS patterns were fitted to Percus-Yevick hard sphere model. Black open circles are experimental data, while the red curves are fitting results.

Table 4.3. Fitting results of the 10 wt% SOS-N_3 SAXS patterns

	R_c (nm)	σ_{Rc} (nm)	R_{HS} (nm)	ϕ	d_0 (nm)	N_{agg}	d_{nn} (nm)
Before	5.6	1.0	12.1	0.38	0.7	127	28.7
Thermal	5.4	1.2	12.2	0.31	1.1	114	31.0

Table 4.3 listed all the Percus-Yevick fitting results from the SAXS patterns. From these results, it is clear that the diameters of the PS-N_3 cores were retained after the cross-linking reactions. The average aggregation number (N_{agg}) and the average closest core to core distance (d_{nn}) of the PS-N_3 cores were also not affected by the reaction. Moreover,

these fitting results of N_{agg} and d_{nn} and are consistent with previous studies on SOS ion gels,[25] which further confirmed the assumption that the incorporation of azide functionalities and the subsequent chemical cross-linking reactions should have no effect on the microstructure of ion gels. Since the cross-linking reaction is confined to the PS domains, it should also have no influence on the mass transport rate of ion gels, such as ionic conductivity and gas permeability.

4.3.5 Ionic conductivity

Figure 4.16 displays the ionic conductivity of the ion gel with 10 wt% SOS-N_3 measured over a temperature range of 25 – 100 °C before and after chemical cross-linking. The conductivities of [EMI][TFSA] taken from a previous literature report and the gel with 10 wt% SOS(2.8-35-2.8) are also plotted for comparison.[45] Clearly, the ionic conductivities of the two gels are essentially the same over the temperature range measured, and chemical cross-linking does not have any measurable effect on ion transport. This result agrees with a previous report that at a polymer concentration of 10 wt%, the ionic conductivity is reduced to very similar extent even with very different polymers.[25,45] In this moderately dilute regime, the T_g of the conducting phase, (i.e., a mixture of ionic liquid and polymer mid-block), remains very low, and therefore ion transport is dominated by the ionic liquid. Additionally, it confirms the conclusion in the same reports that the cross-linked cores only act as physical obstructions to ion paths. These data confirm that ionic conductivity is independent of whether the cores are physically or chemically cross-linked, since the volume fraction of insoluble end-blocks remains the same.

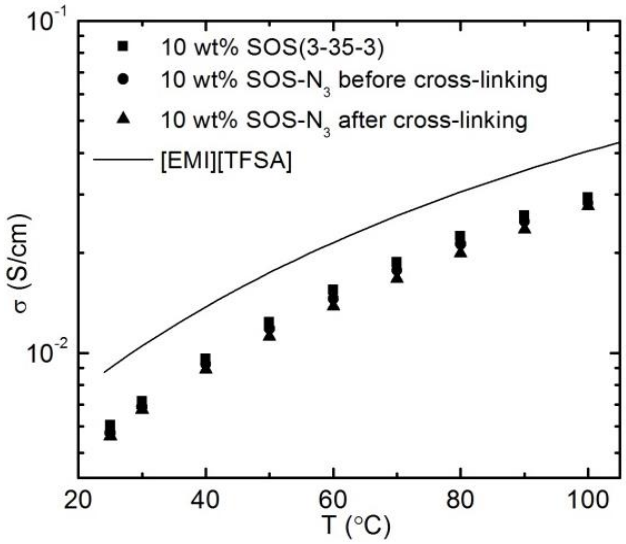

Figure 4.16 Temperature dependence of ionic conductivity for [EMI][TFSA] and ion gels with 10 wt% SOS(2.8-35-2.8) and 10 wt% SOS-N_3(3.8-35-3.8).

4.3.6 Gas separation performances

The gas transport properties of SOS-N_3 ion gels were tested using the same supported membrane structure as described in Chapters 2 and 3. The membranes were prepared by filling the porous PVDF support with ion gels using solvent casting method, while the cross-linked membranes were further annealing 140 ℃ for 16 hours to achieve complete cross-linking. Here, it is necessary to note that the reaction to obtain cross-linked ion gel membranes was conducted at a lower temperature for a much longer time, as the melting point of the PVDF support is ca. 170 ℃. To confirm that the membrane has been completely cross-linked, Figure 4.17 displays the comparison of IR spectra for ion gels cross-linked under different conditions. In these spectra, the absorption peak for the azide group at ~2095 cm^{-1} was used to monitor the cross-linking reaction, and the spectrum of a completely cross-linked ion gel (annealed at 200 ℃ for 45 minutes, see Figure 4.10) was

used as a reference. As shown in Figure 4.17(b), the azide absorption peak was reduced by a similar extent under two reaction conditions, indicating that annealing at 140 ℃ for 16 hours can also achieve a complete cross-linking of the 10 wt% SOS-N_3 ion gels.

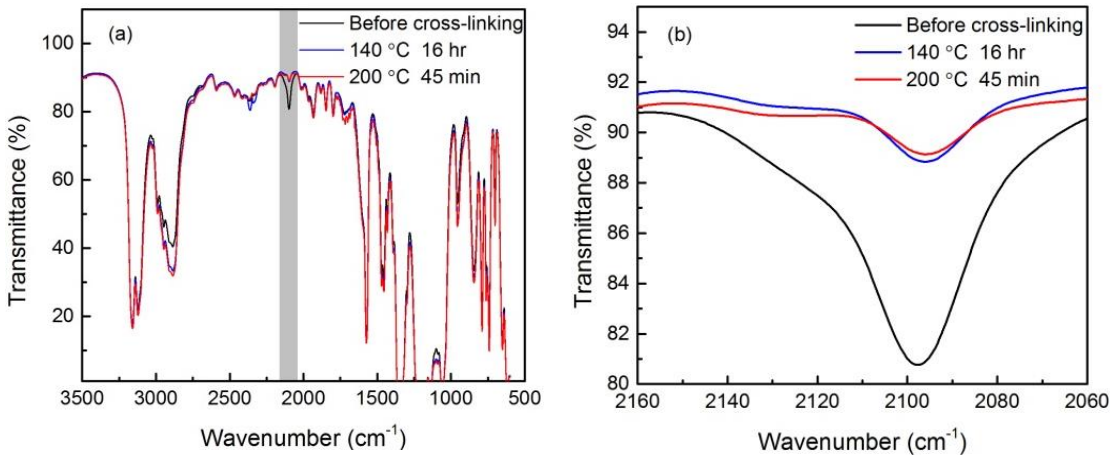

Figure 4.17 (a) Full IR spectra of 10 wt% SOS-N_3 ion gels before cross-linking (black), after heating at 140 ℃ for 16 hours (blue) and after heating at 200 ℃ for 45 minutes (red). The grey area indicates the absorption peak of azide groups; (b) shows the expanded IR spectra in the range of 2160-2060 cm^{-1}.

Table 4.4 summarizes the gas permeation properties of the 10 wt% SOS-N_3 ion gels before and after chemical cross-linking. The permeabilities of CO_2, CH_4 and N_2 for the 10 wt% SOS-N_3 ion gel before cross-linking were found to be 850, 46 and 25 barrers, respectively. The calculated ideal selectivity is 18 for CO_2/CH_4 and 36 for CO_2/N_2, which agrees well with our previous studies of SOS ion gels. More importantly, the two ion gels showed nearly the same permeability for all the three gases measured, and therefore chemical cross-linking have negligible influence on the gas permeation properties. This is because the mass transport path for gas molecules in the ion gel is via the mixtures of

ionic liquid ([EMI][TFSA]) and solvated mid-blocks (PEO), which were not affected by the cross-linking reactions in the PS domains. As revealed by the SAXS studies, the microstructure of the ion gels were not affected by the chemical cross-linking, and therefore the mass transport rate is retained.

Table 4.4 Permeation properties of 10 wt% SOS-N_3 ion gels before and after thermal cross-linking

	P_{CO_2}[a]	P_{CH_4}	P_{N_2}	α_{CO_2/CH_4}	α_{CO_2/N_2}
Before	850 ± 35	46 ± 5	24 ± 3	18	36
Thermal	820 ± 10	44 ± 2	24 ± 2	19	35

[a] Gas permeability results are in the unit of barrer

Apart from the permeation properties, the mechanical stability of gas separation membrane is also essential to further applications beyond lab-scale. The burst pressure of ion gel membranes has been increased after the cross-linking reaction. Typical results of the burst pressure measurements for cross-linked and uncross-linked membranes are shown in Figures 4.17 (a) and (b), respectively. The burst pressures of 10 wt% ion gel membranes before cross-linking were found to be 83 ± 7 Psi. In contrast, the cross-linked ion gel membranes show improved stability with burst pressures of 150 psi (ca. 85% higher). The enhanced mechanical properties of the membranes can be attributed to the higher toughness and tensile strength of the ion gel materials.

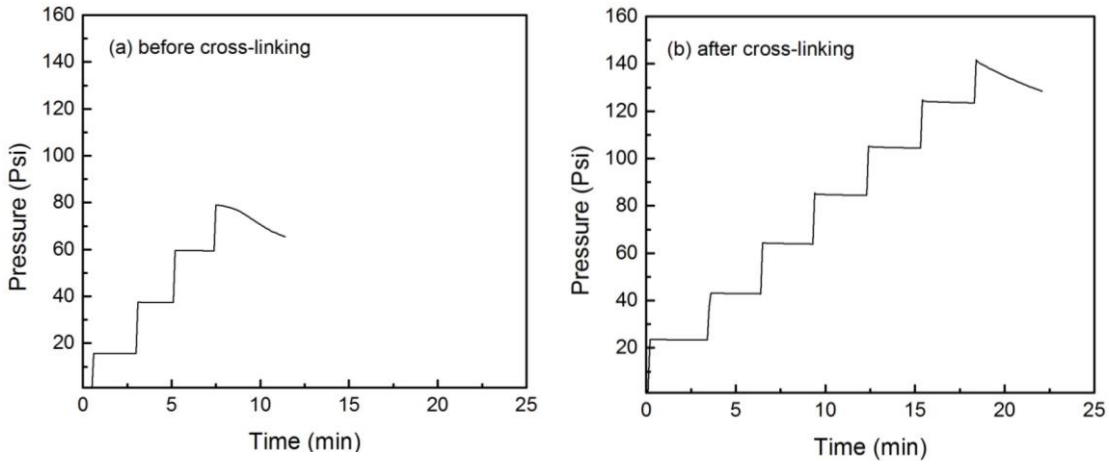

Figure 4.18 Burst pressure measurements of supported ion gel membranes with 10 wt% SOS-N_3 (a) before cross-linking and (b) after cross-linking.

4.4 Summary

We have successfully developed a novel ion gel with high toughness, high conductivity and high gas permeability through sequential block copolymer self-assembly and chemical cross-linking. This strategy combines the key advantages of the physical ion gel, i.e. the thermo-reversibility and facile liquid-state processability, and the enhanced mechanical strength of chemical gels. In addition, the rapid mass transport rate of ion gel was retained after chemical cross-linking, while the ion gel toughness was increased by almost one order of magnitude. SAXS studies confirmed that the ion gel microstructure was not affected by cross-linking reaction, which further explains why the mass transport rates (ionic conductivity and gas permeability) are retained after cross-linking.

4.5 References

(1) Baker, R. W. *Ind. Eng. Chem. Res.* **2002**, *41*, 1393–1411.

(2) Baker, R. W.; Lokhandwala, K. *Ind. Eng. Chem. Res.* **2008**, *47*, 2109–2121.

(3) Harner, J. M.; Hoagland, D. A. *J. Phys. Chem. B* **2010**, *114*, 3411–8.

(4) Voss, B. A.; Bara, J. E.; Gin, D. L.; Noble, R. D. *Chem. Mater.* **2009**, *21*, 3027–3029.

(5) Jansen, J. C.; Friess, K.; Clarizia, G.; Schauer, J.; Izak, P. *Macromolecules* **2011**, *44*, 39–45.

(6) Singh, B.; Sekhon, S. S. *J. Phys. Chem. B* **2005**, *109*, 16539–16543.

(7) Noro, A.; Matsushita, Y.; Lodge, T. P. *Macromolecules* **2008**, *41*, 5839–5844.

(8) Klingshirn, M. A.; Spear, S. K.; Subramanian, R.; Holbrey, J. D.; Huddleston, J. G.; Rogers, R. D. *Chem. Mater.* **2004**, *16*, 3091–3097.

(9) Susan, M. A. B. H.; Kaneko, T.; Noda, A.; Watanabe, M. *J. Am. Chem. Soc.* **2005**, *127*, 4976–4983.

(10) Neouze, M.-A.; Le Bideau, J.; Gaveau, P.; Bellayer, S.; Vioux, A. *Chem. Mater.* **2006**, *18*, 3931–3936.

(11) Cho, J. H.; Lee, J.; Xia, Y.; Kim, B.; He, Y.; Renn, M. J.; Lodge, T. P.; Frisbie, C. D. *Nat. Mater.* **2008**, *7*, 900–906.

(12) Lee, K. H.; Zhang, S.; Gu, Y.; Lodge, T. P.; Frisbie, C. D. *Manuscript Submitted*.

(13) Cordier, P.; Tournilhac, F.; Soulie-Ziakovic, C.; Leibler, L. *Nature* **2008**, *451*, 977–980.

(14) Noro, A.; Matsushita, Y.; Lodge, T. P. *Macromolecules* **2009**, *42*, 5802–5810.

(15) Kofu, M.; Someya, T.; Tatsumi, S.; Ueno, K.; Ueki, T.; Watanabe, M.; Matsunaga, T.; Shibayama, M.; Sakai, V. G.; Tyagi, M.; Yamamuro, O. *Soft Matter* **2012**, *8*, 7888–7897.

(16) Fujii, K.; Asai, H.; Ueki, T.; Sakai, T.; Imaizumi, S.; Chung, U.; Watanabe, M.; Shibayama, M. *Soft Matter* **2012**, *8*, 1756–1759.

(17) Asai, H.; Fujii, K.; Ueki, T.; Sakai, T.; Chung, U.; Watanabe, M.; Han, Y.-S.; Kim, T.-H.; Shibayama, M. *Macromolecules* **2012**, *45*, 3902–3909.

(18) Matsumoto, K.; Endo, T. *Macromolecules* **2008**, *41*, 6981–6986.

(19) Matsumoto, K.; Endo, T. *Macromolecules* **2009**, *42*, 4580–4584.

(20) Bang, J.; Bae, J.; Lowenhielm, P.; Spiessberger, C.; Given-Beck, S. A.; Russell, T. P.; Hawker, C. J. *Adv. Mater.* **2007**, *19*, 4552–4557.

(21) Yoo, M.; Kim, S.; Lim, J.; Kramer, E. J.; Hawker, C. J.; Kim, B. J.; Bang, J. *Macromolecules* **2010**, *43*, 3570–3575.

(22) Park, J.; Kim, J.; Lee, S.; Bang, J.; Kim, B. J.; Kim, Y. S.; Cho, J. *J. Mater. Chem.* **2009**, *19*, 4488–4490.

(23) Kang, D. J.; Kwon, T.; Kim, M. P.; Cho, C.-H.; Jung, H.; Bang, J.; Kim, B. J. *ACS Nano* **2011**, *5*, 9017–9027.

(24) Lee, S.; Lee, B.; Kim, B. J.; Park, J.; Yoo, M.; Bae, W. K.; Char, K.; Hawker, C. J.; Bang, J.; Cho, J. *J. Am. Chem. Soc.* **2009**, *131*, 2579–2587.

(25) Zhang, S.; Lee, K. H.; Sun, J.; Frisbie, C. D.; Lodge, T. P. *Macromolecules* **2011**, *44*, 8981–8989.

(26) Lai, J. T.; Filla, D.; Shea, R. *Macromolecules* **2002**, *35*, 6754–6756.

(27) He, Y.; Lodge, T. P. *Macromolecules* **2008**, *41*, 167–174.

(28) Gu, Y.; Lodge, T. P. *Macromolecules* **2011**, *44*, 1732–1736.

(29) Gu, Y.; Cussler, E. L.; Lodge, T. P. *J. Membr. Sci.* **2012**, *423-424*, 20–26.

(30) Tanaka, F.; Edwards, S. F. *Macromolecules* **1992**, *25*, 1516–1523.

(31) Seitz, M. E.; Burghardt, W. R.; Faber, K. T.; Shull, K. R. *Macromolecules* **2007**, *40*, 1218–1226.

(32) Sato, T.; Watanabe, H.; Osaki, K. *Macromolecules* **2000**, *33*, 1686–1691.

(33) Vega, D. A.; Sebastian, J. M.; Loo, Y.-L.; Register, R. A. *J. Polym. Sci., Part B: Polym. Phys.* **2001**, *39*, 2183–2197.

(34) Hiemenz, P. C.; Lodge, T. P. *Polymer Chemistry*; 2nd ed.; CRC Press: New York, 2007.

(35) Fetters, L. J.; Lohse, D. J.; Richter, D.; Witten, T. A.; Zirkel, A. *Macromolecules* **1994**, *27*, 4639–4647.

(36) Annable, T.; Buscall, R.; Ettelaie, R.; Whittlestone, D. *J. Rheo.* **1993**, *37*, 695–726.

(37) He, Y.; Boswell, P. G.; Bühlmann, P.; Lodge, T. P.; Buehlmann, P. *J. Phys. Chem. B* **2007**, *111*, 4645–52.

(38) Tae, G.; Kornfield, J. A.; Hubbell, J. A.; Lal, J. *Macromolecules* **2002**, *35*, 4448–4457.

(39) Treloar, L. R. G. *Trans. Faraday Soc.* **1944**, *40*, 59–70.

(40) Kinning, D. J.; Thomas, E. L. *Macromolecules* **1984**, 1712–1718.

(41) Bansil, R.; Nie, H.; Li, Y.; Liao, G.; Ludwig, K.; Steinhart, K.; Konak, C.; Lal, J. *Macromol. Symp.* **2002**, *190*, 161–172.

(42) Flanigan, C. M.; Crosby, A. J.; Shull, K. R. *Macromolecules* **1999**, *32*, 7251–7262.

(43) Mischenko, N.; Reynders, K.; Koch, M. H. J.; Mortensen, K.; Pedersen, S.; Fontaine, F.; Graulus, R.; Reynaers, H. *Macromolecules* **1995**, *28*, 2054–2062.

(44) Berg, J. C. *An Introduction to Interfaces and Colloids: The Bridge to Nanoscience*; World Scientific Publishing Co. Pte. Ltd.: Hackensack, NJ, 2010; p. 785.

(45) Zhang, S.; Lee, K. H.; Frisbie, C. D.; Lodge, T. P. *Macromolecules* **2011**, *44*, 940–949.

Chapter 5

Summary and Outlook

5.1 Summary

The overall target of this thesis project is to explore the application of block copolymer ion gels for CO_2 separation, and seek ways to optimize their properties in terms of the gas separation performance and mechanical strength. The ion gels investigated in this thesis comprise a physical network formed by self-assembly of a triblock copolymer, and an ionic liquid that can selectively dissolve the polymer mid-block.[1] In this material, ionic liquids function as the CO_2 separation media, largely due to their highly selective gas solubility and non-volatility. The self-assembled polymer networks provide the mechanical support to ionic liquids without too much sacrifice in terms of their favorable separation performance.

In the pioneering works from Bara, Noble and coworkers, chemically cross-linked polymerized ionic liquids (PILs) have been successfully used for CO_2 separation.[2–4] Inspired by the enhanced separation performance of the PIL composite membranes,[5,6] this thesis research started with the development of a triblock copolymer ion gel with a PIL mid-block. The synthesis of the triblock copolymer was successfully achieved through a sequential RAFT polymerization and post-polymerization reactions. Then the rheological properties of ion gels and the gas separation performance of supported ion gel membranes have been investigated. The polymerized ionic liquid gels exhibited high gas

permeability, due to the high liquid fraction in these systems (≥ 85 wt% of [EMI][TFSA]). Moreover, the permeation selectivity for both CO_2/N_2 and CO_2/CH_4 gas pairs is significantly increased from that of the neat ionic liquid. Robeson plot comparisons indicate very promising separation performance for ion gels. The permeability/selectivity combination lies close to or better than the current "upper bound", which represent the best performance of existing polymer materials.[7,8]

The gas separation study was then extended to two other block copolymer ion gels based on poly(styrene-b-ethylene oxide-b-styrene) (SOS) and poly(styrene-b-methyl methacrylate-b-styrene) (SMS) triblock copolymers and [EMI][TFSA]. Similar to the PIL gels, these two ion gels also exhibit high gas permeability due to the high ionic liquid fractions. Interestingly, the separation performances of the ion gels were found to be strongly dependent on the polymer mid-block dissolved in the ionic liquids. The mid-block effect is further confirmed by gas solubility experiments on homopolymer/[EMI][TFSA] solutions. Added PEO is found to increase the solubility ratio of the ionic liquid solutions for both gas pairs. The separation performance of ion gels can thereby be readily adjusted by changing the polymer structures.

To achieve applications in industrial processes, it is desirable to enhance the mechanical strength of the ion gels without sacrificing their mass transport properties. In Chapter 4 and Appendix B, we described the development of a novel ABA-triblock copolymer ion gel which can be chemically cross-linked by high-temperature annealing or UV-irradiation. The triblock copolymer has about 28% of the end-block repeating units functionalized with cross-linkable azide groups.[9] After self-assembly in the ionic

liquid, the styrene domains can be further cross-linked by annealing at 200 ℃ for ca. 20 minutes or UV-irradiation (λ = 254 nm). The kinetics of the cross-linking reaction has been investigated using rheological measurements and FTIR spectroscopy. After chemical cross-linking, the mechanical strength of the gel showed significant improvement, with over 400% increase in the tensile strength and almost one order of magnitude increase in the gel toughness. The mechanical stability of the supported ion gel membranes was also enhanced. The burst pressure of the membrane almost doubled after cross-linking. More importantly, the mass transport rates (both gas permeability and ionic conductivity) are retained after the cross-linking. Because the cross-linking reaction is restricted to the styrene domains, it does not affect the mass transport path. Results from small angle X-ray scattering (SAXS) also confirmed that the microstructure of the ion gel remains unchanged by the cross-linking reaction.

5.2 Outlook

Research into the application of block copolymer ion gels indicated that they can be tunable and efficient systems for CO_2 separations. However, there are still many opportunities for future research in this area. The following discussion focuses on two specific topics.

5.2.1 Ion gel as gas separation media

From a materials design perspective, block copolymer ion gels represent a flexible platform to tailor the gel properties for different applications. Recent research efforts

have shown that by changing the molecular weight, polymer structure and incorporating certain functional groups, the gel properties can be readily tuned. In this thesis, for instance, we have discovered that the gas separation performance, especially the selectivity for CO_2, can be greatly improved by changing the polymer mid-block. Meanwhile, by incorporating the chemically cross-linkable functionality into the PS end-blocks, the mechanical properties can be significantly enhanced without sacrificing the gas transport rate.

For the future research in this area, it would also be of great interest to study the influence of ionic liquids on the gas separation performance of ion gels. As the major component of an ion gel, the ionic liquid is anticipated to have a significant impact on the gas separation performance. Previous research has shown that although [EMI][TFSA] has a high gas permeability, other ionic liquids such as [EMI][BF_4] and [EMI] dicyanamide ([dca]) exhibit a higher selectivity for CO_2/N_2 and CO_2/CH_4 separations.[10,11] By incorporating these ionic liquids into the system, the separation performance of ion gel membranes might be significantly improved. Preliminary research has also indicated that SOS triblock copolymers should be able to achieve gelation with [EMI][BF_4].[12]

Another research direction would be to explore the moisture effect on the ion gels. In industrial operations, water vapor has a significant influence on the gas separation performance of polymeric membranes.[13] Previous research on supported ionic liquid membranes has indicated that moisture has minimal effect on the separation performance of hydrophobic ionic liquids, such as [EMI][TFSA].[14] However, it would be important to investigate the moisture effect on ion gels containing hydrophilic polymer mid-blocks

such as PEO, or hydrophilic ionic liquids, such as [EMI][BF_4]. The moisture effect can be studied by comparing the separation performance of an ion gel membrane under dry and water-saturated gases. Such experiments will require a water vapor generator connected to the diffusion cell to provide gases with different humidity levels.

Apart from CO_2 separation, ionic liquids have shown promise to achieve separation of other gas pairs, such as alkanes/alkenes. Dai and coworkers have demonstrated a high-selectivity separation of isoprene/pentane by using a "task-specific ionic liquid" containing a silver-based cation.[15] As the silver ions can specifically complex with the double bonds in alkene molecules, the ionic liquid can act as a selective "carrier" for alkene molecules through the membrane, while blocking alkanes, thereby achieving the facilitated transport for alkene. Silver ions could also be introduced into an ion gel membrane to achieve similar purposes. The most straightforward method is to directly blend ionic liquids with miscible silver salts such as $AgBF_4$ and achieve gelation using a triblock copolymer. Ortiz et al. have successfully demonstrated that the ionic liquid-silver mixture can be used as an efficient medium in selective absorption of alkene.[16] However, as silver ions can easily react with oxygen, one of the most challenging targets is to find ways that can effectively avoid degradation of the silver ions in the air.

5.2.2 Further investigation of cross-linkable ion gels

We have already demonstrated that the mechanical properties of cross-linkable SOS-N_3 ion gels have been substantially increased without sacrificing the mass transport rate. This material is expected to be advantageous in applications where ion gels have already shown great promise, such as plastic electronics and CO_2 separation membranes.

However, there are several fundamental questions that need to be elucidated for its further application.

First, the kinetics of the thermal cross-linking reaction needs to be further investigated. As mentioned in Chapter 4, it takes a much longer time to achieve a "complete cross-linking" with a 10 wt% SOS-N_3 ion gel than a PS-N_3 "homopolymer". One possible reason is a slight difference in the experimental condition: the "homopolymer" cross-linking was conducted under vacuum to avoid degradation at high temperature, while the gel cross-linking was conducted under N_2 atmosphere on a rheometer. According to a possible mechanism proposed by Yoo et al., the cross-linking reaction of PS-N_3 will generate N_2 as a side product (Figure 5.1).[17,18] Therefore, the slight difference in experimental condition may cause the difference in the cross-linking kinetics. A potential study that can elucidate this issue would be to conduct an *in-situ* PS-N_3 cross-linking experiment by annealing at 200 ℃ on the rheometer. The modulus change of the polymer will be monitored as a function of time. The gel point can be determined by the modulus change when it converts from a polymer melt (above T_g) to a cross-linked polymer network after the cross-linking.

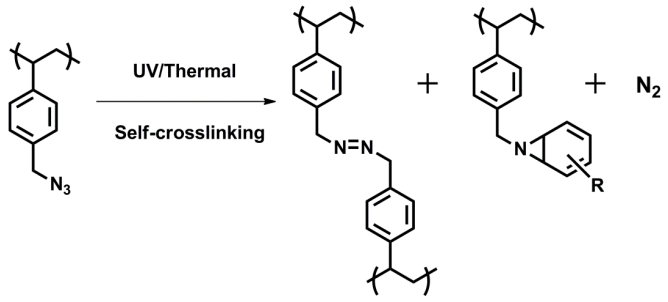

Figure 5.1 Possible cross-linking mechanism of PS-N_3

Second, it would be desirable to explore the possibility of accelerating the reaction kinetics for both thermal and UV cross-linking. By reducing the annealing time at high temperatures or the UV-irradiation time, we can decrease the risk of materials degradation during the cross-linking. One potential solution is to increase the density of azide groups in the PS end-blocks. However, the potential concern is from the synthesis: the increased density of azide groups would require using larger amount of explosive NaN_3 in the reaction. The synthesis will have to be achieved in several smaller batches for safety reasons.

Third, it is also important to understand the mechanical properties of ion gel thin films. In a typical gas separation membrane, the selective layer usually has a thickness between 0.1 to 1 μm. The results from this research will also be beneficial for the other applications of ion gel such as plastic electronics. Previously in the Lodge group, Lee et al. have demonstrated that spin-coating can be used to prepare ion gel thin films with thickness of 1-20 μm.[19] More recent effort has further decreased the thickness of ion gel films to ca. 400 nm. Common methods for measuring the mechanical properties of thin films include nano-indentation and direct tensile test. In nano-indentation, a small diamond tip is pressed into the sample and measures the indentation displacement as a function of the force load on the tip. In a direct tensile test, samples need to be processed into specific shapes and load onto an extensional tool. While the experiment is straightforward, it could be challenging as the mechanical properties of ion gels are relatively weak. Transferring the ion gel thin films without damage will be potentially

difficult. For ion gels with low polymer weight fractions (e.g. 10 wt%), the signal from the measurement could be lower than the instrument limit.

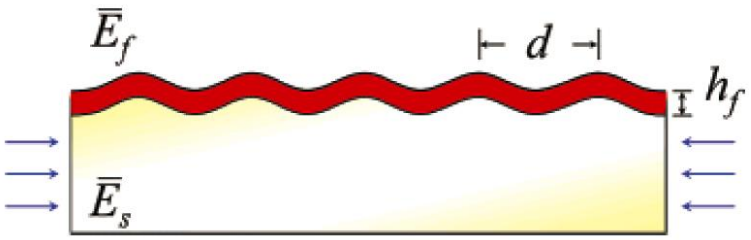

Figure 5.2 Schematics of surface wrinkling test to measure the mechanical properties of a soft material (redrawn from ref. 21). A PS thin film (red) is deposited on a soft gel substrate (yellow).

Another possible approach would to use the buckling test. As demonstrated by Stafford and coworkers, the surface rheological properties of a soft gel can be measured using a "surface wrinkling" technique (Figure 5.2).[20,21] In the wrinkling experiment, a stiff polymer thin film with known mechanical properties (e.g. polystyrene, thickness ≈ 100 nm, red in Figure 5.2) is deposited on the gel (yellow substrate in Figure 5.2). Then, the surface wrinkling is induced by applying a small compressional force on the sample. Simultaneously, the wavelength (*d*) of the wrinkled surface is measured using small angle light scattering or optical microscopy. The rheological properties of ion gel surface can be determined by the following equation.[22]

$$\overline{E}_S = \frac{\overline{E}_f}{3}\left(\frac{d}{2\pi h_f}\right)^{-3} \tag{5.1}$$

In this equation, $\overline{E}_s$ is the modulus of the substrate, $\overline{E}_f$ is the modulus of the polymer thin film, h_f is the thickness of the thin film and d is the wavelength of the wrinkled surfaces.

5.3 Reference

(1) He, Y.; Boswell, P. G.; Buhlmann, P.; Lodge, T. P. *J. Phys. Chem. B* **2007**, *111*, 4645–52.

(2) Bara, J. E.; Lessmann, S.; Gabriel, C. J.; Hatakeyama, E. S.; Noble, R. D.; Gin, D. L. *Ind. Eng. Chem. Res.* **2007**, *46*, 5397–5404.

(3) Bara, J. E.; Hatakeyama, E. S.; Gabriel, C. J.; Zeng, X.; Lessmann, S.; Gin, D. L.; Noble, R. D. *J. Membr. Sci.* **2008**, *316*, 186–191.

(4) Bara, J. E.; Noble, R. D.; Gin, D. L. *Ind. Eng. Chem. Res.* **2009**, *48*, 4607–4610.

(5) Bara, J. E.; Camper, D. E.; Gin, D. L.; Noble, R. D. *Acc. Chem. Res.* **2010**, *43*, 152–159.

(6) Bara, J. E.; Hatakeyama, E. S.; Gin, D. L.; Noble, R. D. *Polym. Adv. Technol.* **2008**, *19*, 1415–1420.

(7) Robeson, L. M. *J. Membr. Sci.* **1991**, *62*, 165–185.

(8) Robeson, L. M. *J. Membr. Sci.* **2008**, *320*, 390–400.

(9) Gu, Y.; Zhang, S.; Martinetti, L.; Lee, K. H.; McIntosh, L. D.; Frisbie, C. D.; Lodge, T. P. *J. Am. Chem. Soc.* **2013**, *135*, 9652–9655.

(10) Bara, J. E.; Carlisle, T. K.; Gabriel, C. J.; Camper, D.; Finotello, A.; Gin, D. L.; Noble, R. D. *Ind. Eng. Chem. Res.* **2009**, *48*, 2739–2751.

(11) Scovazzo, P.; Havard, D.; McShea, M.; Mixon, S.; Morgan, D. *J. Membr. Sci.* **2009**, *327*, 41–48.

(12) Lee, H.-N.; Lodge, T. P. *J. Phys. Chem. Lett.* **2010**, *1*, 1962–1966.

(13) Baker, R. W.; Lokhandwala, K. *Ind. Eng. Chem. Res.* **2008**, *47*, 2109–2121.

(14) Scovazzo, P.; Kieft, J.; Finan, D. A.; Koval, C.; Dubois, D.; Noble, R. D. *J. Membr. Sci.* **2004**, *238*, 57–63.

(15) Huang, J.-F.; Luo, H.; Liang, C.; Jiang, D.; Dai, S. *Ind. Eng. Chem. Res.* **2008**, *47*, 881–888.

(16) Ortiz, A.; María Galán, L.; Gorri, D.; De Haan, A. B.; Ortiz, I. *Ind. Eng. Chem. Res.* **2010**, *49*, 7227–7233.

(17) Yoo, M.; Kim, S.; Lim, J.; Kramer, E. J.; Hawker, C. J.; Kim, B. J.; Bang, J. *Macromolecules* **2010**, *43*, 3570–3575.

(18) Lee, S.; Lee, B.; Kim, B. J.; Park, J.; Yoo, M.; Bae, W. K.; Char, K.; Hawker, C. J.; Bang, J.; Cho, J. *J. Am. Chem. Soc.* **2009**, *131*, 2579–2587.

(19) Lee, K. H.; Zhang, S.; Lodge, T. P.; Frisbie, C. D. *J. Phys. Chem. B* **2011**, *115*, 3315–3321.

(20) Chung, J. Y.; Nolte, A. J.; Stafford, C. M. *Adv. Mater.* **2011**, *23*, 349–68.

(21) Stafford, C. M.; Harrison, C.; Beers, K. L.; Karim, A.; Amis, E. J.; VanLandingham, M. R.; Kim, H.-C.; Volksen, W.; Miller, R. D.; Simonyi, E. E. *Nat. Mater.* **2004**, *3*, 545–50.

(22) Wilder, E. A.; Guo, S.; Lin-Gibson, S.; Fasolka, M. J.; Stafford, C. M. *Macromolecules* **2006**, *39*, 4138–4143.

Bibliography

Ahn, J.; Chung, W.-J.; Pinnau, I.; Song, J.; Du, N.; Robertson, G. P.; Guiver, M. D. *J. Membr. Sci.* **2010**, *346*, 280–287.

Ahn, J.; Chung, W.-J.; Pinnau, I.; Guiver, M. D. *J. Membr. Sci.* **2008**, *314*, 123–133.

Alentiev, A. Y.; Yampolskii, Y. P.; Shantarovich, V. P.; Nemser, S. M.; Plate, N. A. *J. Membr. Sci.* **1997**, *126*, 123–132.

Anderson, J. L.; Dixon, J. K.; Brennecke, J. F. *Acc. Chem. Res.* **2007**, *40*, 1208–1216.

Annable, T.; Buscall, R.; Ettelaie, R.; Whittlestone, D. *J. Rheo.* **1993**, *37*, 695–726.

Anthony, J. L.; Aki, S. N. V. K.; Maginn, E. J.; Brennecke, J. F. *Int. J. Environ. Tech. Manage.* **2004**, *4*, 105–115.

Anthony, J. L.; Anderson, J. L.; Maginn, E. J.; Brennecke, J. F. *J. Phys. Chem. B* **2005**, *109*, 6366–6374.

Aoyagi, N.; Ochiai, B.; Mori, H.; Endo, T. *Synlett* **2006**, 636–638.

Armand, M.; Endres, F.; MacFarlane, D. R.; Ohno, H.; Scrosati, B. *Nat. Mater.* **2009**, *8*, 621–9.

Asai, H.; Fujii, K.; Ueki, T.; Sakai, T.; Chung, U.; Watanabe, M.; Han, Y.-S.; Kim, T.-H.; Shibayama, M. *Macromolecules* **2012**, *45*, 3902–3909.

Babcock, R. E.; Spillman, R. W.; Goddin, C. S.; Cooley, T. E. *Energy Progress* **1988**, *8*, 135–142.

Bai, Z.; He, Y.; Lodge, T. P. *Langmuir* **2008**, *24*, 5284–5290.

Bai, Z.; He, Y.; Young, N. P.; Lodge, T. P. *Macromolecules* **2008**, *41*, 6615–6617.

Bai, Z.; Lodge, T. P. *J. Am. Chem. Soc.* **2010**, *132*, 16265–16270.

Bai, Z.; Zhao, B.; Lodge, T. P. *J. Phys. Chem. B* **2012**, *116*, 8282–8289.

Baker, R. W. *Ind. Eng. Chem. Res.* **2002**, *41*, 1393–1411.

Baker, R. W.; Lokhandwala, K. *Ind. Eng. Chem. Res.* **2008**, *47*, 2109–2121.

Balat, H.; Oz, C. *Energy Exploration & Exploitation* **2007**, *25*, 357–392.

Baltus, R. E.; Counce, R. M.; Culbertson, B. H.; Luo, H.; DePaoli, D. W.; Dai, S.; Duckworth, D. C. *Sep. Sci. Technol.* **2005**, *40*, 525–541.

Baltus, R. E.; Culbertson, B. H.; Dai, S.; Luo, H.; DePaoli, D. W. *J. Phys. Chem. B* **2004**, *108*, 721–727.

Bang, J.; Bae, J.; Lowenhielm, P.; Spiessberger, C.; Given-Beck, S. A.; Russell, T. P.; Hawker, C. J. *Adv. Mater.* **2007**, *19*, 4552–4557.

Bansil, R.; Nie, H.; Li, Y.; Liao, G.; Ludwig, K.; Steinhart, K.; Konak, C.; Lal, J. *Macromol. Symp.* **2002**, *190*, 161–172.

Bara, J. E.; Camper, D. E.; Gin, D. L.; Noble, R. D. *Acc. Chem. Res.* **2010**, *43*, 152–159.

Bara, J. E.; Carlisle, T. K.; Gabriel, C. J.; Camper, D.; Finotello, A.; Gin, D. L.; Noble, R. D. *Ind. Eng. Chem. Res.* **2009**, *48*, 2739–2751.

Bara, J. E.; Gabriel, C. J.; Hatakeyama, E. S.; Carlisle, T. K.; Lessmann, S.; Noble, R. D.; Gin, D. L. *J. Membr. Sci.* **2008**, *321*, 3–7.

Bara, J. E.; Gabriel, C. J.; Lessmann, S.; Carlisle, T. K.; Finotello, A.; Gin, D. L.; Noble, R. D. *Ind. Eng. Chem. Res.* **2007**, *46*, 5380–5386.

Bara, J. E.; Hatakeyama, E. S.; Gabriel, C. J.; Zeng, X.; Lessmann, S.; Gin, D. L.; Noble, R. D. *J. Membr. Sci.* **2008**, *316*, 186–191.

Bara, J. E.; Hatakeyama, E. S.; Gin, D. L.; Noble, R. D. *Polym. Adv. Technol.* **2008**, *19*, 1415–1420.

Bara, J. E.; Lessmann, S.; Gabriel, C. J.; Hatakeyama, E. S.; Noble, R. D.; Gin, D. L. *Ind. Eng. Chem. Res.* **2007**, *46*, 5397–5404.

Bara, J. E.; Noble, R. D.; Gin, D. L. *Ind. Eng. Chem. Res.* **2009**, *48*, 4607–4610.

Bates, E. D.; Mayton, R. D.; Ntai, I.; Davis, J. H. *J. Am. Chem. Soc.* **2002**, *124*, 926–927.

Bates, F. S.; Fredrickson, G. H. *Physics Today* **1999**, 32–38.

Belov, N. A.; Zharov, A. A.; Shashkin, A. V; Shaikh, M. Q.; Raetzke, K.; Yampolskii, Y. P. *J. Membr. Sci.* **2011**, *383*, 70–77.

Berg, J. C. *An Introduction to Interfaces and Colloids: The Bridge to Nanoscience*; World Scientific Publishing Co. Pte. Ltd.: Hackensack, NJ, 2010; p. 785.

Blancard, L. A.; Hancu, D.; Beckman, E. J.; Brennecke, J. F. *Nature* **1999**, *399*, 28–29.

Bonhote, P.; Dias, A.-P.; Papageorgiou, N.; Kalyanasundaram, K.; Graetzel, M. *Inorg. Chem.* **1996**, *35*, 1168–1178.

Brennecke, J. F.; Gurkan, B. E. *J. Phys. Chem. Lett.* **2010**, *1*, 3459–3464.

Budd, P. M.; McKeown, N. B.; Ghanem, B. S.; Msayib, K. J.; Fritsch, D.; Starannikova, L.; Belov, N.; Sanfirova, O.; Yampolskii, Y.; Shantarovich, V. *J. Membr. Sci.* **2008**, *325*, 851–860.

Budd, P. M.; Msayib, K. J.; Tattershall, C. E.; Ghanem, B. S.; Reynolds, K. J.; McKeown, N. B.; Fritsch, D. *J. Membr. Sci.* **2005**, *251*, 263–269.

Cadena, C.; Anthony, J. L.; Shah, J. K.; Morrow, T. I.; Brennecke, J. F.; Maginn, E. J. *J. Am. Chem. Soc.* **2004**, *126*, 5300–5308.

Camper, D.; Bara, J. E.; Gin, D. L.; Noble, R. D. *Ind. Eng. Chem. Res.* **2008**, *47*, 8496–8498.

Camper, D.; Bara, J. E.; Koval, C.; Noble, R. D. *Ind. Eng. Chem. Res.* **2006**, *45*, 6279–6283.

Camper, D.; Becker, C.; Koval, C.; Noble, R. D. *Ind. Eng. Chem. Res.* **2006**, *45*, 445–450.

Carlisle, T. K.; Bara, J. E.; Gabriel, C. J.; Noble, R. D.; Gin, D. L. *Ind. Eng. Chem. Res.* **2008**, *47*, 7005–7012.

Castner, E. W.; Wishart, J. F.; Shirota, H. *Acc. Chem. Res.* **2007**, *40*, 1217–1227.

Chambon, F.; Petrovic, Z. S.; MacKnight, W. J.; Winter, H. H. *Macromolecules* **1986**, *19*, 2146–2149.

Chen, H.; Choi, J.-H.; Cruz, D. S.; Winey, K. I.; Elabd, Y. A. *Macromolecules* **2009**, *42*, 4809–4816.

Chen, H.; Elabd, Y. A. *Macromolecules* **2009**, *42*, 3368–3373.

Cho, J. H.; Lee, J.; He, Y.; Kim, B. S.; Lodge, T. P.; Frisbie, C. D. *Adv. Mater.* **2008**, *20*, 686–690.

Cho, J. H.; Lee, J.; Xia, Y.; Kim, B.; He, Y.; Renn, M. J.; Lodge, T. P.; Frisbie, C. D. *Nat. Mater.* **2008**, *7*, 900–906.

Chu, S. *Science* **2009**, *325*, 1599.

Chung, J. Y.; Nolte, A. J.; Stafford, C. M. *Adv. Mater.* **2011**, *23*, 349–68.

Cong, H.; Radosz, M.; Towler, B. F.; Shen, Y. *Sep. Purif. Technol.* **2007**, *55*, 281–291.

Cordier, P.; Tournilhac, F.; Soulie-Ziakovic, C.; Leibler, L. *Nature* **2008**, *451*, 977–980.

Costello, L. M.; Koros, W. J. *J. Polym. Sci., Part B: Polym. Phys.* **1995**, *33*, 135–146.

Cussler, E. L. *J. Membr. Sci.* **1989**, *43*, 149–164.

Ding, S.; Tang, H.; Radosz, M.; Shen, Y. *J. Polym. Sci., Part A: Polym. Chem.* **2004**, *42*, 5794–5801.

Donohue, M. D.; Minhas, B. S.; Lee, S. Y. *J. Membr. Sci.* **1989**, *42*, 197–214.

Earle, M. J.; Seddon, K. R. *Pure Appl. Chem.* **2000**, *72*, 1391–1398.

Fetters, L. J.; Lohse, D. J.; Richter, D.; Witten, T. A.; Zirkel, A. *Macromolecules* **1994**, *27*, 4639–4647.

Flanigan, C. M.; Crosby, A. J.; Shull, K. R. *Macromolecules* **1999**, *32*, 7251–7262.

Freeman, B. D. *Macromolecules* **1999**, *32*, 375–380.

Freeman, B. D.; Pinnau, I. *ACS Symp. Ser.* **1999**, *733*, 1–27.

Fujii, K.; Asai, H.; Ueki, T.; Sakai, T.; Imaizumi, S.; Chung, U.; Watanabe, M.; Shibayama, M. *Soft Matter* **2012**, *8*, 1756–1759.

Fuller, J.; Carlin, R. T.; De Hugh C., L.; Haworth, D. *J. Chem. Soc., Chem. Commun.* **1994**, 299–300.

Galinski, M.; Lewandowski, A.; Stepniak, I. *Electrochim. Acta* **2006**, *51*, 5567–5580.

Ghanem, B. S.; McKeown, N. B.; Budd, P. M.; Al-Harbi, N. M.; Fritsch, D.; Heinrich, K.; Starannikova, L.; Tokarev, A.; Yampolskii, Y. *Macromolecules* **2009**, *42*, 7881–7888.

Gin, D. L.; Noble, R. D. *Science* **2011**, *332*, 674–676.

Golemme, G.; Jansen, J. C.; Muoio, D.; Bruno, A.; Manes, R.; Buonomenna, M. G.; Choi, J.; Tsapatsis, M. In *Membr. Gas Sep.*; John Wiley & Sons Ltd., 2010; pp. 113–124.

Green, M. D.; Long, T. E. *Polym. Rev.* **2009**, *49*, 291–314.

Gu, Y.; Cussler, E. L.; Lodge, T. P. *J. Membr. Sci.* **2012**, *423-424*, 20–26.

Gu, Y.; Lodge, T. P. *Macromolecules* **2011**, *44*, 1732–1736.

Gu, Y.; Zhang, S.; Martinetti, L.; Lee, K. H.; McIntosh, L. D.; Frisbie, C. D.; Lodge, T. P. *J. Am. Chem. Soc.* **2013**, *135*, 9652–9655.

Hagiwara, R.; Matsumoto, K.; Nakamori, Y.; Tsuda, T.; Ito, Y.; Matsumoto, H.; Momota, K. *J. Electrochem. Soc.* **2003**, *150*, 195–199.

Hammond, G. P.; Akwe, S. S. O. *Int. J. Energ. Res.* **2007**, *31*, 1180–1201.

Harner, J. M.; Hoagland, D. A. *J. Phys. Chem. B* **2010**, *114*, 3411–8.

He, X.; Yang, W.; Pei, X. *Macromolecules* **2008**, *41*, 4615–4621.

He, Y.; Boswell, P. G.; Buhlmann, P.; Lodge, T. P. *J. Phys. Chem. B* **2007**, *111*, 4645–52.

He, Y.; Li, Z.; Simone, P.; Lodge, T. P. *J. Am. Chem. Soc.* **2006**, *128*, 2745–2750.

He, Y.; Lodge, T. P. *Chem. Commun.* **2007**, 2732–2734.

He, Y.; Lodge, T. P. *J. Am. Chem. Soc.* **2006**, *128*, 12666–12667.

He, Y.; Lodge, T. P. *Macromolecules* **2008**, *41*, 167–174.

Hert, D. G.; Anderson, J. L.; Aki, S. N. V. K.; Brennecke, J. F. *Chem. Commun.* **2005**, 2603–2605.

Hiemenz, P. C.; Lodge, T. P. *Polymer Chemistry*; 2nd ed.; CRC Press: New York, 2007.

Hoarfrost, M. L.; Segalman, R. A. *Macromolecules* **2011**, *44*, 5281–5288.

Hu, X.; Tang, J.; Blasig, A.; Shen, Y.; Radosz, M. *J. Membr. Sci.* **2006**, *281*, 130–138.

Huang, J.-F.; Luo, H.; Liang, C.; Jiang, D.; Dai, S. *Ind. Eng. Chem. Res.* **2008**, *47*, 881–888.

Jansen, J. C.; Friess, K.; Clarizia, G.; Schauer, J.; Izak, P. *Macromolecules* **2011**, *44*, 39–45.

Jessop, P. G.; Heldebrant, D. J.; Li, X.; Eckert, C. A.; Liotta, C. L. *Nature* **2005**, *436*, 1102.

Kang, D. J.; Kwon, T.; Kim, M. P.; Cho, C.-H.; Jung, H.; Bang, J.; Kim, B. J. *ACS Nano* **2011**, *5*, 9017–9027.

Katakabe, T.; Kaneko, T.; Watanabe, M.; Fukushima, T.; Aida, T. *J. Electrochem. Soc.* **2005**, *152*, A1913–A1916.

Kawano, R.; Matsui, H.; Matsuyama, C.; Sato, A.; Susan, M. A. B. H.; Tanabe, N.; Watanabe, M. *J. Photochem. Photobiol., A* **2004**, *164*, 87–92.

Kinning, D. J.; Thomas, E. L. *Macromolecules* **1984**, 1712–1718.

Klingshirn, M. A.; Spear, S. K.; Subramanian, R.; Holbrey, J. D.; Huddleston, J. G.; Rogers, R. D. *Chem. Mater.* **2004**, *16*, 3091–3097.

Kofu, M.; Someya, T.; Tatsumi, S.; Ueno, K.; Ueki, T.; Watanabe, M.; Matsunaga, T.; Shibayama, M.; Sakai, V. G.; Tyagi, M.; Yamamuro, O. *Soft Matter* **2012**, *8*, 7888–7897.

Koros, W. J.; Fleming, G. K. *J. Membr. Sci.* **1993**, *83*, 1–80.

Koros, W. J.; Fleming, G. K.; Jordan, S. M.; Kim, T. H.; Hoehn, H. H. *Prog. Polym. Sci.* **1988**, *13*, 339–401.

Krossing, I.; Slattery, J. M.; Daguenet, C.; Dyson, P. J.; Oleinikova, A.; Weingärtner, H. *J. Am. Chem. Soc.* **2006**, *128*, 13427–13434.

Lai, J. T.; Filla, D.; Shea, R. *Macromolecules* **2002**, *35*, 6754–6756.

Lan, W.; Liu, C.-F.; Yue, F.-X.; Sun, R.-C.; Kennedy, J. F. *Carbohydr. Polym.* **2011**, *86*, 672–677.

Lee, H.-N.; Bai, Z.; Newell, N.; Lodge, T. P. *Macromolecules* **2010**, *43*, 9522–9528.

Lee, H.-N.; Lodge, T. P. *J. Phys. Chem. Lett.* **2010**, *1*, 1962–1966.

Lee, H.-N.; Newell, N.; Bai, Z.; Lodge, T. P. *Macromolecules* **2012**, *45*, 3627–3633.

Lee, J.; Aida, T. *Chem. Commun.* **2011**, *47*, 6757–62.

Lee, J.; Panzer, M. J.; He, Y.; Lodge, T. P.; Frisbie, C. D. *J. Am. Chem. Soc.* **2007**, *129*, 4532–4533.

Lee, K. H.; Zhang, S.; Gu, Y.; Lodge, T. P.; Frisbie, C. D. *Manuscript Submitted*.

Lee, K. H.; Zhang, S.; Lodge, T. P.; Frisbie, C. D. *J. Phys. Chem. B* **2011**, *115*, 3315–3321.

Lee, S.; Lee, B.; Kim, B. J.; Park, J.; Yoo, M.; Bae, W. K.; Char, K.; Hawker, C. J.; Bang, J.; Cho, J. *J. Am. Chem. Soc.* **2009**, *131*, 2579–2587.

Li, W.; Sun, N.; Stoner, B.; Jiang, X.; Lu, X.; Rogers, R. D. *Green Chem.* **2011**, *13*, 2038–2047.

Lin, H.; Freeman, B. D. *J. Mol. Struct.* **2005**, *739*, 57–74.

Noble, R. D.; Way, J. D..,*Liquid Membranes: Theory and Applications.*;; ACS Sympos.; American Chemical Society: Washington DC, 1987; p. 196 pp.

Liu, Z.; Wang, H.; Li, Z.; Lu, X.; Zhang, X.; Zhang, S.; Zhou, K. *Mater. Chem. Phys.* **2011**, *128*, 220–227.

Lodge, T. P. *Science* **2008**, *321*, 50–51.

Lozano, L. J.; Godinez, C.; De A. P., los R.; Hernandez-Fernandez, F. J.; Sanchez-Segado, S.; Alguacil, F. J. *J. Membr. Sci.* **2011**, *376*, 1–14.

Lu, J.; Yan, F.; Texter, J. *Prog. Polym. Sci.* **2009**, *34*, 431–448.

Luby, P.; Susta, M. R. *Power* **2007**, *151*, 40,42,44–48,50.

MacFarlane, D. R.; Forsyth, M.; Howlett, P. C.; Pringle, J. M.; Sun, J.; Annat, G.; Neil, W.; Izgorodina, E. I. *Acc. Chem. Res.* **2007**, *40*, 1165–1173.

Marcilla, R.; Mecerreyes, D.; Winroth, G.; Brovelli, S.; Rodriguez Maria del Mar, Y.; Cacialli, F. *Appl. Phys. Lett.* **2010**, *96*, 043308/1–043308/3.

Matsumoto, K.; Endo, T. *Macromolecules* **2008**, *41*, 6981–6986.

Matsumoto, K.; Endo, T. *Macromolecules* **2009**, *42*, 4580–4584.

Mayadunne, R. T. A.; Rizzardo, E.; Chiefari, J.; Krstina, J.; Moad, G.; Postma, A.; Thang, S. H. *Macromolecules* **2000**, *33*, 243–245.

McKeown, N. B.; Budd, P. M.; Msayib, K. J.; Ghanem, B. S.; Kingston, H. J.; Tattershall, C. E.; Makhseed, S.; Reynolds, K. J.; Fritsch, D. *Chem.Eur. J.* **2005**, *11*, 2610–2620.

Mecerreyes, D. *Prog. Polym. Sci.* **2011**, *36*, 1629–1648.

Meli, L.; Lodge, T. P. *Macromolecules* **2009**, *42*, 580–583.

Meli, L.; Santiago, J. M.; Lodge, T. P. *Macromolecules* **2010**, *43*, 2018–2027.

Mischenko, N.; Reynders, K.; Koch, M. H. J.; Mortensen, K.; Pedersen, S.; Fontaine, F.; Graulus, R.; Reynaers, H. *Macromolecules* **1995**, *28*, 2054–2062.

Morgan, D.; Ferguson, L.; Scovazzo, P. *Ind. Eng. Chem. Res.* **2005**, *44*, 4815–4823.

Muhammad, N.; Man, Z.; Khalil, M. A. B.; Elsheikh, Y. A. *J. Appl. Sci.* **2010**, *10*, 1090–1096.

Muldoon, M. J.; Aki, S. N. V. K.; Anderson, J. L.; Dixon, J. K.; Brennecke, J. F. *J. Phys. Chem. B* **2007**, *111*, 9001–9009.

Myers, C.; Pennline, H.; Luebke, D.; Ilconich, J.; Dixon, J. K.; Maginn, E. J.; Brennecke, J. F. *J. Membr. Sci.* **2008**, *322*, 28–31.

Nakajima, H.; Ohno, H. *Polymer* **2005**, *46*, 11499–11504.

Neouze, M.-A.; Le Bideau, J.; Gaveau, P.; Bellayer, S.; Vioux, A. *Chem. Mater.* **2006**, *18*, 3931–3936.

Neves, L. A.; Crespo, J. G.; Coelhoso, I. M. *J. Membr. Sci.* **2010**, *357*, 160–170.

Neyertz, S.; Brown, D.; Pandiyan, S.; Van N. F. A., der V. *Macromolecules* **2010**, *43*, 7813–7827.

Noble, R. D.; Gin, D. L. *J. Membr. Sci.* **2011**, *369*, 1–4.

Noble, R. D.; Stern, S. A., *Membrane Separations Technology: Principles and Applications*; Eds.; 2nd Ed.; Elsevier, 1995; p. 718 pp.

Noro, A.; Matsushita, Y.; Lodge, T. P. *Macromolecules* **2008**, *41*, 5839–5844.

Noro, A.; Matsushita, Y.; Lodge, T. P. *Macromolecules* **2009**, *42*, 5802–5810.

Ohno, H. *Macromol. Symp.* **2007**, *249-250*, 551–556.

Ohno, H.; Ito, K. *Chem. Lett.* **1998**, 751–752.

Ohno, H.; Yoshizawa, M.; Ogihara, W. *Electrochim. Acta* **2004**, *50*, 255–261.

Ortiz, A.; María Galán, L.; Gorri, D.; De Haan, A. B.; Ortiz, I. *Ind. Eng. Chem. Res.* **2010**, *49*, 7227–7233.

Park, J.; Kim, J.; Lee, S.; Bang, J.; Kim, B. J.; Kim, Y. S.; Cho, J. *J. Mater. Chem.* **2009**, *19*, 4488–4490.

Pham, T. P. T.; Cho, C.-W.; Yun, Y.-S. *Water Res.* **2010**, *44*, 352–72.

Phillip, W. A. Block Copolymer Membranes for Selective Separations. Ph.D. Thesis, University of Minnesota, Twin Cities, 2009, p. 202.

Pinnau, I.; Toy, L. G. *J. Membr. Sci.* **1996**, *109*, 125–133.

Puleo, A. C.; Muruganandam, N.; Paul, D. R. *Journal of Polymer Science, Part B: Polymer Physics* **1989**, *27*, 2385–2406.

Qin, Y.; Lu, X.; Sun, N.; Rogers, R. D. *Green Chem.* **2010**, *12*, 968–971.

Remsing, R. C.; Swatloski, R. P.; Rogers, R. D.; Moyna, G. *Chem. Commun.* **2006**, 1271–1273.

Robeson, L. M. *J. Membr. Sci.* **1991**, *62*, 165–185.

Robeson, L. M. *J. Membr. Sci.* **2008**, *320*, 390–400.

Robeson, L. M.; Smith, C. D.; Langsam, M. *J. Membr. Sci.* **1997**, *132*, 33–54.

Rochelle, G. T. *Science* **2009**, *325*, 1652–1654.

Sato, T.; Watanabe, H.; Osaki, K. *Macromolecules* **2000**, *33*, 1686–1691.

Schrag, D. P. *Science* **2007**, *315*, 812–813.

Schuber, T. *Ionic Liquids Today* **2007**, *6*, 2–7.

Scovazzo, P. *J. Membr. Sci.* **2009**, *343*, 199–211.

Scovazzo, P.; Havard, D.; McShea, M.; Mixon, S.; Morgan, D. *J. Membr. Sci.* **2009**, *327*, 41–48.

Scovazzo, P.; Kieft, J.; Finan, D. A.; Koval, C.; Dubois, D.; Noble, R. D. *J. Membr. Sci.* **2004**, *238*, 57–63.

Seitz, M. E.; Burghardt, W. R.; Faber, K. T.; Shull, K. R. *Macromolecules* **2007**, *40*, 1218–1226.

Seki, S.; Susan, M. A. B. H.; Kaneko, T.; Tokuda, H.; Noda, A.; Watanabe, M. *J. Phys. Chem. B* **2005**, *109*, 3886–3892.

Sen, D.; Kalipcilar, H.; Yilmaz, L. *J. Membr. Sci.* **2007**, *303*, 194–203.

Shiflett, M. B.; Yokozeki, A. *Ind. Eng. Chem. Res.* **2005**, *44*, 4453–4464.

Simone, P. M.; Lodge, T. P. *ACS Appl. Mater. Interfaces* **2009**, *1*, 2812–20.

Simone, P. M.; Lodge, T. P. *Macromolecules* **2008**, *41*, 1753–1759.

Simons, K.; Nijmeijer, K.; Bara, J. E.; Noble, R. D.; Wessling, M. *J. Membr. Sci.* **2010**, *360*, 202–209.

Singh, B.; Sekhon, S. S. *J. Phys. Chem. B* **2005**, *109*, 16539–16543.

Smith, G. D.; Borodin, O.; Li, L.; Kim, H.; Liu, Q.; Bara, J. E.; Gin, D. L.; Nobel, R. *Phys. Chem. Chem. Phys.* **2008**, *10*, 6301–6312.

Snedden, P.; Cooper, A. I.; Scott, K.; Winterton, N. *Macromolecules* **2003**, *36*, 4549–4556.

Spillman, R. W. *Chem. Eng. Prog.* **1989**, *85*, 41–62.

Stafford, C. M.; Harrison, C.; Beers, K. L.; Karim, A.; Amis, E. J.; VanLandingham, M. R.; Kim, H.-C.; Volksen, W.; Miller, R. D.; Simonyi, E. E. *Nat. Mater.* **2004**, *3*, 545–50.

Stancik, C. M.; Lavoie, A. R.; Achurra, P. A.; Waymouth, R. M.; Gast, A. P. *Langmuir* **2004**, *20*, 8975–87.

Stern, S. A. *J. Membr. Sci.* **1994**, *94*, 1–65.

Stern, S. A.; Shah, V. M.; Hardy, B. J. *Journal of Polymer Science, Part B: Polymer Physics* **1987**, *25*, 1263–1298.

Sun, N.; Rodriguez, H.; Rahman, M.; Rogers, R. D. *Chem. Commun.* **2011**, *47*, 1405–1421.

Susan, M. A. B. H.; Kaneko, T.; Noda, A.; Watanabe, M. *J. Am. Chem. Soc.* **2005**, *127*, 4976–4983.

Swatloski, R. P.; Holbrey, J. D.; Rogers, R. D. *Green Chem.* **2003**, *5*, 361–363.

Swatloski, R. P.; Spear, S. K.; Holbrey, J. D.; Rogers, R. D. *J. Am. Chem. Soc.* **2002**, *124*, 4974–4975.

Tae, G.; Kornfield, J. A.; Hubbell, J. A.; Lal, J. *Macromolecules* **2002**, *35*, 4448–4457.

Tanaka, F.; Edwards, S. F. *Macromolecules* **1992**, *25*, 1516–1523.

Tanaka, K.; Okano, M.; Toshino, H.; Kita, H.; Okamoto, K. *J. Polym. Sci., Part B: Polym. Phys.* **1992**, *30*, 907–914.

Tang, H.; Tang, J.; Ding, S.; Radosz, M.; Shen, Y. *J. Polym. Sci., Part A: Polym. Chem.* **2005**, *43*, 1432–1443.

Tang, J.; Radosz, M.; Shen, Y. *Macromolecules* **2008**, *41*, 493–496.

Tang, J.; Shen, Y.; Radosz, M.; Sun, W. *Ind. Eng. Chem. Res.* **2009**, *48*, 9113–9118.

Tang, J.; Tang, H.; Sun, W.; Plancher, H.; Radosz, M.; Shen, Y. *Chem. Commun.* **2005**, 3325–3327.

Tang, J.; Tang, H.; Sun, W.; Radosz, M.; Shen, Y. *J. Polym. Sci., Part A: Polym. Chem.* **2005**, *43*, 5477–5489.

Tokuda, H.; Hayamizu, K.; Ishii, K.; Susan, M. A. B. H.; Watanabe, M. *J. Phys. Chem. B* **2004**, *108*, 16593–16600.

Tokuda, H.; Hayamizu, K.; Ishii, K.; Susan, M. A. B. H.; Watanabe, M. *J. Phys. Chem. B* **2005**, *109*, 6103–6110.

Tokuda, H.; Ishii, K.; Susan, M. A. B. H.; Tsuzuki, S.; Hayamizu, K.; Watanabe, M. *J. Phys. Chem. B* **2006**, *110*, 2833–2839.

Treloar, L. R. G. *Trans. Faraday Soc.* **1944**, *40*, 59–70.

Ueki, T.; Karino, T.; Kobayashi, Y.; Shibayama, M.; Watanabe, M. *J. Phys. Chem. B* **2007**, *111*, 4750–4754.

Ueki, T.; Watanabe, M. *Chem. Lett.* **2006**, *35*, 964–965.

Ueki, T.; Watanabe, M. *Langmuir* **2007**, *23*, 988–990.

Ueki, T.; Watanabe, M. *Macromolecules* **2008**, *41*, 3739–3749.

Ueki, T.; Watanabe, M.; Lodge, T. P. *Macromolecules* **2009**, *42*, 1315–1320.

Vega, D. A.; Sebastian, J. M.; Loo, Y.-L.; Register, R. A. *J. Polym. Sci., Part B: Polym. Phys.* **2001**, *39*, 2183–2197.

Virgili, J. M.; Nedoma, A. J.; Segalman, R. A.; Balsara, N. P. *Macromolecules* **2010**, *43*, 3750–3756.

Visser, A. E.; Swatloski, R. P.; Reichert, W. M.; Davis Jr., J. H.; Rogers, R. D.; Mayton, R.; Sheff, S.; Wierzbicki, A. *Chem. Commun.* **2001**, 135–136.

Visser, T.; Koops, G. H.; Wessling, M. *J. Membr. Sci.* **2005**, *252*, 265–277.

Voss, B. A.; Bara, J. E.; Gin, D. L.; Noble, R. D. *Chem. Mater.* **2009**, *21*, 3027–3029.

Vu, D. Q.; Koros, W. J.; Miller, S. J. *Ind. Eng. Chem. Res.* **2002**, *41*, 367–380.

Walden, P. *Bull. Sci. Acad. Imp. Sci. St. Petersb.* **1914**, 405–422.

Wang, H.; Gurau, G.; Rogers, R. D. *Chem. Soc. Rev.* **2012**, *41*, 1519–37.

Washiro, S.; Yoshizawa, M.; Nakajima, H.; Ohno, H. *Polymer* **2004**, *45*, 1577–1582.

Wasserscheid, P.; Welton, T.; Editors. *Ionic Liquids in Synthesis.*; Wiley-VCH Verlag GmbH & Co. KGaA, 2003; p. 364 pp.

Welton, T. *Chem. Rev.* **1999**, *99*, 2071–2084.

Wilder, E. A.; Guo, S.; Lin-Gibson, S.; Fasolka, M. J.; Stafford, C. M. *Macromolecules* **2006**, *39*, 4138–4143.

Wilkes, J. S. *Green Chem.* **2002**, *4*, 73–80.

Wilkes, J. S.; Levisky, J. A.; Wilson, R. A.; Hussey, C. L. *Inorg. Chem.* **1982**, *21*, 1263–1264.

Wilkes, J. S.; Zaworotko, M. J. *J. Chem. Soc., Chem. Commun.* **1992**, 965–967.

Wind, J. D.; Paul, D. R.; Koros, W. J. *J. Membr. Sci.* **2004**, *228*, 227–236.

Wind, J. D.; Staudt-Bickel, C.; Paul, D. R.; Koros, W. J. *Ind. Eng. Chem. Res.* **2002**, *41*, 6139–6148.

Winter, H. H.; Chambon, F. *J. Rheo.* **1986**, *30*, 367–382.

Winterton, N. *J. Mater. Chem.* **2006**, *16*, 4281–4293.

Yampolskii, Y. *Macromolecules* **2012**, *45*, 3298–3311.

Yan, F.; Texter, J. *Angew. Chem., Int. Ed.* **2007**, *46*, 2440–2443.

Yang, C.; Nuxoll, E. E.; Cussler, E. L. *AIChE J.* **2001**, *47*, 295–302.

Yang, T.; Xiao, Y.; Chung, T.-S. *Energy & Environmental Science* **2011**, *4*, 4171–4180.

Yoo, M.; Kim, S.; Lim, J.; Kramer, E. J.; Hawker, C. J.; Kim, B. J.; Bang, J. *Macromolecules* **2010**, *43*, 3570–3575.

Yoshizawa, M.; Hirao, M.; Ito-Akita, K.; Ohno, H. *J. Mater. Chem.* **2001**, *11*, 1057–1062.

Yuan, J.; Antonietti, M. *Polymer* **2011**, *52*, 1469–1482.

Yuan, J.; Mecerreyes, D.; Antonietti, M. *Prog. Polym. Sci.* Ahead of Print.

Zhang, S.; Lee, K. H.; Frisbie, C. D.; Lodge, T. P. *Macromolecules* **2011**, *44*, 940–949.

Zhang, S.; Lee, K. H.; Sun, J.; Frisbie, C. D.; Lodge, T. P. *Macromolecules* **2011**, *44*, 8981–8989.

Appendix A

Small Angle Neutron Scattering (SANS) Investigation of Homopolymer Conformations in Ionic Liquid

In Chapter 3, we have examined the separation performance of block copolymer ion gels with PEO and PMMA mid-blocks. It is well recognized that PEO and PMMA are soluble in [EMI][TFSA], as well as in several other ionic liquids. Indeed, many polymer/ionic liquid composite materials, including block copolymer ion gels, are developed based on the compatibility of the ionic liquid and polymers.[1–4] However, only a few studies have investigated the interaction between polymers and ionic liquids.[5] Polymer conformation in a solvent provides information about the solvent quality. For instance, a flexible polymer such as PEO and PMMA adopts a swollen coil conformation in a good solvent. The relationship between the molecular weight (M) of the polymer and its radius of gyration (R_g) is $R_g \sim M^{3/5}$. Here, we describe some preliminary efforts to study the polymer chain conformations in ionic liquids using small angle neutron scattering (SANS). SANS is a useful technique to investigate the conformation of polymer chains in dilute solution or melt state. In previous reports, Yamakawa et al. have systematically studied the chain conformation of PMMA in the good solvents (acetone) and theta solvent (acetonitrile, MeCN).[6] Devanand and Brown have also studied the

radius of gyration (R_g) of PEO in water and methanol.[7–9] Kugler and Smith have studied the R_g of PEO in melt.[10,11] Their results are used as reference values in this research.

A preliminary set of experiments were conducted to study the radius of gyration (R_g) of PEO, PMMA and PIL in dilute ionic liquid solutions. The PIL (112kDa, $Đ$ = 1.28) and deuterated ionic liquid d_5-[EMI][TFSA] were synthesized following previously reported procedures.[12,13] PEO (M_n = 145 kDa, $Đ$ = 1.07) was a polymer standard for SEC, which is obtained from Toyo Soda MFG. Co. PMMA (M_n = 100 kDa, $Đ$ = 1.10) was previously synthesized by Dr. Ilan Zeroni. PMMA (M_n = 480 kDa, $Đ$ = 1.05) was obtained from Polymer Lab Inc. Polymer solution samples were prepared using the solvent casting method as described in the Chapter 2. CH_2Cl_2 was used as the co-solvent.

SANS experiments were performed on the CG-2 General Purpose SANS instrument at the High Flux Isotope Reactor (HFIR) facility of the Oak Ridge National Laboratory (ORNL) in Oak Ridge, Tennessee. The incident neutron beam had a wavelength of 4.75 Å. The samples were dilute polymer solutions sealed in banjo cells with 1 mm thickness. All samples were exposed to neutron irradiation for 20-30 minutes at 30 ℃. Data were corrected for empty cell, solvent scattering and detector sensitivity. The obtained 2-dimensional patterns were then azimuthally averaged to obtain 1-dimensional I versus q representation of the data.

The I vs q curves for PEO/[EMI][TFSA] and PMMA/[EMI][TFSA] solutions are displayed in Figure A.1. The radius of gyration (R_g) of all these solutions were determined by fitting the scattering data to the Debye function (Equation A.1) using non-linear regression

$$I(q) = \left[\frac{2A}{(qR_g)^4}\right]\left[e^{-(qR_g)^2} - 1 + (qR_g)^2\right] + B \qquad \text{(A.1)}$$

where A is a prefactor, B is the baseline correction and R_g is the radius of gyration. In an ideal condition, Guinier plot can be used to extract information of R_g instead of Debye function, to avoid making assumptions about chain conformations. However, the Guinier fitting was not adopted here because the q range investigated in this experiment does not fully extend into the Guinier regime to avoid uncertainties at low q. The assumption of $qR_g < 1$ cannot be met in the current experimental setting. On the other hand, by using the Debye function, the data obtained over the entire q range can be utilized to analyze the results. The original I vs. q curves for PMMA are displayed in Figure A.1 and those for PEO and PIL are displayed in Figures A.2 and A.3.

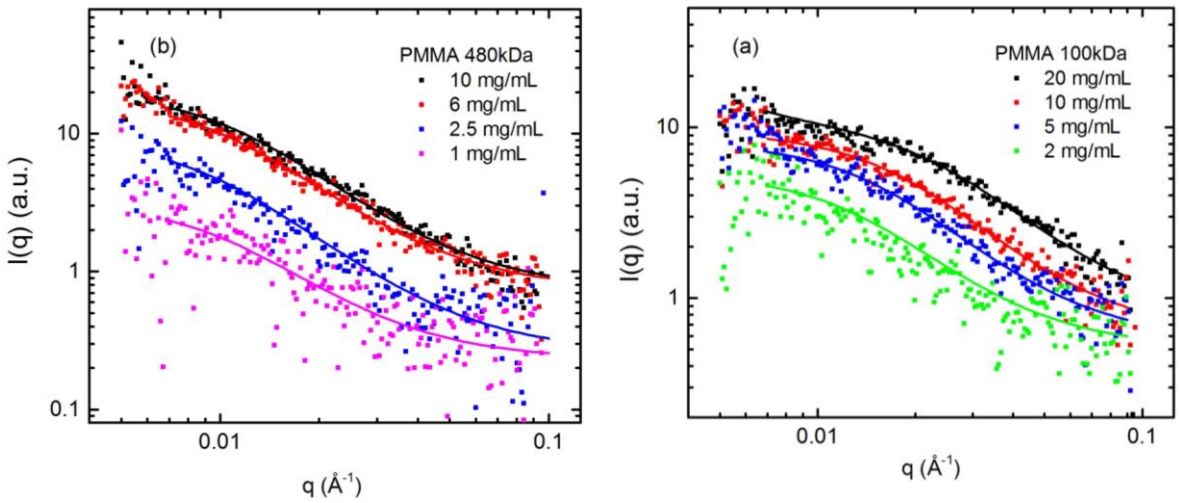

Figure A.1 Intensity profiles of dilute solutions with different concentration (a) PMMA (100kDa) in d_5-[EMI][TFSA], and (b) PMMA (480kDa) in d_5-[EMI][TFSA].

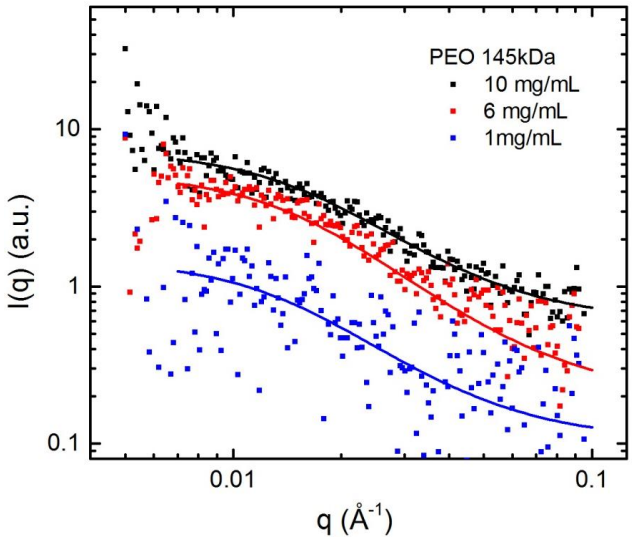

Figure A.2 Intensity profiles of dilute polymer solutions at various concentrations for PEO (145kDa) in d_5-[EMI][TFSA].

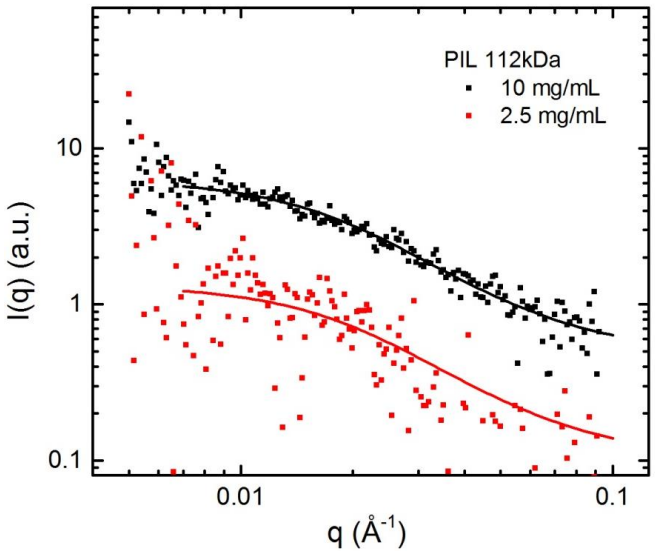

Figure A.3 Intensity profiles of dilute polymer solutions at various concentrations for PEO (145kDa) in d_5-[EMI][TFSA].

Table A.1 Apparent radius of gyration from Debye fitting

Polymer	Concentration (mg/mL)	R_g (Å, Debye)
PMMA 100 kDa	20	67 ± 3
	10	88 ± 6
	5	103 ± 11
	2	118 ± 25
PMMA 480 kDa	10	146 ± 8
	6	157 ± 13
	2.5	170 ± 19
	1	175 ± 55
PEO 145 kDa	10	100 ± 7
	6	101 ± 14
	1	112 ± 45
PIL 112 kDa	10	81 ± 8
	2.5	86 ± 22

Table A.1 listed the apparent R_g values at various concentrations obtained from Debye fitting. The values of infinite dilution R_g for PEO and PMMA in d_5-[EMI][TFSA] were obtained by extrapolation to zero concentration, as shown in Figure A.4. The infinite dilution R_g for PIL cannot be obtained due to the limited data points available. The obtained infinite dilution R_g was 119 ± 4 Å and 176 ± 3 Å for PMMA (100kDa) and PMMA (480kDa), respectively. The infinite dilution R_g for PEO (145kDa) was 113 ± 6 Å. These results were also compared with the literature values of these two polymers in either good solvent or theta solvent. As shown in Figure A.5, the R_g for PMMA is in

reasonable expect with that of the common organic solvents, indicating that the solvent quality of [EMI][TFSA] for PMMA is between a typical good solvent and a typical theta solvent. On the other hand, the value of R_g for PEO in [EMI][TFSA] is smaller than that in the good solvents and the melt, which suggests that PEO in [EMI][TFSA] may not be a swollen coil. However, it is necessary to point out the error bar of the fitting results are fairly large at low concentration, which is mainly due to the very low scattering intensity of the dilute solutions. Therefore, additional experiments to confirm the data reproducibility and to more extensively analyze the effect of polymer molecular weight on R_g are required before a reliable conclusion can be drawn. Future experiments should also consider reaching a lower q range to allow accessing the Guinier regime (qR_g < 1).This should allow using the Guinier analysis to obtain information of R_g without making prior assumptions about the polymer chain conformation.

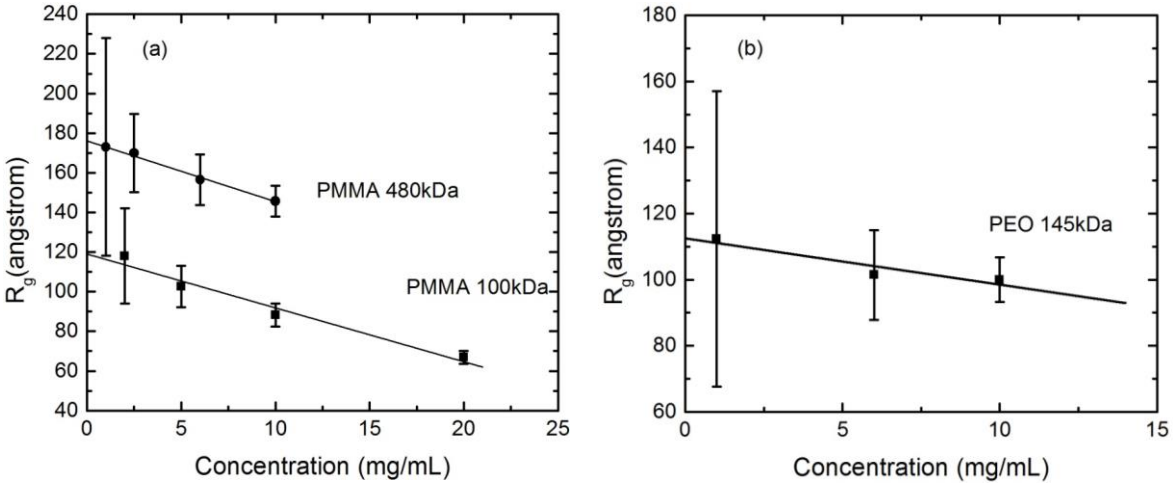

Figure A.4 Concentration dependence of radius of gyration for (a) PMMA (100kDa and 480 kDa) in d_5-[EMI][TFSA], and (b) PEO (145 kDa) in d_5-[EMI][TFSA]. Intercept on vertical axis indicated the infinite dilution values of R_g.

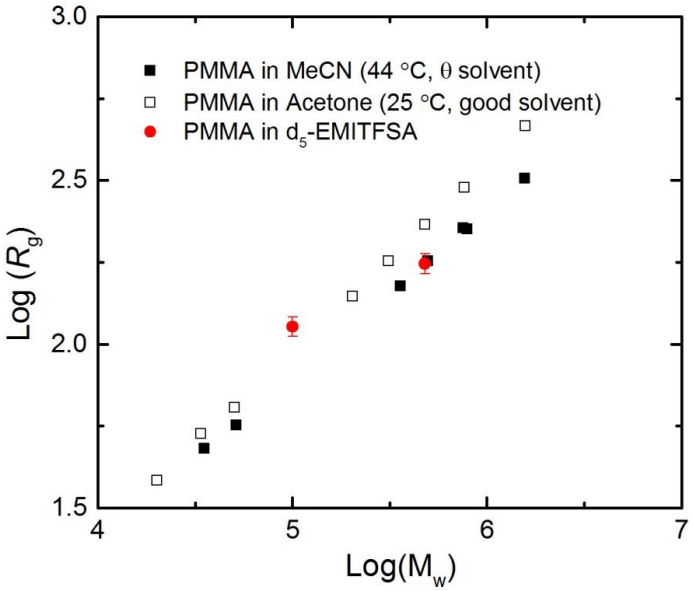

Figure A.5 Comparison of *R*g for PMMA in [EMI][TFSA] with previous literature values for PMMA in theta solvent and good solvent. *R*g values were adapted from Ref.6.

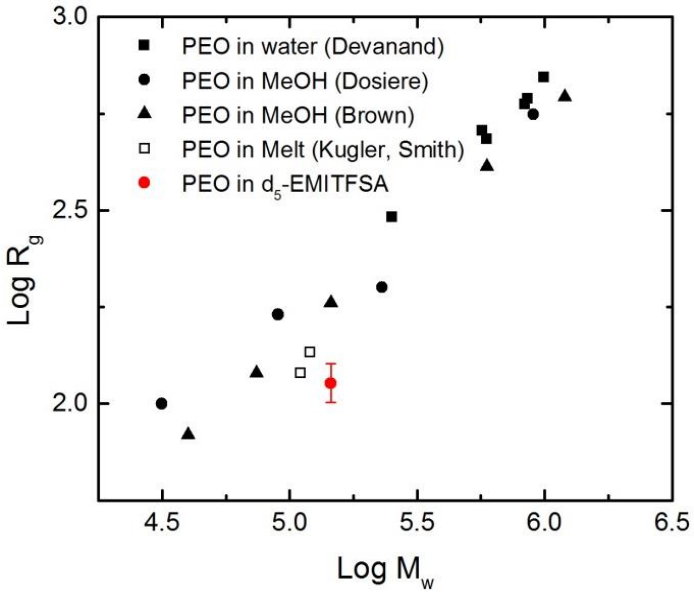

Figure A.6 Comparison of *R*g for PEO in [EMI][TFSA] with previous literature values for PEO in good solvents (water and methanol) and in melt. *R*g values were adapted from Ref.7-11.

References

(1) Fujii, K.; Asai, H.; Ueki, T.; Sakai, T.; Imaizumi, S.; Chung, U.; Watanabe, M.; Shibayama, M. *Soft Matter* **2012**, *8*, 1756–1759.

(2) Asai, H.; Fujii, K.; Ueki, T.; Sakai, T.; Chung, U.; Watanabe, M.; Han, Y.-S.; Kim, T.-H.; Shibayama, M. *Macromolecules* **2012**, *45*, 3902–3909.

(3) Susan, M. A. B. H.; Kaneko, T.; Noda, A.; Watanabe, M. *J. Am. Chem. Soc.* **2005**, *127*, 4976–4983.

(4) Zhang, S.; Lee, K. H.; Frisbie, C. D.; Lodge, T. P. *Macromolecules* **2011**, *44*, 940–949.

(5) Mok, M. M.; Liu, X.; Bai, Z.; Lei, Y.; Lodge, T. P. *Macromolecules* **2011**, *44*, 1016–1025.

(6) Abe, F.; Horita, K.; Einaga, Y.; Yamakawa, H. *Macromolecules* **1994**, *27*, 725–732.

(7) Zhou, P.; Brown, W. *Macromolecules* **1990**, *23*, 1131–1139.

(8) Devanand, K.; Selser, J. C. *Macromolecules* **1991**, *24*, 5943–5947.

(9) Vandermiers, C.; Damman, P.; Dosiere, M. *Polymer* **1998**, *39*, 5627–5631.

(10) Kugler, J.; Fischer, E. W.; Peuscher, M.; Eisenbach, C. D. *Makromol. Chem.* **1983**, *184*, 2325–2334.

(11) Smith, G. D.; Yoon, D. Y.; Jaffe, R. L.; Colby, R. H.; Krishnamoorti, R.; Fetters, L. J. *Macromolecules* **1996**, *29*, 3462–3469.

(12) Gu, Y.; Lodge, T. P. *Macromolecules* **2011**, *44*, 1732–1736.

(13) Lee, H.-N.; Newell, N.; Bai, Z.; Lodge, T. P. *Macromolecules* **2012**, *45*, 3627–3633.

Appendix B

Photo-Induced Cross-Linking of Ion Gels*

In Chapter 4, a new ABA-triblock copolymer ion gel with cross-linkable end-blocks was described. Azide functional groups in the end-blocks were cross-linked by annealing the gel at elevated temperatures. We have discovered that the mass transport rate through the ion gel was unaffected by the cross-linking, while the toughness was increased by almost an order of magnitude.[1] Practically, however, heating the ion gel at 200 ℃ for 45 minutes under inert atmosphere is a very harsh condition for materials processing. For applications in both gas separation and plastic electronics, degradation of the other components in the membrane or electronic devices at such a high temperature will be a big concern. Previous studies by Bang et al. have shown that azide groups can also be cross-linked by UV-irradiation at 254 nm.[2–4] Compared with thermal cross-linking, photo-induced cross-linking of ion gels will require a lower energy cost and easier processing.[5,6] It is also possible achieve photo-patterning of the ion gels via UV cross-linking. Here, initial research efforts to achieve UV cross-linking of the same SOS-N_3 ion gels were described. This Appendix also serves as a supplement to Chapter 4.

In this project, all the chemicals and materials were the same as described in Chapter 4, or synthesized following the same procedure. The research described here was also

* This work is conducted in collaboration with Dr. Jae-Hong Choi.

focused on the cross-linking of 10 wt% SOS-N_3(3.8-35-3.8) ion gels for a direct comparison with the thermally cross-linked samples.

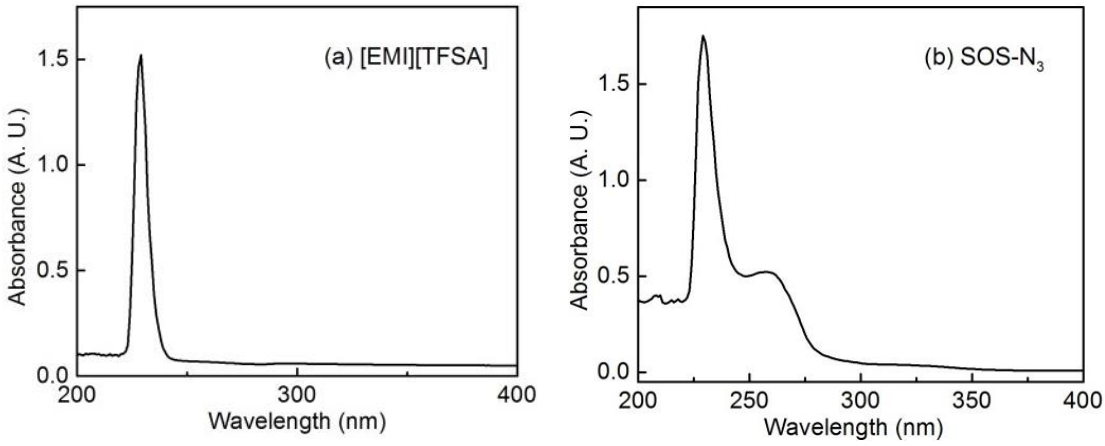

Figure B.1 UV-Vis absorption spectra of (a) [EMI][TFSA], and (b) SOS-N_3(3.8-35-3.8) in the wavelength range of 200 – 400 nm.

To examine the viability of using UV-irradiation to achieve chemical cross-linking of ion gels, UV-Vis spectroscopy has been used to study the UV-absorption of different components in the ion gels. Figure B.1 displays the UV-absorption spectra of both SOS-N_3 triblock copolymer and ionic liquid [EMI][TFSA]. While both components of the ion gel show strong absorption peaks near 229 nm, the SOS-N_3 triblock copolymer can also strongly absorb UV light at around 256 nm, which happened to be very close to the wavelength of commercial mercury vapor lamps (254 nm). Therefore, a hand-held mercury lamp was used for cross-linking in this project.

Ion gel samples were prepared using a solvent casting method. Premixed stock solution for ion gels was prepared by dissolving the mixture of SOS-N_3 triblock copolymer, [EMI][TFSA] at a weight ratio of 1:9 in CH_2Cl_2. Then, the solution was drop

casted onto a polished NaCl salt plate. After the sample was purged under N_2 flow for 2 hours, a thin layer of ion gel film formed on top of the salt plate. The residual solvents were then removed under vacuum at 60 ℃ for 24 hours. The average thickness of the ion gel was calculated by weight.

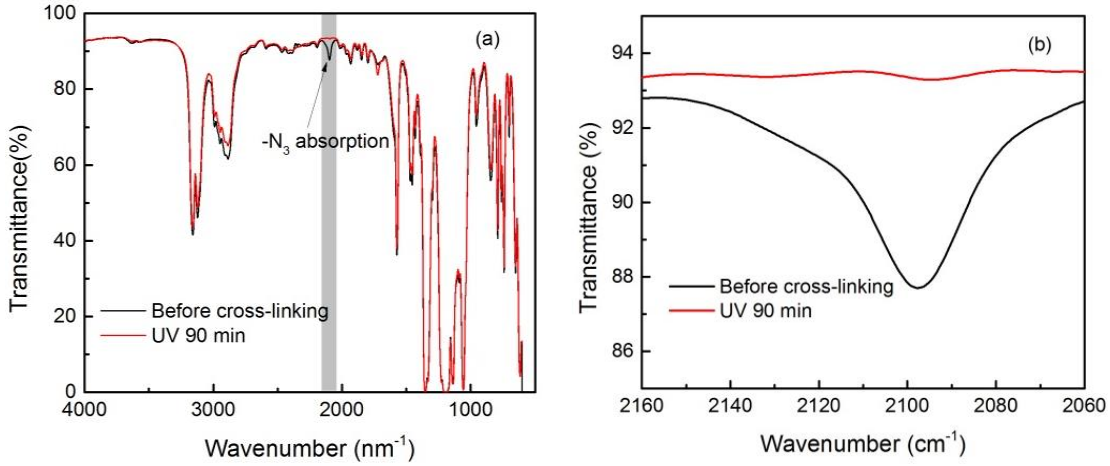

Figure B.2 (a) Full IR spectra of a 10 wt% SOS-N_3 ion gel film (ca. 30 μm) before cross-linking (black) and after UV exposure for 90 min (red); (b) expanded IR spectra for the azide absorption peak in the range of 2160-2060 cm^{-1}.

A UVGL-55 hand-held UV lamp (UVP Inc., intensity = 1.29 mW/cm^2 at 254 nm) was used to investigate the cross-linking of ion gel samples. In a typical experiment, the sample was placed under the UV lamp in a glove box, and exposed for a certain amount of time (e.g. 90 minutes). After UV exposure, FTIR was used to monitor the cross-linking reaction of the azide groups in ion gel samples (Figure B.2). The absorption peak of azide group (ca. 2095 cm^{-1}) gradually decreases with increased amount irradiation time, while the gel film remains a solid. Through comparison with the IR spectra of thermally cross-linked ion gel samples (Chapter 4, Figure 4.15), it is discovered that 90 minutes of UV-

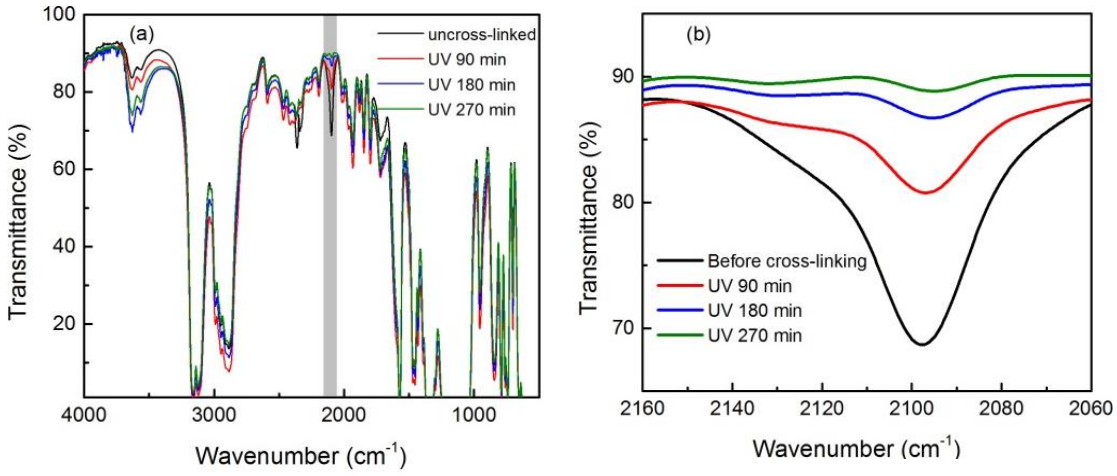

Figure B.3 (a) Full IR spectra of a 10 wt% SOS-N_3 ion gel film (ca. 60 μm) before cross-linking (black) and after UV exposure for 90, 180 and 270 min (red, blue and green, respectively); (b) expanded IR spectra for the azide absorption peak in the range of 2160-2060 cm^{-1}.

exposure can achieve a similar level of cross-linking on the ion gel film as 200 ℃ annealing for 45 minutes. In addition, the ion gel samples before after UV exposure were also immersed in CH_2Cl_2, a good solvent for both [EMI][TFSA] and SOS-N_3 triblock copolymer, to check their solubility. While the uncross-linked physical gel quickly dissolved in the CH_2Cl_2, the sample exposed to UV-irradiation could only swell in the solvent. This result further confirmed the chemical cross-linking of SOS-N_3 ion gels by UV-irradiation.

Furthermore, we also found that the rate of UV cross-linking strongly depends on the thickness of ion gel films, as it required a significantly longer time (270 min, as shown in Figure B.3) to achieve complete cross-linking of a 60-μm-thick ion gel film than the cross-linking of the ion gel samples with ca. 30 μm thickness (90 min). This is likely due

to the UV-absorption of [EMI][TFSA]. It also suggested that UV-irradiation should be more suitable for cross-linking the ion gel thin films instead of bulk materials.

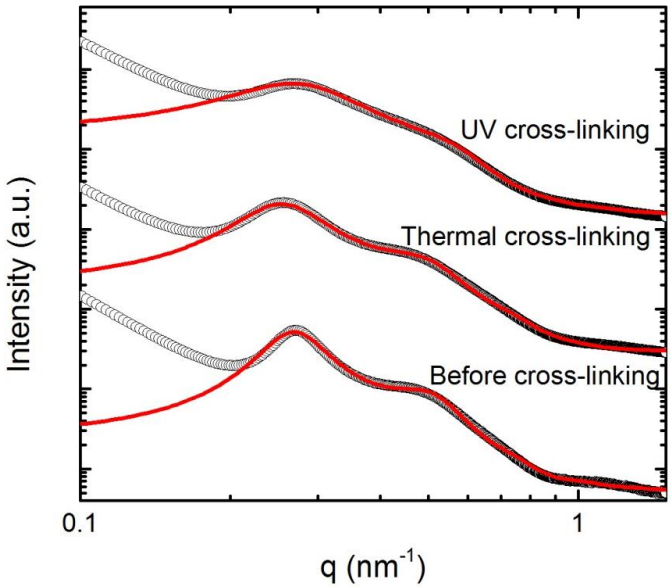

Figure B.4 1D SAXS profiles of 10 wt% SOS-N_3 ion gels before cross-linking and after UV or thermal cross-linking. SAXS patterns were fitted to Percus-Yevick hard sphere model. Black open circles are experimental data, and the red curves are fitting results.

Small angle X-ray scattering (SAXS) has also been used to study the microstructure of the UV cross-linked ion gels. Figure B.4 showed the SAXS scattering patterns of the UV cross-linked samples, and their fitting to the Percus-Yevick hard sphere model.[7–11] This model assumes a dense core of the PS-N_3 domains, with radius R_c, which is surrounded by an outer shell of dissolved PEO chains defining an effective hard-core radius, R_{HS}. The model also incorporates the standard deviation of the core size, σ_{Rc}. The

microstructure of the gel is assumed as a liquid with interacting hard spheres, at a volume fraction ϕ. The average aggregation number of the PS-N_3 micelle cores, N_{agg}, and the average core-to-core distance, d_{nn}, were calculated from the fitting results of R_c, effective hard-core radius R_{HS}, and the volume fraction ϕ (please see Chapter 4 for more detailed descriptions).

Table B.1 summarizes the fitting results of the SAXS patterns for UV cross-linked ion gels, and the results for the same ion gels before and after thermal cross-linking were also included for comparison. By comparing the SAXS patterns changing before and after the cross-linking, it is clear that the microstructure of the ion gel was not significantly affected by the UV cross-linking reaction. In fact, the SAXS patterns of these three gels look quite similar to each other. The fitting results also confirmed that both the core radius R_c, and the average core to core distance, d_{nn}, are essentially unchanged after UV-irradiation. This is also consistent with our previous conclusions on thermal cross-linking that the reaction of azide groups are confined to the PS domains, which should not affect the morphology of ion gels.

Table B.1 Fitting parameters for SAXS patterns of 10 wt% SOS-N_3 ion gels

	R_c (nm)	σ_{Rc} (nm)	R_{HS} (nm)	ϕ	d_0 (nm)	N_{agg}	d_{nn} (nm)
Before	5.6	1.0	12.1	0.38	0.72	127	28.7
UV	5.7	1.1	10.7	0.22	0.47	134	30.7
Thermal	5.4	1.2	12.2	0.31	1.15	114	31.0

Here, it is necessary to mention that the UV cross-linking method described in this project can only be achieved under inert atmosphere (in glove box). Preliminary results showed that ion gels exposed to UV-irradiation in the air suffered severe degradation. The gel sample becomes a liquid and starts to flow after UV exposure. It is speculated that ozone generated by UV-irradiation caused the degradation of PEO mid-block chains in ion gel, which damaged the cross-linked network structure.[12] Therefore, conducting UV cross-linking under inert atmosphere could prevent ozone degradation, thereby keeping the network structure intact. From the standpoint of materials design, one possible solution is to increase the density of azide functional groups in the PS end-blocks, which should accelerate the cross-linking kinetics and help decreasing the UV-exposure time. A potential concern is from the synthesis: the increased density of azide groups would require using larger amount of explosive NaN_3 in the reaction. Due to the limit of NaN_3 that can be used in each batch of synthesis (< 2 g), polymers may have to be synthesized in several smaller batches for safety reasons.

References

(1) Gu, Y.; Zhang, S.; Martinetti, L.; Lee, K. H.; McIntosh, L. D.; Frisbie, C. D.; Lodge, T. P. *J. Am. Chem. Soc.* **2013**, *135*, 9652–9655.

(2) Bang, J.; Bae, J.; Lowenhielm, P.; Spiessberger, C.; Given-Beck, S. A.; Russell, T. P.; Hawker, C. J. *Adv. Mater.* **2007**, *19*, 4552–4557.

(3) Yoo, M.; Kim, S.; Lim, J.; Kramer, E. J.; Hawker, C. J.; Kim, B. J.; Bang, J. *Macromolecules* **2010**, *43*, 3570–3575.

(4) Lee, S.; Lee, B.; Kim, B. J.; Park, J.; Yoo, M.; Bae, W. K.; Char, K.; Hawker, C. J.; Bang, J.; Cho, J. *J. Am. Chem. Soc.* **2009**, *131*, 2579–2587.

(5) Park, J.; Kim, J.; Lee, S.; Bang, J.; Kim, B. J.; Kim, Y. S.; Cho, J. *J. Mater. Chem.* **2009**, *19*, 4488–4490.

(6) Lee, S. W.; Lee, H. J.; Choi, J. H.; Koh, W. G.; Myoung, J. M.; Hur, J. H.; Park, J. J.; Cho, J. H.; Jeong, U. *Nano Lett.* **2010**, *10*, 347–351.

(7) Bansil, R.; Nie, H.; Li, Y.; Liao, G.; Ludwig, K.; Steinhart, K.; Konak, C.; Lal, J. *Macromol. Symp.* **2002**, *190*, 161–172.

(8) Kinning, D. J.; Thomas, E. L. *Macromolecules* **1984**, 1712–1718.

(9) Mischenko, N.; Reynders, K.; Koch, M. H. J.; Mortensen, K.; Pedersen, S.; Fontaine, F.; Graulus, R.; Reynaers, H. *Macromolecules* **1995**, *28*, 2054–2062.

(10) Flanigan, C. M.; Crosby, A. J.; Shull, K. R. *Macromolecules* **1999**, *32*, 7251–7262.

(11) Seitz, M. E.; Burghardt, W. R.; Faber, K. T.; Shull, K. R. *Macromolecules* **2007**, *40*, 1218–1226.

(12) Kaczmarek, H.; Kowalonek, J.; Klusek, Z.; Pierzgalski, S.; Datta, S. *J. Polym. Sci., Part B: Polym. Phys.* **2004**, *42*, 585–602.